THE UNIVERSITY OF ALBERTA

A TRACE ELEMENT STUDY OF THE TEXAS GULF ORE BODY, TIMMINS, ONTARIO

by

© ARPAD FARKAS

A THESIS

SUBMITTED TO THE FACULTY OF GRADUATE STUDIES AND RESEARCH

IN PARTIAL FULFILMENT OF THE REQUIREMENTS FOR THE DEGREE

OF MASTER OF SCIENCE

DEPARTMENT OF GEOLOGY

EDMONTON, ALBERTA

Spring, 1973

ABSTRACT

Trace and minor element partitioning between sulfide minerals of the Texas Gulf Sulfur massive sulfide deposit at Timmins, Ontario, was studied by means of electron microprobe analysis, in order to examine the question of chemical equilibrium in the sulfide depositional processes, to establish the paragenetic sequence and learn about the temperature and chemical environment of ore formation. Textures and chemical compositions of ore minerals were correlated.

The distribution of Co, Ni, Cu and Zn between the sulfide minerals can either indicate tendency to equilibrium partitioning at very high temperature or postdepositional homogenization of sulfide minerals by diffusion processes. Some evidence favours the latter alternative. The high abundance of Co relative to Ni in the sulfide minerals is interpreted as an original depositional feature and conforms to the type of deposit and its geological environment. It follows from both theoretical considerations on partitioning and application of experimental data on the partitioning of Co and Ni between high temperature hydrothermal fluid and pyrite that the high Co/Ni ratios of the Kidd Creek sulfides indicate a high concentration of Co relative to Ni in the ore depositing fluid.

The exact paragenetic sequence of mineralization is impossible to establish from the partitioning data, but the generally accepted

view stating the lack of paragenetic sequence in massive sulfide mineralization cannot be substantiated in relation to the Texas Gulf deposit because (a) the trace element distribution does not support diagenetic or metamorphic recrystallization of the sulfides at low temperature and (b) the difference in chemical composition of pyrites indicates different generations of this mineral.

Iron content of sphalerite which is resistant to postmineral changes indicates equilibrium deposition for pyrite, pyrrhotite and sphalerite as well as equilibrium fugacity of sulfur. Pressure of deposition calculated from the iron content of sphalerite is about 5.5 kilobars. Temperature of deposition calculated from partitioning of Cd between sphalerite and galena is about 550°C.

The mineralogical composition of ore (presence of Co, Sn, Ag minerals, lack of Fe oxide minerals) and perhaps the high temperature and pressure of deposition reflect the significant differences in geological-chemical environment of ore formation between Archean massive sulfides and massive sulfides of younger geological age.

ACKNOWLEDGEMENTS

Grateful acknowledgement is made to Dr. R.E. Folinsbee who initially suggested the Texas Gulf Timmins deposit for investigations, made it financially possible through a research assistantship and supervised many phases of the thesis work.

Dr. B.R. Hollebone's and Dr. H. Baadsgaard's interest, criticism and invaluable suggestions in interpreting the analytical data are deeply appreciated.

The assistance and patience of Dr. M. Coleman in the gas extraction for the planned sulfur isotopic analysis is acknowledged. Unfortunately the isotopic analysis has not yet been carried out because the mass spectrometer of the Physics Department has been inoperable.

D.A. Tomlinson and R. Bliss assisted in the electron microprobe analysis. The operation of the Microprobe Laboratory at this Department is supported in part through N.R.C. grant 44254 to Dr. D.G.W. Smith. Dr. Smith helped in the interpretation and assessment of microprobe data.

I also wish to acknowledge the friendly cooperation of personnel of the Texas Gulf Company and Kidd Creek Mine for permission to obtain the thesis material, for guidance in sample collection and for providing geological information.

The assistance of Mrs. N. Badham and F. Dimitrov in typing, editing and drafting is deeply appreciated.

Gratitude is also extended to my friend, L. Angus.

TABLE OF CONTENTS

LIST OF FIGURES

LIST OF PHOTOGRAPHIC PLATES

CHAPTER I: HISTORY, GENERAL GEOLOGY AND DESCRIPTION OF THE DEPOSIT

History of the Deposit

Prior to 1964 the Texas Gulf Sulfur Company performed an airborne and ground electromagnetic survey in Kidd Township in the vicinity of Timmins, Ontario, which indicated a high conductivity zone in a terrain mainly covered by glacial deposits. Drilling of this geophysical anomaly located an orebody 400 feet wide and 2000 feet long. Ore reserves are greater than 90 million tons (Northern Miner, April 15, 1971); at a yearly rate of 3,600,000 tons production the mine can operate for more than 25 years. The ore averages 4.85 oz Ag per ton, 1.33 per cent Cu and 7.08 per cent Zn. In 1966 mining was started by the open pit method with production increasing to 9000 tons per day.

Presently the Kidd Creek Mine is the biggest single producer of Ag and Zn in the world. In 1972 the open pit mining progressed down to the 10th bench (400 feet) while underground the 800 feet level was developed but still without any production. The ore is transported by train to a concentrator in Hoyle Township which produces zinc concentrate, copper concentrate and lead concentrate. The concentrator is designed to provide for the addition of a fourth circuit for producing tin and pyrite concentrates. The lead concentrate contains 28% Pb, the zinc concentrate contains 48% Zn and the copper concentrate has 23% Cu.

General Geology

The Timmins area belongs to the Superior Province and it is characterized by a thick Archean complex. The Archean rocks at Timmins can be divided into three stratigraphic units: (i) Keewatin volcanics, (ii) Keewatin sediments, and (iii) Timiskaming sediments. The oldest rocks are the Keewatin volcanics which comprise basic to acidic flows, pyroclastics and some intrusive rocks. The basic lava flows are either massive or pillowed and they are often associated with some minor breccias and basic tuffs. The basalt and andesite flows are conformably overlain by acidic pyroclastics and some acidic lavas.

Acidic flows occur in the northwest, central and south part of the Timmins area, while the acidic tuffs and breccias are located northwest of Timmins. Thin layers of argillite and cherty rocks typical of iron formations, are interbedded with the lavas. Stocks of quartz and feldspar porphyry occur within the volcanic pile. At the Kamiskotia area a layered gabbro with some anorthositic and ultramafic phases intrudes the Keewatin volcanics. Some of these ultramafic intrusions (peridotite and dunite) are serpentinized. West of Timmins a granitic batholith is intruded into the volcanics.

The Keewatin sediments are composed mainly of graywacke, argillite, arkose and some conglomerate and occur mainly in the central part of the area. The alternating graywacke and shale beds associated with some quartzite and conglomerate are representative of the Timiskaming Group. The Keewatin and Timiskaming sediments

are separated by an unconformity. The youngest rocks of the sequence, excluding the glacial lacustrine deposits, are the ultrabasic intrusions which are usually intruded along faults.

The Archean rocks exhibit folds, faults and also some domical structure. The folds usually have easterly trending axes. The trend of the faults is often easterly and they usually occur at or near the axes of synclines. Beside this there are northeast and northwest trending faults which are younger in age. The younger faults are in some cases accompanied by diabase dikes.

In the vicinity of Timmins, the Destor Porcupine Fault Zone is the major structural feature. North of this fault there is a large synclinorium which is accompanied by a series of smaller folds. South of the Destor Porcupine Fault is a northeast trending anticline. Domical structures located south of Timmins are accompanied by isoclinal folds (D.R. Pyke, R.S. Middleton, 1971).

Unfortunately only very basic geological information is available on the deposit itself. All the data presented here are based on personal communication with the mine personnel, supplemented by observations made during the few days of our sample collection.

The deposit is located in northeast Kidd Township, 15 miles north of Timmins. The Timmins area lies at the northeast edge of Abitibi Greenstone Belt which is characterized by metamorphosed early Precambrian (Archean) volcanic and sedimentary rocks and by

the occurrence of economically very significant massive sulfide deposits. It was formed in an Archean volcanic environment, in a geological setting typical of many Canadian massive sulfide deposits of the same age.

The Archean rocks spatially related to the massive sulfide mineralization are felsic and mafic volcanics, basic and ultrabasic intrusives and some slightly metamorphosed sediments. The mine area is covered by thick glacial-lacustrine deposits with only one major outcrop of Archean rocks; a rhyolite breccia located east of the orebody exhibiting no sulfide mineralization. The volcanic sequence grades from andesite through dacite to rhyolite and is composed of massive flows, breccias, tuffs and tuff agglomerates. Stratigraphically the sulfide bodies occur within rhyolite breccias or along a contact between rhyolitic and andesitic rocks and they are concordant with the enclosing steeply-dipping volcanic rocks. The orebody strikes about N20E, dips steeply E and plunges 75°N. Coarse pyroclastic rocks are more abundant than tuffs, although some of the flows can be interpreted as welded tuffs. All the volcanics exhibit some degree of sericitization, chloritization and silicification. Rhyolite breccias are usually strongly silicified and they form a circular pattern outlining a volcanic pipe (Middleton, Pike, 1971). The close association with acidic volcanics is characteristic of this type of deposit and implies genetic relationship between volcanism and ore deposition.

The rhyolite lavas are fine-grained, dense, massive, structureless rocks with colours varying from black to light, yellowish grey. No definite pillowed structures can be recognised. Microscopic examination revealed that the groundmass is very fine feldspar and quartz with varying amounts of chlorite. In highly chloritized rocks, almost all the groundmass is made up of chlorite. Quartz and feldspar phenocrysts are present in some specimens. The few feldspar phenocrysts proved to be orthoclase and some albite. The characteristic feature is the strong silicification and chloritization. In the vicinity of the ore the silicification is more pronounced, the amount of cryptocrystalline silica is so high that the rock has a cherty appearance. In the strongly silicified varieties only cherty silica, quartz and chlorite can be microscopically determined. Veinlets of quartz and carbonate of secondary origin are not so common as in the andesitic lavas. Opaque constituents are pyrite and chalcopyrite. The dark grey andesitic lavas are composed of quartz, chlorite and sericite with some epidote and carbonate. Quartz phenocrysts are rare: only some of the dacitic lavas contain conspicuous eye-shaped phenocrysts. Often the massive andesite, dacite lavas have been altered to sericite schists, particularly in

contact with the orebody or along dislocations and shear zones. These sericitic schists contain cherty quartz, some carbonate, and considerable amounts of epidote. In altered andesite-dacite lavas the groundmass is highly chloritic and sericitic. Carbonization is more pronounced than in the case of rhyolites.

Opaque constituents of the andesite lavas include both oxide and sulfide. The sulfide is exclusively pyrite. The oxide is ilmenite and titaniferous magnetite. In polished sections no sign of sulfurization or replacement of oxides by pyrite can be observed.

Ilmenite and titaniferous magnetite lamellae are very frequent (Photograph 18). Spectral scan of the oxides detected both iron and titanium. It has been shown (Verhoogen, 1962) that exsolution of ilmenite from the magnetite ulvospinel series takes place parallel to {100} or {110}.

If the lava cools quickly, the metastable magnetite--ulvospinel solid solution does not exsolve. It is obvious that these oxides were formed at high temperatures in an oxidizing environment. Pyrite formation occurred at lower temperatures (even lower than the temperature of oxide exsolution) so that its chemical environment did not prevent the oxide formation.

Rhyolite tuffs are light grey in colour and exhibit no banding. Quartz, sericite and chlorite constitute most of the groundmass,

often with a small amount of albite and orthoclase. They usually have some cherty aggregates. Disseminated pyrite makes up the associated sulfide phase. Rhyolite-tuff breccias exhibit similar lithological features except that the lithic fragments are not chloritized to the same extent as the fine-grained groundmass, the felsic patches are imbedded in a dark chloritic and sericitic matrix. Disseminated pyrite, some chalcopyrite and sphalerite are the associated sulfides.

Often it is hard to distinguish between tuff agglomerates and tuff breccias because the lithic fragments vary in shape from angular to subangular or subrounded. A particular feature of the tuff agglomerates is the presence of massive sulfide fragements. A more detailed microscopic and macroscopic description of these sulfide fragments will be presented later, since they have important genetic significance in regard to ore deposition.

Rhyolite breccias: these are dense, fine-grained strongly silicified rocks. At the base of the massive sulfide mineralization (structural hanging wall) they exhibit a cherty appearance due to the high amount of cryptocrystalline silica. Quartz phenocrysts may occur in the highly siliceous matrix. Pyrite and chalcopyrite are the associated sulfides. All the volcanic rocks exhibit hydrothermal alteration in the vicinity of the orebody. The most conspicuous processes are silicification and chloritization, while carbonatization is not as important.

Tuff agglomerates usually contain fragments of massive sulfides, mainly sphalerite and pyrite and some disseminated chalcopyrite mineralization. The lithic fragments are not mineralized, all the mineralization is restricted to the highly chloritic groundmass. The size of the massive sphalerite fragments varies from some millimeters to several centimeters. These massive sphalerite fragments are elongated parallel to the planes of shearing. The lithic fragments show a much less pronounced elongation in the same direction. The few pyrite fragments exhibit strong cataclastic deformation. It is believed (Sinclair, 1971) that sulfide fragments in volcanic rocks overlying massive sulfide ore deposits derived from the deposit either by volcanic explosion in the same way as the associated pyroclastic debris, or by slumping of the sulfides along with the volcanic breccias on the flank of a volcano. These sulfide fragments do not exhibit the noticeable reaction rim of oxides and silicates observed at Horne Mine, Noranda (Sinclair, 1971), so that they have never been in contact with lava or pyroclastic debris of magmatic temperature. This is not conclusive proof against an explosive origin of tuff agglomerates containing sulfide fragments, because the explosion could have occurred at lower, hydrothermal temperatures (e.g. steam explosion) intermixing formerly deposited tuff agglomerates and massive sulfides. This would imply that the explosive volcanism revived after or during the deposition of massive sulfides, and also suggests that, since the sulfides are formed as an integral part of the volcanic cycle,

they are syngenetic with the volcanism. As we have mentioned, thermal metamorphism was not operative in the case of the sulfide fragments. The lack of thermal metamorphism is well evidenced by the fact that even pyrrhotite was not formed from the pyrite fragments. Clear signs of dynamometamorphism following the formation of the sulfide-bearing tuff agglomerates is evidenced by the elongation of sulfide fragments parallel to the shear planes. Further evidence is supplied by microscopic examination of the sulfide fragments: the quartz-carbonate gangue associated with the massive sphalerite, exhibits a preferred orientation parallel to the elongation of the fragments. Fragments of massive pyrite exhibit cataclastic deformation compared to the plastic deformation of sphalerite. The tectonic deformation affected not only the physical nature of the sulfides, but also resulted in phase alteration. Along the shear zones of tuff agglomerates pyrrhotite is present instead of pyrite. Similarly, it has been observed that in the shear zone of the main N-W fault structure, pyrrhotite is the almost exclusive iron sulfide. The most likely reason is that tectonic deformation and movement of the rocks along the fault planes locally generated high enough temperatures for the breakdown of pyrite to pyrrhotite + sulfur. This type of explanation is in agreement with the fact that in minor shear zones pyrrhotite is restricted to a thin surface layer 1-2 mm in thickness. Later, high temperature sulfur deficient solutions depositing pyrrhotite, or causing the breakdown of pyrite to pyrrhotite, probably would effect larger areas and were not restricted to slippage planes.

The intrusive bodies are represented by peridotite exhibiting talc carbonate alteration and large bodies of gabbro and serpentine. The altered peridotite is located east of the orebody, along a west, northwest-trending fault. Gabbro and serpentinite were encountered in a drill hole east of the orebody. These intrusive bodies are believed to be younger than the volcanics. Chloritic and biotitic sediments (greenschist facies) are subordinate in amount: thin beds of graphitic schist can be found in the north orebody exhibiting only disseminated pyrite mineralization. These layers are concordant with the stratigraphy and are located at the structural footwall.

The structure of the deposit is complex with evidence of folding and faulting. The orebody is folded along with the enclosing volcanics. Considering the zoning of sulfide minerals, their distribution, and the whole stratigraphic sequence, it seems to be likely that the deposit is overturned. This way the rhyolite tuffs and breccias can be taken as hanging wall only in structural sense; stratigraphically they must be the footwall of the deposit. As a part of the major fold structure, bodies of andesite and dacite dip steeply or are overturned, forming the hanging wall and footwall of the orebody (Angelo Petulik, personal communication).

The most prominent fault structure is in the E-W direction dividing the orebody into a northern and southern part. This fault seems post ore in nature. Metamorphism of the enclosing rocks is in the grade of greenschist facies.

Ore Types, Mineralogy, Zoning and Texture of the Ore.

Two major ore types can be distinguished: disseminated and massive. The disseminated mineralization is either pyrite or chalcopyrite. Disseminated sphalerite ores are hardly ever encountered, they are insignificant local features.

The host rock for disseminated pyrite mineralization can be both volcanics (mainly acidic) and sedimentary rocks. Host rocks for the disseminated chalcopyrite include sericite schist and silicified rhyolite lavas or pyroclastics. Massive ores can be banded or structureless. Massive ores without banding include chalcopyrite, sphalerite and pyrite ore.

Massive chalcopyrite ores usually carry sphalerite, some pyrite and pyrrhotite. A characteristic type of massive chalcopyrite is the "siliceous copper ore" occurring in strongly silicified rhyolite breccia and is accompanied by very little pyrite or sphalerite.

Massive sphalerites usually contain substantial amounts of pyrite and some pyrrhotite. Similarly, the massive pyrites usually contain some sphalerite and pyrrhotite.

Massive ores with banding are: banded pyrite-sphalerite ores with occasional bands of galena, banded chalcopyrite-sphalerite ore with alternating chlorite bands. As mentioned before, a major shear zone divides the orebody into a north and south part.

The north orebody is Zn-rich, and characterized by massive sphalerite ore with some chalcopyrite. Locally, some banded chalcopyrite-sphalerite ore occurs in the north orebody. The south

orebody is Cu-rich and mainly pyritic. Disseminated and massive pyrite and chalcopyrite with some sphalerite is characteristic of the south orebody.

The major sulfide minerals are pyrite, sphalerite and chalcopyrite in the order of decreasing abundance. Pyrrhotite and particularly galena are much less abundant. Other sulfides reported to be present are: bornite, covellite, digenite, stromeyerite, marcasite, arsenopyrite, greenockite (Douglas, 1970). Of these no covellite, digenite, stromeyerite and greenockite were identified by us. Presence of trace bornite is established only tentatively, no microprobe analysis supports the optical data. One microprobe analysis was made on an optical phase looking like bornite; this particular grain proved to be a tarnished chalcopyrite.

We identified cobaltite, antimonial silver, allargentum, freibergite, native silver and cassiterite. In all cases quantitative electron microprobe analysis was performed to ensure the identification.

The associated gangue minerals are quartz, cherty silica, chlorite and carbonate.

A definite stratigraphic zoning is noticeable in the deposit, particularly in the south orebody. In a drill hole (#204) intersecting the south orebody, the successive zones from top of the drill hole to bottom are: disseminated pyrite of about 400 feet thickness,

400-500 feet of disseminated and massive chalcopyrite and a 200 feet intersection characterized by massive sphalerite with some pyrite and traces of galena. These are not true thicknesses, the angle of drill hole is not known by us. The Fe-Cu-Zn-Pb zonal arrangement is clearly recognizable, but the order is reversed; just the opposite is found in many similar deposits, Canada and abroad. There is a strong likelihood that rather than that the zoning and the stratigraphic sequence of volcanics is reversed, the deposit is overturned.

At the north orebody the zones from structural hanging-wall to footwall are: disseminated chalcopyrite, massive chalcopyrite and massive sphalerite.

Many textural features encountered in the Texas Gulf deposit are characteristic of massive sulfides of similar origin. Excellent references are available on this subject (Stanton, 1960, 1964; Kalliokoski, 1965) so that instead of giving a detailed description, we describe and discuss only the more important textures which have some bearing on the genesis and geological history of the deposit.

Texture of the ore can be grouped into two categories:

1. Original depositional textures
2. Textures indicative of metamorphism

Unmodified or partially modified original textures include: colloform texture, banding, indicators of equilibrium coprecipitation between the sulfide minerals, textures indicating lack of replacement

and finally a few replacement textures.

Colloform textures are rare, they are encountered in massive pyrite or sphalerite. They appear as fine-grained masses of sphalerite included in pyrite or reversely pyrite included in sphalerite, having spherical or arched outlines (Photograph 1). Rhythmic alternation with concentric shells of pyrite and sphalerite is common, with occasional chalcopyrite layers. These concentric shells have a radial, fibrous internal structure. Colloform carbonate with radial structure was also observed. More often the colloform textures exhibit various degrees of recrystallization. At the first stage of recrystallization the radial structure is still recognizable (Photograph 2) at a later stage polygonal network of the minor phase in the host is the result.

Banding was observed on both microscopic and macroscopic scale and exhibited all the usual features of banded massive sulfide ores. It is not a general characteristic of this ore, but more widespread than colloform texture. One observation is worth mention, concerning the controversial subject of banding. The origin of banded texture in massive-sphalerite ores with alternating bands of pyrite and sphalerite cannot be explained by simple metamorphism for the following reason. Due to the different mechanical properties of pyrite and sphalerite even a unidirectional deformation is not able to produce bands of pyrite from former pyritic aggregates included in sphalerite, because there is no evidence that confining pressures were high enough to result in cohesive flow of pyrite. Oppositely,

pyrite of this deposit invariably shows only brittle deformation without any sign of cohesive flow. Brittle deformation of pyrite is not so noticeable on pyrites included in massive sphaleritic ores, which can be expected if we have a mechanically elastic matrix (sphalerite) with brittle enclosed material (pyrite). Photograph 3 represents a fine-grained pyritic band in massive sphalerite, the individual pyrite grains do not exhibit cataclastic deformation. Similar arguments apply to pyrite bands found in chalcopyritic ore. The general lack of replacement rules out this type of origin for the banded ores so that banding of ore is regarded as an original depositional feature which was modified by later tectonic agencies. It is essentially a result of the rhythmic deposition of different sulfides or sulfide and gangue minerals. At this point there is a strong similarity with colloform textures except that banding is a more regional, larger scale feature, and the constituent particles have coarser grain size.

Generally the sulfides do not replace the gangue minerals. During the microscopic investigations, special attention was paid to carbonates, because they are the most reactive, the most favourable host for replacement. Photograph 4 represents a rhombohedral calcite included in massive chalcopyrite, while Photograph 5 shows a calcite rhombohedron in banded pyritic sphalerite ore with no obvious sign of replacement. The subhedral or anhedral carbonate grains encountered are not necessarily of replacement origin, they might well be equilibrium coprecipitates with sulfides.

Pyrite often surrounds the formerly deposited euhedral carbonate, with boundary following the rhombohedral crystal faces of the carbonates (Photograh 6). This texture cannot be of later metamorphic origin since pyrite did not respond with cohesive flow to stresses which affected the orebody.

Evidence of pseudomorphism is very rare; in one case it was observed that cobaltite included in massive chalcopyrite forms pseudomorphs after calcite and the cobaltite itself shows possible signs of later replacement by chalcopyrite.

In summary it can be stated that selective replacement of gangue minerals by sulfides was not operative to the extent of determining the ore deposition process.

Photographs 7 and 8 represent primary unmodified textures: the subhedral and anhedral pyrite grains included in and embayed by sphalerite are indicators of equilibrium coprecipitation between pyrite and sphalerite. This question will be discussed later in connection with the chemical evidence presented in the section dealing with the Cu and Zn analysis of sulfides.

Deformation textures involve cataclastic deformation of pyrite, flattening of chalcopyrite and sphalerite, preferred orientation of gangue minerals, plastic flow of galena, deformation veins of galena, chalcopyrite and sphalerite intruding into fractured pyrite or silicates, and finally partial or complete recrystallization of original textures.

Tectonic brecciation of pyrite resulted in the formation of sharp, angular fragments. It is exhibited mostly by massive pyrites or disseminated pyrites and is most conspicuous along shear planes. Tension fractures of pyrite (Photograph 9) and silicate gangue (Photograph 10) are veined by sphalerite and chalcopyrite, minerals able to react to the stresses with plastic flow. If pyrite occurs in a cherty groundmass unable to take up stresses by plastic flow, it becomes highly strained, pitted on polished surface (Photograph 11). Photograph 12 exemplifies the importance of the mechanical properties of enclosing material. Pyrite enclosed in a more plastic chalcopyrite band is subhedral with no evidence of fracturing while pyrite occurring in silicate has a strongly cataclastic appearance.

Plastic deformation of chalcopyrite and sphalerite resulted in the flattening, elongation of grains parallel to the stresses. Photograph 13 shows flattened, slightly oriented grains of sphalerite from disseminated sphaleritic ore. Galena also shows evidence of plastic deformation: the cleavage planes are slightly bent (Photograph 14).

Orientation of gangue minerals enclosed in a plastic matrix (chalcopyrite or sphalerite) is one clear evidence of late, metamorphic deformation (Photographs 10 and 15). This feature is only locally noticeable at contacts with the enclosing volcanic rocks and it probably indicates higher pressure zones localized along folds or other types of structures.

Recrystallization of sulfides is also a late, superimposed feature and can involve two different processes (Stanton, 1964):

1. Recrystallization resulting in grain growth.
2. Recovery from the strain by annealing.

No definite annealing textures were observed on pyrite; large deformed crystals are not recrystallized into fine-grained mosaic or polygonal textures. There are definite evidences of recrystallization (grain growth of fine-grained pyritic masses. Colloform textures are affected the most (Photograph 2) but fine-grained pyrite can also exhibit some degree of recrystallization.

Photograph 16 exhibits aggregates of fine-grained pyrite with a tendency to recrystallization to cubes of varying perfection. In this case there is no sign of brittle deformation. Although theoretically it would be possible that complete annealing could erase the effect of deformation, it is practically impossible, since at many other places cataclastic deformation is conspicuous. This way this particular texture is more likely to be of grain growth type of recrystallization, which can also develop during the diagenesis of the deposit and does not necessarily imply metamorphism.

Conclusions drawn from the Textural Study can be summarized as follows:

1. Replacement origin is not favoured on the ground of ore textures and its relationship with gangue minerals.
2. Sulfides were fine-grained and perhaps at a certain stage of the deposition a minor fraction of the precipitated sulfides was of colloidal grain size. Although much more detailed textural study would be necessary to ensure the general nature of the observation, it seems that relics of colloform textures (and fine-grained pyrite)

are found near to the structural footwall, i.e. stratigraphically at the upper part of the orebody in the pyritic Zn-Pb zone which might suggest that the colloidal or fine-grained sulfide fraction was transported to and deposited at higher levels by the upward-flowing mineralizing solutions. This type of distribution also can be expected as a result of deposition in a submarine, exhalative environment.

3. Regional metamorphism of the deposit was of low grade and many of the deformation textures observed on sulfides were localized to minor or major shear zones and probably folds.

Some of the fine-grained sulfides exhibit partial recrystallization, but this might happen during the diagenesis of the deposit when the temperature was still high and relics of the mineralizing solutions were present. Recrystallization of the colloform textures also might be diagenetic in nature.

The same low-grade regional metamorphism with many preserved primary ore textures was observed in the neighbouring massive sulfide deposit at the Kam Kotia Mine (Kalliokoski, 1965).

CHAPTER II: APPLICATION OF TRACE ELEMENT STUDIES TO METALLOGENETIC PROBLEMS

Mode of Occurrence and Source of Trace Elements in Sulfides

Trace elements in sulfides may be present in different types of solid solutions: in diadochic substitution, in interstitial sites, in lattice defects, or they are present as trace minerals captured during the growth of host mineral, or formed by exsolution during cooling. Adsorption and various fluid inclusions may also contribute to the total trace element content of sulfide minerals. All these factors together can cause an irregular distribution of trace elements in the mineral assemblage. If the erratic distribution is caused by surface adsorption we will be unable to detect any regularity in partitioning due to the lack of a suitable analytical technique.

Surface adsorption is a result of the attraction between surface atoms whose bonding is not completely satisfied and foreign ions held in a diffuse layer. The adsorption capability increases with surface area and gains more importance where the mineral is fine-grained or has colloidal dimensions. This way, if sulfide minerals from volcanogenic types of deposits were colloidal in nature as has been suggested by Kinkel et al. (1966), we could not expect any regular distribution of the trace elements.

It is possible to detect trace mineral contaminations by utilizing high sensitivity analytical techniques and to establish a relationship, if there is any, in the partition of trace elements between coexisting minerals. The source of trace elements may or may not be the same as that of the major components. In whole or

in part, the provenance of trace elements is likely to have been the ore fluid from which the sulfides have been deposited.

The minor element content of the ore depositing fluid and sulfide minerals depends on many factors:

1. Minor element content of the source rock.
2. Partition ratio between the ore depositing fluid and source rock.
3. Partitioning of the minor elements between the ore depositing fluid and precipitating sulfide minerals, i.e. the physical chemical environment of ore deposition.

Obviously the number of variables which determine the trace element content of sulfides are more than we can determine. In the case of a sedimentary-exhalative type of deposit, a further complication is the varying rate of interaction between the sedimentary and volcanic environment. Despite these complications, certain types of deposits are characterized by the higher or lesser abundance of certain trace elements. Characteristic concentrations of certain trace constituents can also be observed in the sedimentary-exhalative type of deposits.

There is also a definite consistency in the association of certain types of ore deposits with certain types of rocks. So that, despite the significant differences in the mineralogical compositions of the individual deposits, the characteristic geological environment and trace element concentration of a given deposit type must imply a very similar physical-chemical environment, or genetic source of ore deposition in every individual case.

Trace element studies on sulfides

Numerous investigations of trace elements in hydrothermal as well as sedimentary sulfide minerals have been carried out so far (Fleischer, 1955; Hawley and Nichol, 1961). Early reconnaissance type investigations were limited mainly to correlation with temperature of deposition and crystal chemistry.

The distribution of trace elements has been studied on many scales; in single crystals, individual orebodies and mining districts. Attempts have been made to discriminate between different types of ore deposits and between different deposits of similar types (Hawley and Nichol, 1961; Loftus-Hills and Solomon, 1967). In some cases connection was established between the lateral and vertical zoning of trace elements and the hypogene mineral zining.

It has been proposed that the partition of trace elements can be used as an indicator of the temperature of ore deposition (McIntire, 1963).

Recently a revival of the geothermometrical application of trace element studies has occurred, but on a more quantitative basis utilizing the results of laboratory experiments on synthetic

sulfide systems at high temperature and pressure (Bethke and Barton, 1971; Hall et al., 1971). This way the present trend of application of trace element studies is toward geothermometric problems, estimation of temperatures of sulfide deposition, coupled with possible information about the question of chemical equilibrium during the deposition. Successful attempts have been made in applying the trace element data to environmental problems of mineral deposition.

Two indicators of depositional environment have been used by various workers. These are the abundances of Co and Se relative to Ni and S. With the help of Co/Ni ratios we can discriminate between magmatic-hydrothermal, sedimentary and possibly sedimentary-exhalative (volcanogenic) environments of deposition.

It has been shown that high Co contents in pyrites may be related to volcanic processes. Preliminary results show (Loftus-Hills and Solomon, 1967) that on the basis of cobalt content and Co/Ni ratios, pyrites can be grouped as follows:

1. Sedimentary or diagenetic pyrites have high Co and Ni content and Co/Ni ratios smaller than 1.

2. a) Pyrites from volcanogenic deposits without accompanying Pb-Zn mineralization have Co/Ni ratios greater than 1.

b) Volcanogenic pyrites from Pb-Zn rich deposits are characterized by low Co and Ni and Co/Ni ratios smaller than 1.

Partitioning of Trace Elements

In developing the theoretical basis of trace element partitioning between coexisting phases only trace elements present in solid solution were considered which can be described adequately in terms of thermodynamics (McIntyre, 1963). The occurrence of trace elements in the form of solid or liquid inclusions adds additional complications, inaplicability of simple thermodynamic rules.

If the crystal growing from an aqueous solution or melt is in equilibrium with the solution or melt, each component will partition between solid and liquid in such a way that its chemical potential becomes equal in each phase. The chemical potential of a given component (say, component 1) in each phase (mineral) A is defined by the expression:

$$\text{Eq I} \quad \mu_1^A = \mu_1^\circ + RT \ln N_1^A$$

where μ_1° is the chemical potential of pure component in its standard state.

N_1^A is the mole fraction of component 1 in the solid solution in mineral A.

R is the gas constant and T is the absolute temperature.

The same must be true for another phase (mineral) B:

$$\text{Eq II} \quad \mu_1^B = \mu_1^\circ + RT \ln N_1^B$$

In the case of equilibrium distribution of component 1 between phase A and B:

$$\mu_1^A = \mu_1^B$$

If we have a multicomponent system, the equality of chemical potential of a given compound must be held for all the phases present in order to have a chemical equilibrium. A more useful definition of chemical equilibrium in our case is: the activity of component 1 must be the same in all phases present.

The definition of activity $a = e^{\mu/RT}$

where μ is the chemical potential, R the gas constant and T is the temperature.

In equilibrium

Eq III $\quad a_1^A = a_1^B = a_1^{solution}$ i.e. the activity of component 1 in mineral A, in mineral B, and in the solution must be equal.

The relationship between activity and concentration (mole fraction)

Eq IV $\quad N_1^A = a_1^A/\gamma_1^A$

where γ_1^A is the activity coefficient of component 1 in phase A.

The activity coefficient is an inverse measure of the ability of host phase to accommodate the minor component. Its magnitude varies with temperature, pressure and composition of the host (Bethke and Barton, 1971).

Substituting IV into III

Eq V $\quad N_1^A \gamma_1^A = N_1^B \gamma_1^B = N_1^{solution} \gamma_1^{solution}$

The partition coefficient K is defined as the ratio of the concentrations of the minor component (component 1) in any two phases

Eq VI $\quad K_1^{solution\text{-}A} = \dfrac{N_1^{solution}}{N_1^A} = \dfrac{\gamma_1^A}{\gamma_1^{solution}}$

Or in the case of two minerals (A and B)

$$\text{Eq VII} \qquad K_1^{A-B} = \frac{N_1^A}{N_1^B} = \frac{\gamma_1^B}{\gamma_1^A}$$

The activity coefficient of a minor component in a solid solution varies with the concentration of the component, excluding a range of dilute concentrations where γ has a constant value analogous to the Henry's Law constant. This way in the dilute solution range K depends only on the temperature and independent of the concentrations.

It is also possible to examine the problem of trace element partitioning between coexisting sulfide minerals on the ground of crystal field theory. The extent of splitting of transition metal d orbitals in the electrostatic crystal field of the ligand (sulfur) determines the magnitude of crystal field stabilization energy (CFSE). Crystal field stabilization energies for divalent cations increase in the order Fe, Co, Ni, Cu as calculated from thermodynamic data (Burns, 1970). Since transition metal ions are concentrated in the phase giving largest crystal field stabilization, the relative enrichment of Co, Ni, Cu in coexisting sulfides can be estimated. CFSE is greatly enhanced when the transition metal ion occurs in the low spin configuration. In coexisting pyrite and pyrrhotite there is a relative enrichment of Co over Ni in pyrite, whereas Ni is enriched over Co in pyrrhotite.

These relative enrichments may be explained by the higher stabilization energy of low spin Co^{2+} in pyrite compared to Ni^{2+} and the higher stabilization energy of Ni^{2+} in pyrrhotite compared to high spin Co^{2+} (Burns, 1970).

Because in sulfide minerals there are a large variety of substituting transition metal ions with different electronic structures the molecular orbital occupancy and hence the CFSE cannot be adequately determined. "Interaction" of different ions in a particular sulfide mineral may result from an equilibrium CFSE which is determined by the weighted average of the number of d electrons of substituting transition metal ions (see partitioning of Co and Ni in the next section). Due to the lack of CFSE measurements on sulfides, the applicability of crystal field theory and the validity of Burn's statements are very questionable.

Generally three distinctive types of partitioning curves can be observed. The patterns of partition coefficients can vary from linear through curvilinear to completely scattered. There is no correlation between the same pairs of minerals and different elements, or between the same elements and different pairs of minerals regarding the type of partitioning curve.

The linear distribution of an element between two minerals resulting in a constant partitioning coefficient very likely indicates that the constraints of the dilute distribution law have been fulfilled; the two minerals were precipitated in equilibrium with each other regarding the particular trace constituents.

The other two types of partitioning pattern (curvilinear and scattered) cannot be taken unequivocally as indicators of the lack of equilibrium coprecipitation. We have to consider the possible causes of departures from the dilute solution law to find explanation for

these types of partitioning patterns. One of the most obvious explanations for the curvilinear and scattered patterns is that the trace elements were not sufficiently diluted to obey Henry's Law. A curvilinear partitioning pattern means increasing partition coefficients with increasing concentration of the element in one or both phases. Besides that the solution was not sufficiently dilute to yield constant partitioning conditions, the other reason can be the presence of "induced point imperfections" in the crystal lattice (McIntyre, 1963).

If the mineral contains solid solution substitution by an element of higher valency than that of the substituted elements, to neutralize the charge disparity vacant lattice sites formed ("induced point imperfections") and the Henry's Law will not be obeyed. The effect of the induced point imperfections on the partitioning coefficient can best be described by McIntyre's equation:

$$\frac{N_i^A}{N_i^B} = \frac{1}{N_1^B} N_i^B + \frac{N_2^B}{C_{(T\ P)}}$$

$$C_{(T\ P)} + \frac{N_i^B\ N_1^B}{N_i^A}$$

where N_i^A and N_i^B are the mole fractions of element "i" in phase A and B respectively.

N_1^B and N_2^B are the "mole fractions" of vacant sites in phase B in the position of element 1 and 2 respectively, induced by the

substituting element "i".

This equation means that if the partitioning coefficient (N_i^A/N_i^B) increases as N_i^A increases, phase B contains induced vacancies. If N_i^B remains constant the partition coefficient will also do so. Curvilinear partitioning pattern is due to changes in N_i^B by this equation.

The reason for scattered type of partitioning can be three-fold:

1. Lack of equilibrium coprecipitation
2. Solutions were not sufficiently dilute
3. Chemical composition of the host mineral changed

Any one of these factors, or any combination of these, as well as the three together can give rise to scattered type of partitioning.

Let us examine the reason for non-dilute behaviour and trace element interaction in a crystal chemical context, considering the solubility of Co and Ni in pyrite and pyrrhotites. We can postulate that the solubility of a certain trace element in a sulfide mineral is related to the distortion of the accommodating mineral's crystal lattice; i.e. in the case of ideal solutions, the lattice of the accommodating mineral is unchanged (the heat of mixing is zero). This way the solubility is related to:

a) the radius ratio of the cation/anion for the substituting element. If the latter is significantly different from the cation/anion radius ratio of the accommodating lattice, a distortion of the host mineral's lattice and hence a limited solubility of the particular trace element can be expected.

b) The electronic structure of the substituting and substituted cation. The number of d electrons in transition metals (and hence the oxidation state) determine the structure and coordination number of transition metal compounds, d^5, d^7, d^9 and d^{10} ions prefer tetrahedral while d^3, d^6 and d^8 ions prefer octahedral or square planar structures. Crystal field stabilization energies (electronegativity of ligand) and spin pairing energies of d antibonding electrons determine the most favourable structure of the compound. If the d electronic structure of the substituted and substituting cation prefer different geometry with the ligand (in our case sulfur) the crystal lattice of the host mineral is distorted. Consider now the most favourable geometry of Co^{2+}, Ni^{2+} with S^{2-} as the ligand, i.e. the substitution of these elements in the pyrrhotite lattice. Co^{2+}, a d^8 ion, prefers a tetrahedral structure with S^{2-} as ligand. Ni^{2+}, a d^7 ion, prefers a square planar or strongly distorted five coordinated structure with S^{2-} as ligand.

Pyrrhotite and jaipurite (γ-CoS) has the same crystal structure (hexagonal). In these lattices Co^{2+} and Fe^{2+} occur in sixfold coordination. Millerite (β-NiS) is rhombohedral in which Ni is in fivefold coordination. The structural similarity of hexagonal pyrrhotite and jaipurite favours a higher solubility of Co than Ni in the pyrrhotite lattice. Ni forced in a sixfold coordinated position in the pyrrhotite lattice, bonded less strongly to the sixth sulfur atom and decreases the stability of the lattice. The above considerations are in agreement with the predicted most stable

geometry of Co^{2+} and Ni^{2+} (d^7 and d^8 ions) with low electronegativity ligand like S^{2-}. These structural differences of Co^{2+} and Ni^{2+} compounds are observed also on aqueous chemical species. With low electronegativity ligands Co^{2+} forms tetrahedral complexes, while Ni^{2+} forms square planar or strongly distorted five coordinate species (Hollebone, 1971).

In the case of Co, Ni, Fe disulfides the ligand is S_2^{2-} ion, in which the oxidation number of sulfur is -1. Compared to S^{2-}, the persulfide ion (S_2^{2-}) has higher electronegativity. The latter fact explains why all Co, Ni and Fe disulfides have the same crystal structure with the metal ion in a sixfold coordination. The structural similarities of pyrite, cattierite and vaesite indicate high solubility of Co and Ni in pyrite. Natural bravoites have a nearly continuous variation in their Fe/Ni ratio from FeS_2 to NiS_2 (Springer et al., 1964) but are believed to be metastable because phase studies in the FeS_2-CoS_2-NiS_2 system indicate a large miscibility gap between pyrite and vaesite at low temperatures. A lower solubility of Ni compared to Co can be expected in pyrite because of:

1. Rapid increase in the electronegativity of the metal ion going from Fe^{2+} to Ni^{2+} due to the increasing effective nuclear charge as a result of the imperfect shielding of d electrons. This way the electronegativity difference in pauling units between the metal and the persulfide ion (S_2^{2-}) is 1.0 for pyrite and 0.5 for vaesite, i.e. vaesite is more covalent than pyrite.

If metal acquires too much charge by covalent acceptance from the ligand, it will distort the structure of the complex and eliminate one or more ligands to reduce its own charge density. In the case of millerite (Ni^{2+} S^{2+} system) the metal ligand electronegativity difference is 0.3; consequently, Ni^{2+} is bonded only to five ligands (S^{2-}).

2. Lower crystal field stabilization energy for Ni^{2+} due to the presence of two antibonding electrons in octahedral crystal field. This effect is small (about 20-25 kcal/mole) compared to the total bond strength of about 1000 kcal/mole. The order of magnitude of CFSE versus covalent bonding is about 5% to 95% in terms of the total bond energy (Figgis, 1966).

3. Larger ionic radius for Ni^{2+} which is related to the change in spin state. Six coordinated low spin Fe^{2+} and Co^{2+} have radii of 0.61Å and 0.65Å respectively, while high spin Ni^{2+} has a radius of 0.70Å. A decreasing metal to sulfur bond strength is reflected by the increasing unit cell edge in the order FeS_2, CoS_2, NiS_2.

In summary, it can be stated that a significant enrichment of Co and Ni can be expected in pyrite over pyrrhotite if the two minerals coprecipitate in equilibrium. Similarly, a departure from ideal behaviour of Co and particularly Ni in the pyrrhotite solid solution can be indicated at a much lower concentration than in the case of pyrite solid solution. Let us consider now how the solubility (activity) of one element influences the solubility of another element in a given crystal lattice; i.e. how the chemical composition of host can influence the activity of the substituting element and this way the partitioning coefficient.

It can again be postulated that if a certain element has high solubility in a sulfide mineral (ideal behaviour) its presence will have a negligible effect on the solubility of another element If the substitution of an element results in the distortion of the host mineral's lattice, the solubility of another element in the same lattice is decreased.

Ghosh-Dastidar et al. (1970) stated that almost all the partition coefficients are influenced by the concentrations of other trace elements in the phases. Authors above proposed that if the partitioning coefficients K_i^{A-B} for element i is a function of i/j element ratios in phase A, interaction of elements i and j in phase A has affected the distribution of element i between phase A and B. Using these "interaction plots" they demonstrated that many of the scattered partitioning patterns are a result of trace "element interactions" in the host mineral. Interaction curves of similar shape were obtained by them "from elements which are known to exhibit similar chemical behaviour", citing In and Cd as examples! Furthermore, in interpreting the partitioning of Co and Ni between pyrrhotite and other sulfide minerals, they stated that "both Co^{2+} and Ni^{2+} are known to have a high capacity to form compounds which are isostructural (i.e. same coordination number, hybrid bonds, etc.) with pyrrhotite". From our former discussion it is obvious that these statements are wrong. Co-Ni "interaction" in the pyrrhotite lattice is not a result of their "similar chemical behaviour". Ni is likely to influence the solubility of Co in the pyrrhotite lattice because nickel distorts the lattice to a greater extent than cobalt.

All these considerations hold only if both Co and Ni are present as divalent ions in the pyrrhotite lattice.

Finally, let us examine the possibility of direct chemical interaction between two trace elements in a certain crystal lattice. Direct chemical interaction could occur via spin pairing between possible sites. In the case of trace amounts of substituting elements, the probability that the two substituting elements occupy neighbouring lattice sites is very small and so is the probability of chemical interaction.

Requirements for the successful application of trace element partitioning

Concentrations of trace constituents in sulfides will be used in this study for a two-fold purpose. By element abundances and ratios we shall try to define the environment of mineral deposition by comparing our results with publisehd data on the same type of deposits. By examining the partition of trace constituents between coexisting mineral pairs we shall attempt to gain information about the question of temperature of formation and existence or nonexistence of equilibrium. This way the elucidation of paragenesis is a basic requirement so that it is one of the major targets of this study.

In order to obtain meaningful analytical results which can be applied to partitioning and paragenetic problems we have to have

nearly absolute degree of sample purity. Even a minute contamination by the phase enriched in the trace constituent would give apparently high concentrations for the impoverished phase. Measuring those trace constituents of a mineral which happens to be the major component of some other minerals we have an absolute constraint on the sample purity (e.g. measuring Cu and Zn content of pyrites associated with sphalerites or chalcopyrites).

There is another analytical restriction: the technique utilized must be highly sensitive and precise. The above requirements can be fulfilled choosing the electron microprobe analysis as the method of analysis. This method of investigation also has the advantage of offering a possibility for obtaining simultaneous chemical and textural information on the ore minerals. The simultaneous microscopical-textural and chemical information gives the best way of classifying the paragenesis of mineralization.

There is a paragenetic restriction on the partitioning of trace elements and their successful application to the problems of ore deposition. The minerals considered must have been deposited simultaneously and in equilibrium with each other.

It has been suggested by Stanton (1960, 1964) that textures of stratiform ores are the result of grain growth in the solid phase, and phase boundaries reflect solid: solid surface tensions dictated by the crystalloblastic properties of the minerals involved.

In his opinion sulfide minerals of stratiform volcanogenic ores are not deposited in a paragenetic (time) sequence, but rather the textures represent low temperature segregation during crystallization of an amorphous or cryptocrystalline sulfide mixture.

In the case of the Kidd Creek deposit, plastic deformation of ore, veining of tension fractures and possibly recrystallization are further complications hindering the interpretation of ore texture with regard to paragenesis. A possible approach to the problem is to assume a more likely paragenetic sequence and test the assumption by trace element abundances and partitioning of trace elements, i.e. to support or discard the assumption utilizing coupled chemical-textural information.

In the following, we list all the assumptions made in interpreting the trace element distribution among the sulfide minerals:

1. The most likely paragenetic sequence is: cobaltite, pyrite, pyrrhotite, chalcopyrite and sphalerite.

2. Interaction or concentration plots are not coincidental. If interaction or concentration plot is established, equilibrium (either depositional or postdepositional) on grain to grain or hand specimen scale is likely.

3. In applying Springer's experimental data (Springer et al., 1964) to the disseminated pyrite mineralization of the Kidd Creek deposit it was assumed that (a) we deal with a pyrite-hydrothermal fluid system, (b) pyrite was precipitated from aqueous sulfide complexes.

CHAPTER III: TRACE ELEMENTS IN THE TEXAS GULF DEPOSIT

Introduction - Elements Analyzed

Cobalt and nickel were chosen for analysis since they have been shown to be useful environmental indicators. It has been shown that they exhibit characteristic concentrations and Co/Ni ratios in the type of deposit to which the Kidd Creek deposit likely belongs.

Sulfide minerals are generally undersaturated with respect to their trace element content. If these elements are trace constituents of one phase and major constituents of another phase and the two phases have simultaneous appearance in the paragenetic sequence with equilibrium coprecipitation, the concentrations of some elements can be present in saturation amounts. This is the reason why Cu or Zn or both were analyzed as trace constituents in pyrites, pyrrhotites, chalcopyrites and sphalerites. Analysis of the later elements also can yield some information about the genesis of pyrrhotite, which is an essential question in clarifying the chemical environment of ore deposition or possible post-depositional metamorphic deformation of the deposit.

Sn and Ag were analyzed because, despite the fact that they have very high abundances in the Kidd Creek deposit, there was not enough information about their mode of occurrence.

Finally, Mn and Cd were chosen for partitioning study and possible use in geothermometry because quantitative data on their equilibrium distribution in coexisting pairs of minerals as a function of temperature are available (Barton and Bethke, 1971).

To obtain information about the gross chemical composition of phases carrying Cu, Zn, Sn and Ag as major constituent, a reconnaissance analysis was performed on several minerals. These measurements were also aimed at identifying some of the minor minerals in cases where the optical methods of identification were not adequate due to the minute grain size or similar optical properties of the minor mineral to that of the host mineral.

Sample Collection and Preparation

Ore samples that were studied and analyzed were obtained from three different sources: from the open pit mining operations, from underground (800' level) and cores from deep drilling hole (Hole No. 204). The samples include both the North and South orebody and the shear zone. The location and description of these samples is given in the appendix. Adequate polished mounts were made for electron microprobe analysis. Detailed ore microscopic investigation was performed on all the samples before chemical analysis.

Analytical Method

The electron microprobe analyses were performed using an A.R.L. "EMX" microprobe applying an operating voltage of 19 KV for Co, Ni,

Cu, Zn, Sn and Ag and 15 KV for Mn and Cd. Lines analyzed and crystals used for each element are as follows: Mn, Co, Ni, Cu and Zn: $K\alpha_{1,2}$ and lithium fluoride. Ag and Cd: $L\alpha_{1,2}$ and EDDT (Ethylene Diamine Ditartrate). Sn: $L\alpha_{1,2}$ and lithium fluoride. An emission current of 200 μa and a beam current of 0.1 μa was applied. This gives a sample current of about 0.01 μa. The above elements were measured in pairs; Co with Ni, Cu with Zn, Sn with Ag and Mn with Cd, using separate channels for the simultaneous measurements.

To obtain quantitative analyses, the raw X-ray intensity data were corrected for background, atomic number, absorption and characteristic fluorescence effects. These corrections were made by an APL language computer program (Smith and Tomlinson, 1970).

In accomplishing the atomic number correction the computer program makes use of the formulae and data of Duncumb and Reed (1968). In calculating the absorption correction the Philibert (1963) and Heinrich (1967) expressions were applied, and where the possibility of characteristic fluorescence excitation existed, the corrections are computed according to the method of Reed (1965). Standards used in the analysis were synthetic CoS, NiS, CuFeS,

Ag and Sn metal, and sphalerite from Picos de Europa, N. Santander, Spain.

Analytical Error

Assuming that all instrumental errors arising from sample inhomogeneity, correction procedures, etc. are negligible, the analytical error in the electron microprobe measurements may be determined by statistical factors; i.e. the number of counts obtained on the standard and sample at the peak and background positions. By increasing the number of measurements (and thus the total counts recorded) and by utilizing standards with high concentrations of the analyzed elements, which therefore give high count rates, the precision of the analysis can be increased.

The following approximation is used in calculating the limit of detectability at approximately the 99% confidence level (D.G.W. Smith; personal communication).

$$0 < I_p - I_b - 2.6\,(I_p/t_p + I_b/t_b)^{\frac{1}{2}}$$

where I is the intensity in counts per second and t is the time in seconds (subscript p refers to peak while b refers to background). This expression is only an approximation since two terms (I_p and I_b) are varying independently and thus the distribution of background-corrected peak counts will not be strictly normal. The term 2.6 in the above approximation refers to a confidence level of 99.06% for a normal distribution. The numerical values of this expression as well as the standard deviations and confidence levels for the different elements at different concentrations are listed in the appendix (Appendix A- 1).

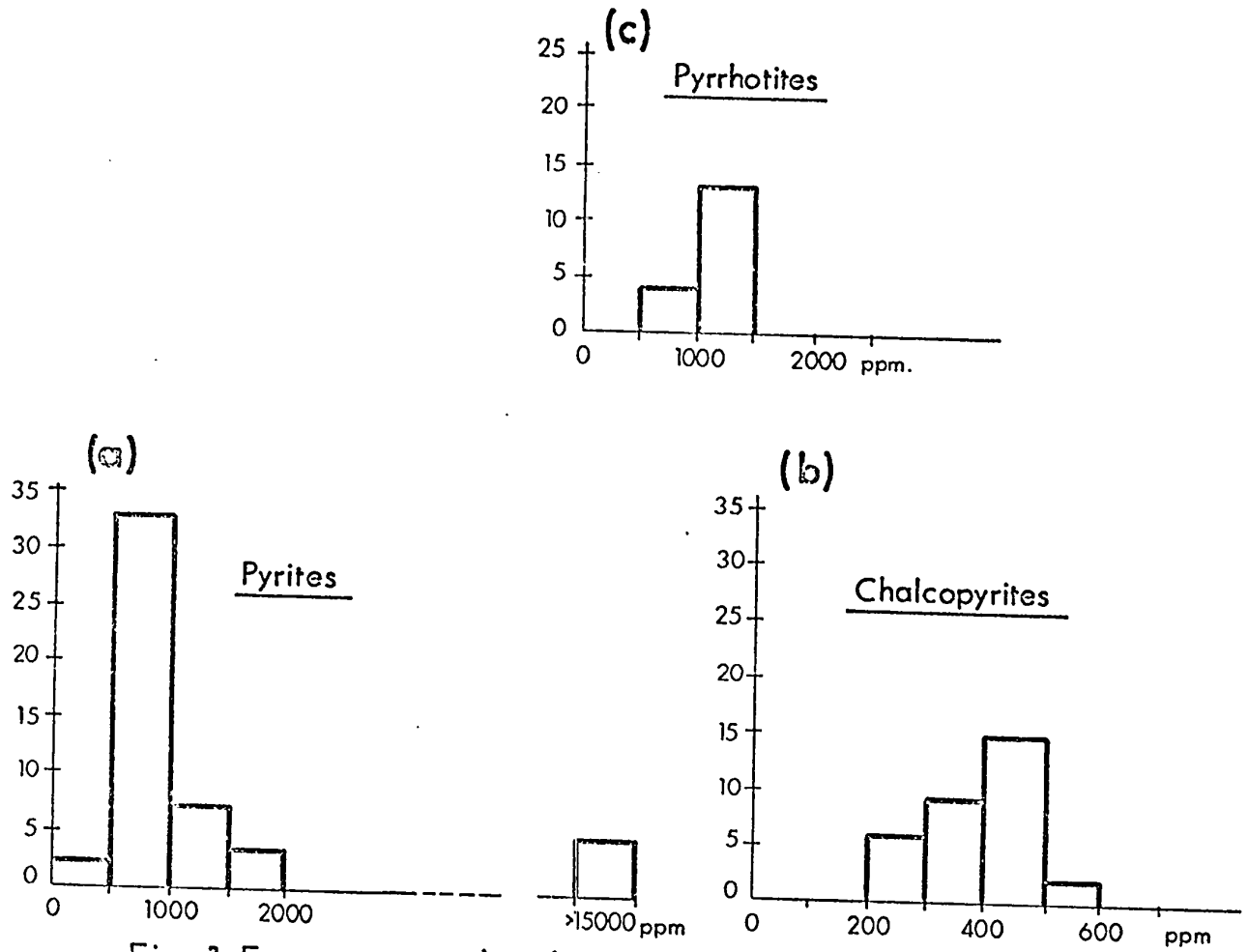

Fig. 1. Frequency distribution of Co concentrations

Results and Interpretation of the Co-Ni Analysis

Co results

Fifty analyses of cobalt were performed on pyrites, thirty-two on chalcopyrites and seventeen on pyrrhotites (see Appendix A-3 and A-4).

The concentration of cobalt in the pyrites ranges from 390 ppm to 27670 ppm. Three features of the frequency distribution of cobalt concentrations in pyrite (see Fig. 1a) are worth mention:

1. The frequency distribution shows a pronounced peak between 500 and 1000 ppm.
2. There is a discontinuity in the range of values: no intermediate Co concentrations are encountered between 2000 and 15,000 ppm.
3. Every analysis detected some hundreds of ppm of cobalt.

The observed high cobalt concentrations in pyrite conform with the type deposit to which the Kidd Creek deposit likely belongs. High cobalt values are exhibited by several pyrite-chalcopyrite ores of probable volcanogenic origin. The trace element composition and geological setting of the Kidd Creek deposit are in accordance; they both support a volcanogenic origin. Compared with other massive sulfide deposits of similar origin, the Kidd Creek deposit is characterized by high cobalt concentrations. The appearance of Co in a mineral of its own is also a manifestation of the very high Co content of the deposit as a whole. Among the Canadian massive sulfide deposits Noranda pyrites show the highest Co concentrations, ranging from 330 to 2850 ppm (Hawley and Nichol, 1961).

Excluding the very high (> 15000 ppm) values, pyrites from the Kidd Creek deposit exhibit a very narrow range of Co concentration with a variation of three times the minimum value. Other Canadian occurrences have a range between the minimum and maximum values which differ by one or two orders of magnitude.

The highest Co content of pyrite for the Kidd Creek deposit is 27670 ppm (Sample No. 15P) for disseminated pyrite occurring in andesitic host rock. Highest values found in massive sulfides are about 17000 ppm (Sample No. 1P and 17P'). Sample 1P is close to the andesitic hanging wall.

The lowest Co concentration is found in massive pyritic ore associated with an acidic tuff agglomerate (Sample No. II). Because of the narrow range of the distribution of Co concentrations, a statistically large number of analyses would be needed to establish a clearcut relationship between types of host rock and cobalt content of pyrites. It may be suggested that pyrites associated with rhyolites have a lower Co content than those coming from andesitic host rock. Samples 5P, 6P and 7P represent a section of the North part of the South orebody from the lower contact of the massive ore with the structural footwall (andesite) to the upper contact with the structural hanging wall (rhyolite). In this case pyrites from the massive ore in contact with the rhyolite have 100-200 ppm lower Co contents than those associated with andesite.

Disseminated pyrites from the graphitic schists have about the

same Co content as the average pyrites from massive sulfides. This would mean that these pyrites are not sedimentary in nature, but formed by the same volcanogenic processes as the massive sulfides. Disseminated pyrites from the shear zone between the North and South orebody have a similar Co content to that of the average pyrite from massive sulfides. No significant differences in Co content of pyrites from different types of ore could be found. Whether the pyrites come from disseminated types of ore or from different kinds of massive ore they always seem to have similar Co contents.

Cobalt content of chalcopyrites ranges from 200 to 590 ppm. The frequency distribution of Co concentrations in chalcopyrites (Fig. 1b) has three characteristic features.

1. Most frequent values are those between 400-500 ppm.
2. The distribution is characterized by a narrow range.
3. Every analysis detected some hundreds ppm of cobalt.

Compared with other massive sulfide deposits, these chalcopyrites have a high cobalt content. Among the Canadian massive sulfide deposits only Flin Flon has higher cobalt containing chalcopyrites (Hawley and Nichol, 1961).

There are no definite differences in the cobalt content of chalcopyrites of different ore types. Even minute inclusions of chalcopyrite found in the disseminated pyrites of the graphitic schists have similar Co content to that of massive or disseminated ores. There is also no clear correlation between Co content of chalcopyrites and type of host rocks.

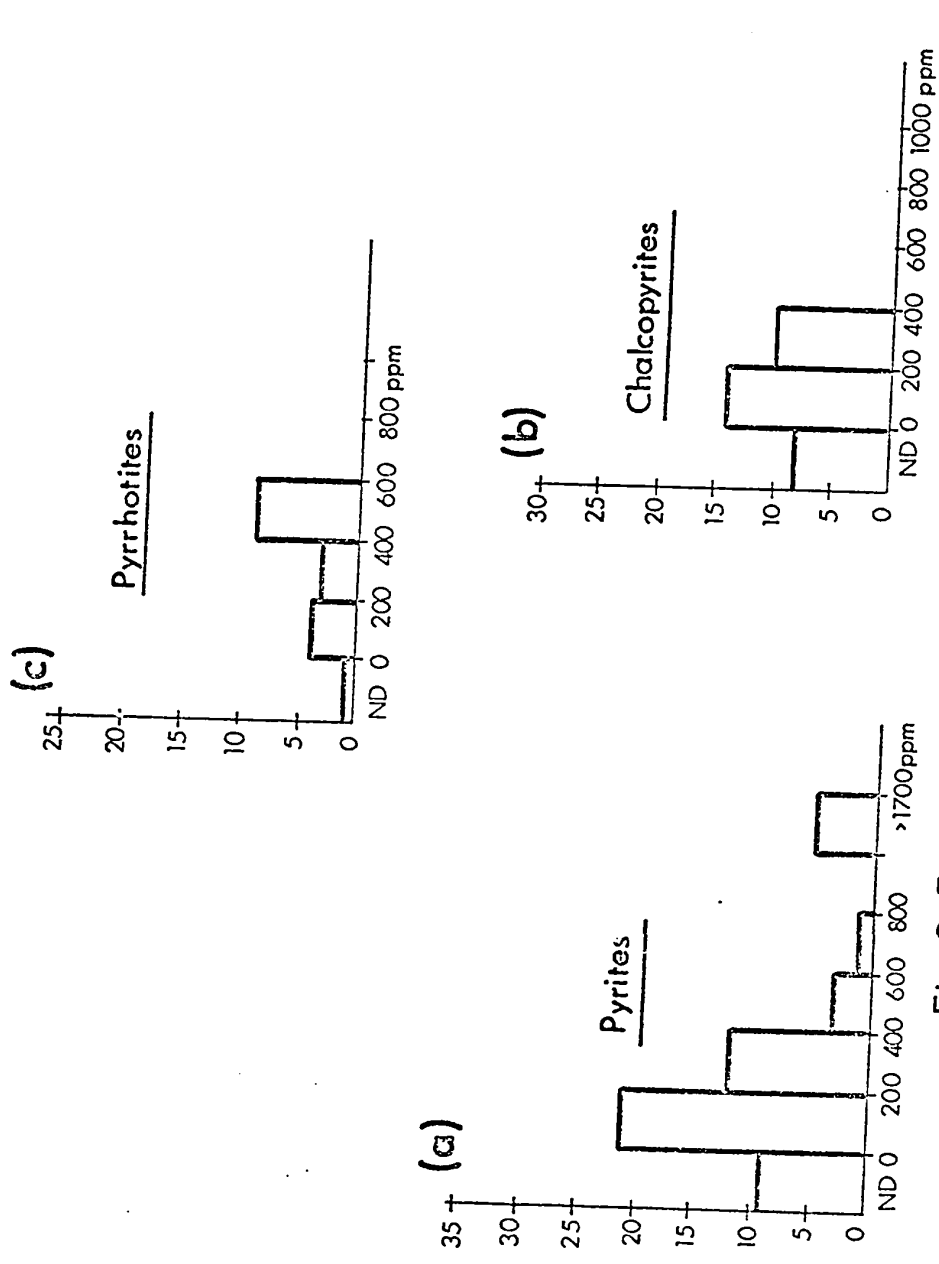

Fig. 2. Frequency distribution of Ni concentrations

The cobalt content of pyrrhotites ranges from 630 to 1380 ppm. The frequency distribution of Co concentrations (Fig. 1c) has the same characteristic features as that of the chalcopyrites, except that the most frequent concentrations are between 1000 and 1500 ppm. Compared with other deposits of the same type, these Co concentrations are high.

The lowest Co values encountered are from pyrrhotites associated with massive chalcopyrites in contact with the hanging wall (rhyolites) and from pyrrhotites of the shear zone, but again we cannot state whether or not there is a difference in Co content of pyrrhotites from different types of ore or host rock.

One analysis was made on cobaltite aiming to confirm the identity of the mineral (Sample 3P). First a spectral scan was made by the microprobe, to establish the qualitative composition. After detecting Co, Ni, S, As we measured Co and Ni. 35.24 weight % Co and 0.65 weight % Ni was measured, giving a formula of $(Co_{0.98} Ni_{0.02})$ As S.

Ni results

The same number of analyses for Ni were performed on pyrites, chalcopyrites, pyrrhotites as in the case of Co.

The concentration of nickel in the pyrites varies from the limit of analytical sensitivity (about 50 ppm) to 3830 ppm. The frequency distribution of the nickel content of pyrites is characterized by (Fig. 2a):

1. A pronounced peak between 0-200 ppm.

2. A relatively wide range of distribution.

The relatively low average nickel content of pyrites is in agreement with the literature data on other massive sulfide occurrences of probable volcanogenic origin. Pyrites from the Kidd Creek deposit, compared with other Canadian massive sulfide occurrences, are characterized by about the same average Ni content (e.g. Quemont and Noranda; Roscoe, 1965), but with a wider range of concentrations.

The highest analyzed nickel content is that of disseminated pyrites from the North orebody andesite sample (Sample No. 15P). It may be mentioned that the same sample also exhibited the highest Co content, but there is no general correlation between the Co and Ni values; high cobalt pyrite grains may have low Ni content and vice versa.

The highest Ni concentrations found in pyrites from the massive sulfide are about 1700 ppm (Sample No. 1P"). The lowest Ni containing pyrites from massive sulfides are associated with acidic host rocks (rhyolites, acidic tuff agglomerates), e.g. Samples 5P II and IV.

In this case there seems to exist a more definite relationship between nickel content and host rock. The trend of higher nickel content going from rhyolitic to andesitic host rock is clearly shown by samples 5P, 6P and 7P. This conforms well with the lower crustal abundance of Ni in acidic rocks than that of the intermediate or basic rocks. Disseminated pyrites from the graphitic schists fall into the same range of Ni content as pyrites from the massive ore,

except one sample (19P) which has high enough Ni content (630 ppm) for sedimentary pyrite. No significant differences in the nickel content of pyrites of different ore types could be found.

On the basis of Ni content we can again distinguish an early and a later generation of pyrite. The low nickel containing generation also has low cobalt content, and except for one case the high nickel pyrite generation has also high cobalt content.

The frequency distribution of nickel concentrations in pyrites is similarly characterized by a discontinuity as in the case of cobalt, but in this case the discontinuous concentration range is narrower (from 630 to 1700 ppm). A significant difference exists between the frequency distribution of Ni and Co content of the pyrites: in the case of Ni we have a much wider range of distribution.

The nickel content of chalcopyrites ranges from the limit of analytical sensitivity (some 10 ppm) to 310 ppm (Fig. 2b). The frequency distribution is characterized by:

1. A definite peak between 0-200 ppm Ni.
2. A wide range of distribution.

Compared with other Canadian massive sulfide deposits these chalcopyrites have a very high nickel content and a wide range of distribution (Hawley and Nichol, 1961). Chalcopyrites associated with rhyolitic host rock have the lowest Ni content. Disseminated chalcopyrites from graphitic schists have variable Ni content, but not out of the range of chalcopyrites from massive sulfides. No systematic differences were found in Ni content of different types of ore.

The concentration of Ni in the pyrrhotites ranges from the limit of analytical sensitivity (some 50 ppm) to 560 ppm (Fig. 2c). The frequency distribution of nickel content in pyrrhotites is similar to that of the chalcopyrites (wide range), but it has a less pronounced peak which is located at higher Co concentrations, between 400 and 600 ppm.

Compared with other Canadian deposits of the same type, these pyrrhotites have high Ni content. The relationship between the nature of host rock is similar in the case of chalcopyrites and pyrites. Pyrrhotites of massive sulfides associated with rhyolitic host rock have the lowest Ni content. Again, no systematic differences in the Ni content of different types of ores could be found.

Some relationship between the Ni content of sulfide minerals and the nature of the host rock has been established. In the case of Co any relationship is much more dubious. The lower Ni content of pyrites, chalcopyrites and pyrrhotites associated with rhyolitic host rock can be explained by:

1. Smaller abundance of Ni in these rocks.
2. The ore depositing solutions were equilibrated with the host rock, and solutions in equilibrium with rhyolitic host rock did not mix with solutions in equilibrium with andesitic host rock. Naturally, we can also visualize two pulses of ore fluids, the first was associated with rhyolitic volcanism, and the next was connected with andesitic volcanism.
3. Partitioning of Ni between the hydrothermal fluid and sulfide minerals and among the sulfide minerals did not conceal the host rock-

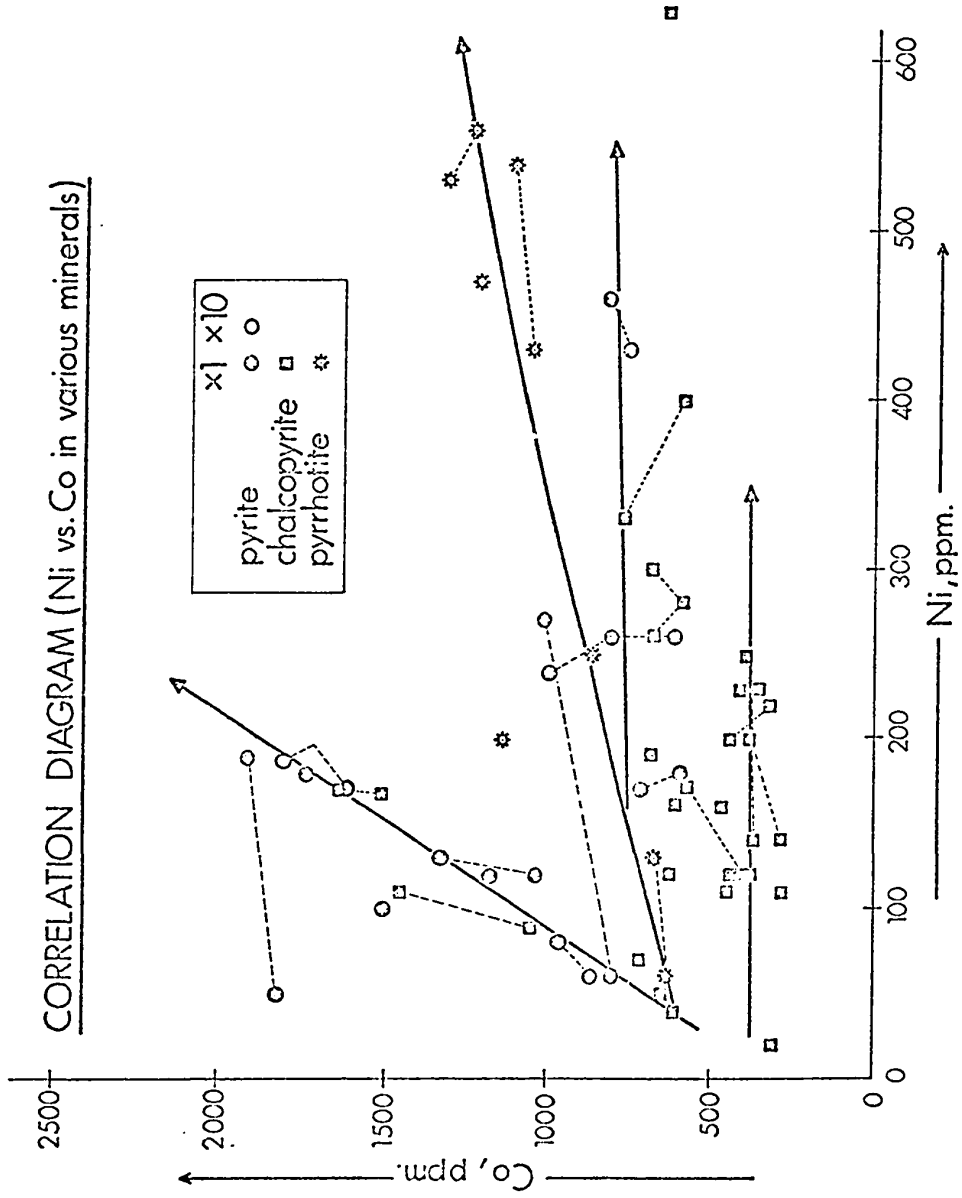
CORRELATION DIAGRAM (Ni vs. Co in various minerals)
×1 ×10
pyrite
chalcopyrite
pyrrhotite
Co, ppm.
Ni, ppm.
2500
2000
1500
1000
500
0
0
100
200
300
400
500
600

Figure 3.

sulfide-trace element relationship. An alternative explanation would be that there were different partitioning conditions at the base of mineralization (rhyolites) due to the different physical-chemical conditions.

The wide range of Ni concentrations can also be explained by one or both of the two alternatives; abundance of Ni, varying partitioning conditions.

There are two features common in the frequency distributions of Ni in pyrites, chalcopyrites and pyrrhotites.

1. They are all characterized by a wide range of values.
2. They all have a definite peak.

The frequency distribution of Ni in chalcopyrites and in pyrites (excluding the early pyrites) have a striking similarity regarding the magnitude of concentrations, position of peak, and shape of the curve. It would suggest that if there was any partitioning of Ni between these minerals it was very small regarding its magnitude. We can use the frequency distribution curves in judging the absence or presence of partitioning in sulfides. If the frequency distributions of the same element in different sulfides shows similar shapes, we can expect a well-defined partitioning of the trace element

Covariance of Co and Ni

In Fig. 3 a correlation diagram for Co and Ni in various sulfide minerals is plotted. We can postulate that if both elements have equilibrium partitioning and the Co/Ni ratio of the ore fluid stayed

at a relatively constant level, a parallel behaviour between Co and Ni in the various sulfide minerals can be expected. The reverse is not necessarily true; lack of parallel behaviour between Co and Ni does not inevitably imply lack of equilibrium partitioning for both of the elements because it may be that:

a) There is only surface equilibrium (zoning) for one of the elements, i.e. Co/Ni ratio of ore fluid can change drastically, while the domain of equilibrium is larger for the other element.

b) Co/Ni ratio of the ore fluid changes due to changes at the source.

c) Lack of correlation is caused by post-mineral changes, in which one of the elements is affected more than the other.

On the correlation diagram chalcopyrites and a few pyrites plot along a horizontal line with approximately constant Co and increasing Ni values. Equilibrium partitioning of Co between these pyrites, chalcopyrites and other minerals is not likely. Pyrrhotites and the majority of pyrites plotted on the correlation diagram exhibit similar behaviour between Co and Ni, indicating a possibility of equilibrium partitioning. Some pyrites plot along a line with slope (Co/Ni ratio) of about 10, while pyrrhotites plot along a line with slope of about 2 or 3. All the pyrites, chalcopyrites and pyrrhotites are characterized by Co/Ni ratios.between 1 and 10. The narrowest range of Co/Ni ratios is exhibited by pyrrhotites. The grouping of pyrites along two separate lines on the correlation diagram can imply the existence of at least two pyrite generations.

Despite the almost constant level of Co in chalcopyrites, the Co/Ni ratios are still high which imposes the question: what process (if not

equilibrium partitioning) are responsible for the high Co/Ni ratios in chalcopyrites?

As mentioned, high Co/Ni ratios are characteristic of pyrites of volcanogenic exhalative deposits. Loftus-Hills and Solomon (1967) attempted to make a subdivision of these types of ores on the basis of Co/Ni ratios of pyrites. From the preliminary results of these workers, pyrites of volcanic origin without accompanying Pb-Zn minerals have Co/Ni> 1 and those associated with Pb-Zn minerals have Co/Ni < 1. Our results are not in agreement with this finding; the Kidd Creek deposit is of the Pb-Zn rich subdivision with high Co/Ni ratios.

However, any application of ratio in elemental abundances has to consider the actual geological situation. The rate of volcanic to sedimentary contribution to the process of ore deposition is a basic geochemical factor if we are dealing with exhalative-sedimentary type deposits. Greater contribution from sedimentary sources should lower the Co/Ni ratio obscuring the normal volcanic trace element assemblage. On the other hand, the extremely high abundance of Pb and Zn in a volcanogenic exhalative deposit (the case of the Kidd Creek deposit) may mean a greater or exclusive volcanic contribution to the mineralization rather than sedimentary under special conditions accompanied by lesser volcanic-exhalative addition.

This way it may be thought that if the subdivision of volcanic exhalative deposits into pyritic and Pb-Zn rich types reflects some difference in their genesis, then the Pb-Zn rich types should have high Co/Ni ratio. Naturally, it is also possible that we cannot sub-divide these types of deposits by using elemental ratios and mineralogical

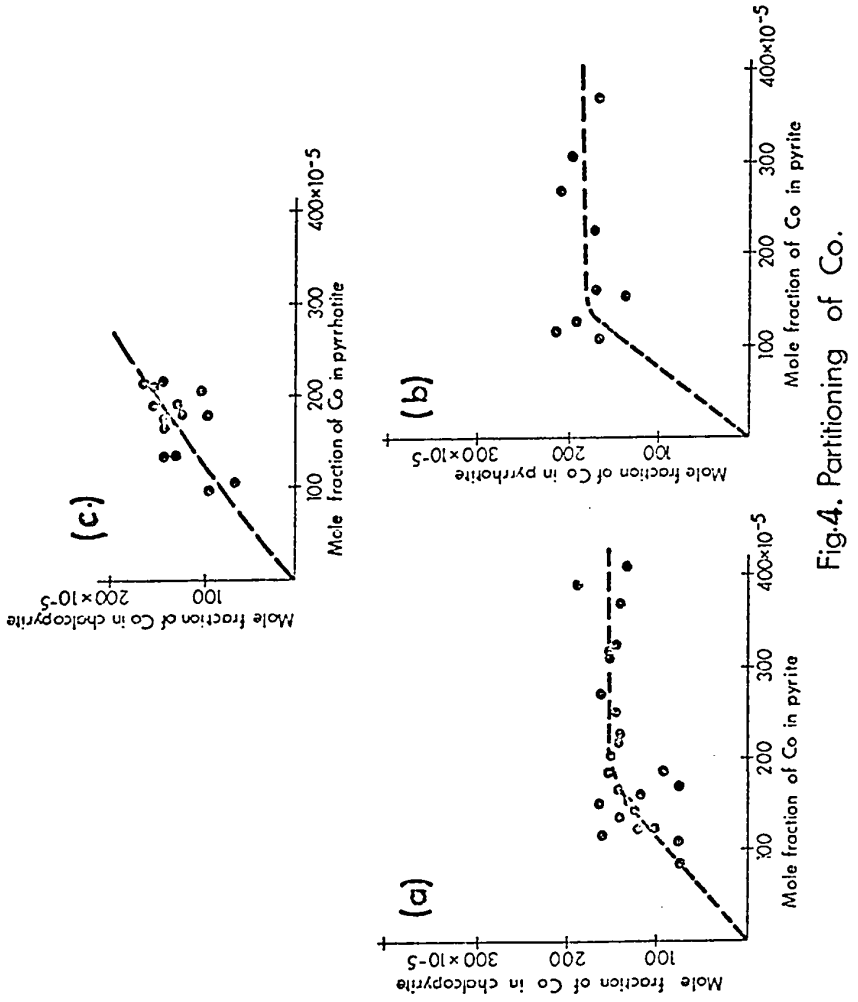

Fig.4. Partitioning of Co.

composition as the only criteria, because of the unrecognized factors causing the separation or parallel behaviour of trace and major components, or because of the different provenance for the trace and major constituents.

We also have to mention that pyrites and pyrrhotites from other Canadian massive sulfides of high Pb-Zn content have a similarly high or even higher Co/Ni ratio than pyrites and pyrrhotites of the Kidd Creek deposit (e.g. Noranda Mine; Hawley and Nichol, 1961). Further, it was shown (Sinclair, 1971) that in the Noranda deposit the No. 5 zone (a massive pyritic zone without economic Cu-Au mineralization) has about 100 times lower Co content in pyrites than the Cu-Au rich zones of the deposit.

Due to the consistent association of the massive sulfide deposits with acidic volcanics, the lower abundance of Ni versus Co can be expected (considering the ore depositing fluids have their source in these acidic volcanics) if solubility, partitioning and other chemical physical factors do not reverse their relative abundance during the deposition process. Some of these variables and their effect on the Co/Ni ratios will be discussed in detail in the section on partitioning.

Partitioning of Co

On Figure 4a the mole fraction of Co in pyrite against the mole fraction of Co in chalcopyrite is plotted. The curve on the diagram

represents a visual estimation of best fit. The partitioning of Co between these two phases follows a bilinear pattern. It can be seen on Figure 4a that at lower Co concentrations the curve is linear with a K_{Co}^{py-cp} slightly larger than 1. This means only a slight enrichment of Co in pyrite. Samples exhibiting constant content of Co are mainly disseminated pyrites, chalcopyrites from rhyolites, graphitic schists and from the shear zone. Few of the massive sulfides plot along the initial linear part of the partitioning curve.

Massive sulfides plot along the horizontal part of the partitioning curve, which is characterized by high Co concentrations (> 1000 ppm for pyrite and about 450 ppm for chalcopyrite).

The fact that above a certain Co concentration K_{Co}^{py-cp} increases with increasing N_{Co}^{py} and that K_{Co}^{py-cp} is no more the function of N_{Co}^{cp} (i.e. the Co content of pyrite is not a function of the Co content of chalcopyrite), implies the lack of equilibrium partitioning between the two minerals.

Two alternative explanations can be found:

1. Lack of coprecipitation for pyrite and chalcopyrite.
2. Pyrite and chalcopyrite were precipitated together but:
   a) above 450 ppm Co chalcopyrite was saturated with respect to cobaltite at the temperature of its formation;
   b) above 450 ppm Co chalcopyrite suffered a sudden increase in induced lattice point imperfections, due to increasing concentrations of Sn, In, etc.

It is hard to visualize that due to induced point imperfections or interactions of Co with other elements, the partitioning curve would

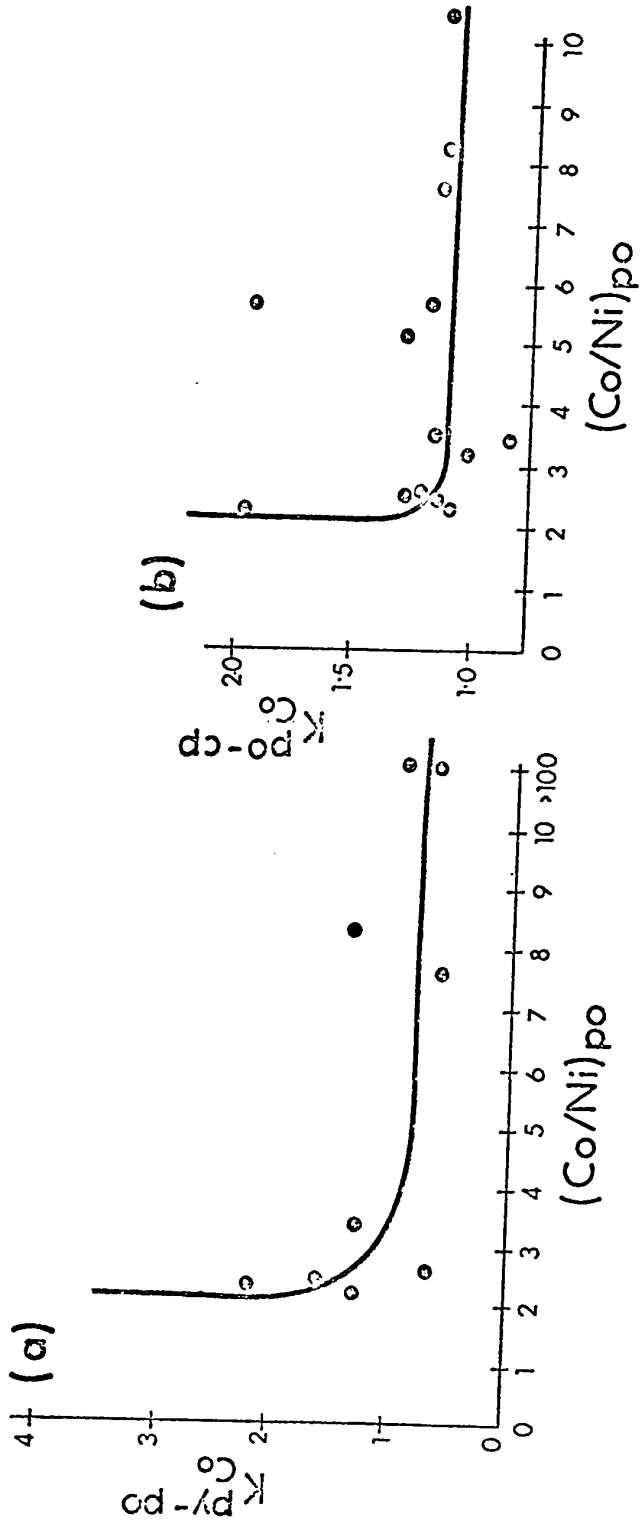

Fig. 5. Interaction plots for Ni.

exhibit so sudden a break, because all these effects must be built up continuously.

3. Diffusion of Co during diagenesis or following the deposition. The very narrow range of Co concentrations in chalcopyrite can also be a manifestation of Co diffusion.

Interaction plots for Ni and Zn against K_{Co}^{py-cp} and a concentration plot of K_{Co}^{py-cp} versus N_{Co}^{Cp} did not give a regular functional relationship.

Partitioning of Co between pyrite and pyrrhotite is represented on Figure 4b. The few data can be either taken as scattered distribution or as a saturation, in this case for pyrrhotite. On Fig. 5a we plotted K_{Co}^{py-po} against (Co/Ni)po and we obtained a hyperbolic type of function. (Co/Ni)po is the Co/Ni elemental ratio in pyrrhotite. At low Co/Ni ratios (between 2 and 3) K_{Co}^{py-po} changes exponentially, increases towards decreasing Co/Ni ratios. "Interaction" of Ni with Co in pyrrhotite has affected the distribution of Co between pyrite and pyrrhotite. Because $K_{Co}^{py-po} = \gamma_{Co}^{po}/\gamma_{Co}^{py}$, increasing K_{Co}^{py-po} with decreasing (Co/Ni)po means that at high Ni content (relative to Co) in the pyrrhotite the activity coefficient of cobalt in pyrrhotite (γ_{Co}^{po}) is increasing. Because the activity coefficient is an inverse measure of the ability of host phase to accommodate the minor component, this means a decreasing solubility of Co in pyrrhotite with increasing Ni content relative to Co, in agreement with our crystal chemical considerations made in the former chapter.

If we accept that an interaction plot indicates equilibrium

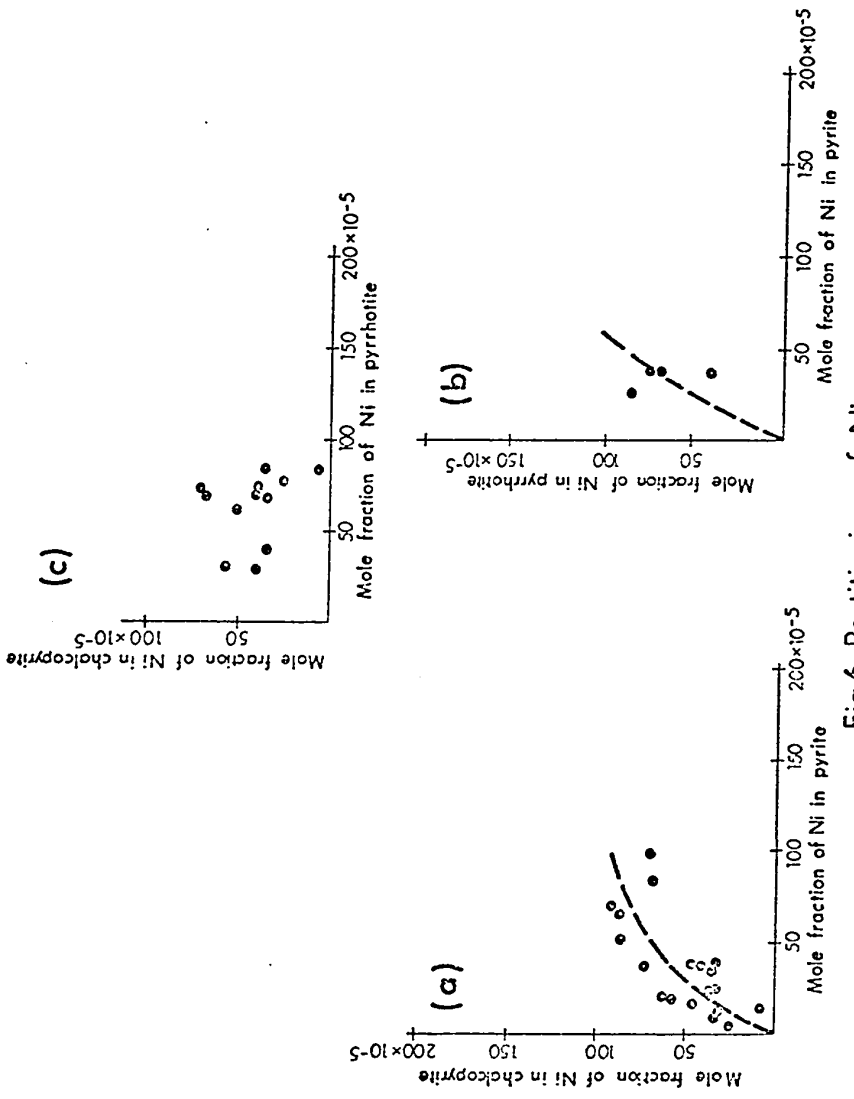

Fig.6. Partitioning of Ni.

partitioning, it can be stated that pyrite and pyrrhotite are in depositional or postdepositional equilibrium with each other. The partitioning coefficient describing the dilute "interactionless" system can be obtained from the interaction curve by extrapolating it to infinitely diluted concentrations of the interacting element (i.e. when the differential $dK_i^{A-B}/d(i/j)_{A \text{ or } B} = 0$). In our case at very high Co/Ni ratios K_{Co}^{py-po} is about 0.8.

On Fig. 4c a near linear partitioning of Co between chalcopyrite and pyrrhotite can be observed.

Interaction plot for Ni against K_{Co}^{po-cp} (Fig. 5b) revealed again that "interaction" of Ni with Co in pyrrhotite has affected the distribution of Co between pyrrhotite and chalcopyrite.

It is interesting to note that the (Co/Ni)po range where K_{Co}^{po-cp} starts to increase suddenly is again between 2 and 3, as in the case of the pyrite-pyrrhotite mineral pair. The K_{Co}^{po-cp} value extrapolated to high (Co/Ni)po values is about 1.2.

Partitioning of Ni

Partitioning of Ni between pyrite and chalcopyrite is of a curvilinear type as in the case of Co (Fig. 6a) with a significant scatter of the values. The major difference from the Co curve, is that chalcopyrite does not show a "saturation plateau" in regard to its Ni content. Extrapolating to zero concentrations, the curve has a slope (K_{Ni}^{py-cp}) of about 0.5 - 0.6. Interaction plots for Co and Zn against K_{Ni}^{py-cp} did not show any regular relationship, and

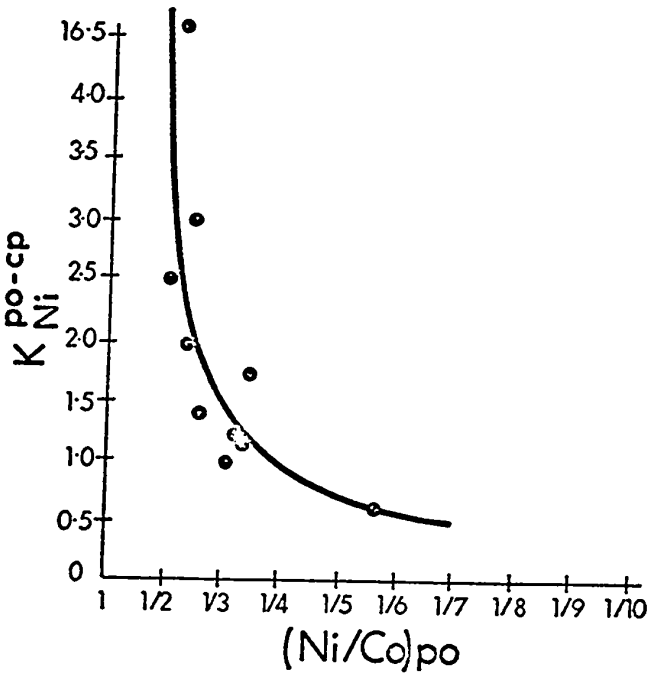

Fig. 7. Interaction plot for Co against K_{Ni}^{po-cp}

similarly the concentration plot of K_{Ni}^{py-cp} versus N_{Ni}^{cp} failed to reveal the reason for curvilinear distribution of Ni.

Partitioning of Ni between pyrite and pyrrhotite is plotted on Fig. 6b. Data are too limited to make an evaluation.

Partitioning of Ni between pyrrhotite and chalcopyrite is plotted on Fig. 6c. Figure 6c exhibits a random distribution of Ni between pyrrhotite and chalcopyrite. Despite the wide scatter of data, such was the case when we have the most clearcut interaction plots. Fig. 7 shows the interaction plot for Co against K_{Ni}^{po-cp}. At high (Ni/Co)po ratios (between 1.2 and 1/4) K_{Ni}^{po-cp} changes exponentially, increases towards increasing (Ni/Co)po ratios. Now the "interactor" cobalt has affected the distribution of Ni between pyrrhotite and chalcopyrite. In this case we have a decreasing solubility of Ni in pyrrhotite with increasing Co content relative to Ni. The K_{Ni}^{po-cp} partitioning coefficient obtained from the dilute Ni range of the interaction curve is about 0.5 - 0.6.

There is some difference between the interaction plots (Figs. 5 and 7). On the interaction plot for Ni versus K_{Co}^{py-po} or K_{Co}^{po-cp} the partitioning coefficient changes much more abruptly than in the case of interaction plot for Co

against K_{Ni}^{po-cp}, implying that the pyrrhotite lattice can take up less Ni than Co, in agreement with the crystal chemical considerations made in the previous chapter.

In summary it can be stated that the near unity partitioning coefficients (extrapolated or observed ones) for Co and Ni either indicate postdepositional homogenization of sulfide minerals by diffusion of Co and Ni, or partitioning at very high temperature.

Problems of Paragenesis

As mentioned before, we observed cobaltite (CoAsS) grains in some pyrites and chalcopyrites. Cobaltite is usually an early member of the paragenetic sequence preceding pyrite or coprecipitating with it. We feel that there are at least two generations of pyrite. The early generation was probably simultaneously or nearly simultaneously precipitated with cobaltite being more or less in equilibrium with it. This way these pyrites are characterized by very high (> 15000 ppm) Co content. The second and later generations of pyrite were formed after the deposition of cobaltite and all have similar Co content which does not exceed 2000 ppm, but they differ with regard to correlation between Co and Ni.

We think that the lack of cobaltite precipitation during the deposition of the later generations of pyrite is not due to the smaller availability of Co in the ore depositing fluid. We rather visualize a process in which the precipitation of cobaltite was superimposed on the continuous deposition of pyrite. When the mass of pyrite was formed (second or later generations) due to the high solubility of Co in pyrite, Co was taken up in solid solution by pyrites rather than precipitating as cobaltite.

Since this process would require the tailing off of the Co concentrations in pyrites, we should encounter not only high and low but also some intermediate Co values. Opposite to this expectation the frequency distribution of Co concentrations in pyrites shows a discontinuity in the values from 2000 to 15000 ppm.

There seem to be two alternative explanations:

1. The ore depositing fluid drastically changed its chemical composition
2. The two generations of pyrite were not deposited continuously one after the other; the pyrite deposition was interrupted by deposition of chalcopyrite. The later point cannot be proved by the Co and Ni content of chalcopyrites.

Partitioning between the Sulfide Minerals and the Ore Depositing Fluid

Because one of the possible interpretations of the observed Co-Ni distribution in the sulfide minerals is partitioning at very high temperature, in the following section, making use of the available experimental data on the partitioning of Co and Ni between a high

temperature aqueous fluid and precipitating cobaltiferous and nickeliferous pyrite, we attempt to gain some chemical information about the ore depositing fluid and to find an explanation for the high Co/Ni ratios of sulfide minerals at Kidd Creek.

Springer et al. (1964) hydrothermally synthesized $(Fe,Co)S_2$ and $(Fe,Ni)S_2$ from a high temperature (100-300°C) acidic aqueous solution (pH = 1 and a_{H_2S} = 0.1 mole/litre) introducing H_2S and sulfur into $FeSO_4$, $CoSO_4$ and $NiSO_4$ solutions of 0.1 mole/litre concentration.

By measuring the $N_{Fe}^{solution}/N_{Co}^{solution}$ and $N_{Fe}^{solid}/N_{Co}^{solid}$ ratios, the partitioning of Co between the fluid and the precipitated bravoite (cobaltian pyrite) is established. The same was done for Ni. They found that at 300°C $K_{Co}^{solid\text{-}fluid} = 16$ and $K_{Ni}^{solid\text{-}fluid} = 7$ which means that Co and Ni are highly enriched in the solid phase. Using these partitioning coefficients and the equation (for equilibrium situations):

$$\frac{N_{Fe}^{fluid}}{N_{Co\ or\ Ni}^{fluid}} = K_{Co\ or\ Ni}^{solid\text{-}fluid} \frac{N_{Fe}^{solid}}{N_{Co\ or\ Ni}^{solid}}$$

together with the measured composition of our pyrites, we can estimate the ratio of the concentrations of metal ions in the ore-bearing solutions. Taking an average pyrite with 1000 ppm Co content:

$$\frac{N_{Fe}^{fluid}}{N_{Co}^{fluid}} = 16\,\frac{99.8}{0.2} \simeq 8000$$

Taking an average pyrite with 200 ppm Ni content

$$\frac{N_{Fe}^{fluid}}{N_{Ni}^{fluid}} = 7\,\frac{99.94}{0.04} \simeq 17500$$

From these we can get the Co/Ni ratio of the ore bearing solution by dividing the two equations: Co/Ni ≃ 2.

Let us consider now what the extremely narrow range of Co content of the Kidd Creek chalcopyrites means in terms of partitioning against the ore fluid. To keep the mole fraction of Co in chalcopyrite N_{Co}^{cp} constant (in accordance with the narrow range of Co in chalcopyrites) it follows from the equation $K_{Co}^{cp\text{-}fluid} = N_{Co}^{cp}/N_{Co}^{fluid}$, that we either have to have both $K_{Co}^{cp\text{-}fluid}$ and N_{Co}^{fluid} to be constant or they have to vary systematically in order to keep N_{Co}^{cp} constant. It is hard to visualize that the change in Co content of the hydrothermal fluid was accompanied by a temperature change (change in K) resulting in a balanced situation with relatively constant N_{Co}^{cp}. To explain the near unity $K_{Co}^{po\text{-}cp}$ value (Fig. 4c) in terms of equilibrium partitioning of Co between chalcopyrite and pyrrhotite also requires the unlikely assumption: very constant partitioning condisitons at very high temperature. The same can be stated with regard to the observed distribution of Ni between pyrite and chalcopyrite.

Although the observed distribution of Co and Ni between pyrite, chalcopyrite and pyrrhotite is likely effected by postmineral changes, the overall higher abundance of Co than that of Ni is an original depositional feature. In the following the most important factors defining the relative abundance of Co compared to Ni are discussed.

To explain the strikingly similar and consistently high Co/Ni ratios in all of these minerals, the following equation has to be satisfied.

$$\text{Eq. I} \qquad \frac{N_{Co}^{fluid}}{N_{Ni}^{fluid}} \times \frac{K_{Co}^{solid\text{-}fluid}}{K_{Ni}^{solid\text{-}fluid}} > 1$$

which allows either a lower Co content of the fluid than that of Ni, or a smaller $K_{Co}^{solid\text{-}fluid}$ than $K_{Ni}^{solid\text{-}fluid}$ until their multiplication is > 1. The same must hold for all the solid phases (A, B, C etc.) present, if they partition only against the ore-bearing fluid. If mineral A and B partition also against each other

$$\text{Eq. II} \qquad \frac{K_{Co}^{A\text{-}B}}{K_{Ni}^{A\text{-}B}} \times \frac{N_{Co}^{B}}{N_{Ni}^{B}} > 1$$

also must be satisfied in order to have higher than 1 Co/Ni ratios in mineral A.

One way to satisfy Eq. I is to have $K_{Co}^{solid\text{-}fluid}$ values higher than $K_{Ni}^{solid\text{-}fluid}$ for all the three minerals (pyrite, pyrrhotite, chalcopyrite). It is likely that pyrrhotite and pyrite can take up more cobalt than nickel in solid solution, and it may be expected

that $K_{Ni}^{po\text{-}fluid}$ and $K_{Ni}^{py\text{-}fluid}$ are smaller than $K_{Co}^{po\text{-}fluid}$ and $K_{Co}^{py\text{-}fluid}$, respectively (experiments by Springer et al., 1964, support this assumption). On the other hand, crystal chemical considerations indicate higher solubility of Ni than that of Co in the chalcopyrite lattice. Thus, $K_{Ni}^{cp\text{-}fluid}$ may be larger than $K_{Co}^{cp\text{-}fluid}$.

Pyrite and pyrrhotite can also have high Co/Ni ratios partitioning against an ore-bearing fluid having somewhat higher Ni than Co content. Chalcopyrites can have high Co/Ni ratios only partitioning against an ore fluid having high Co/Ni ratio. If chalcopyrite is partitioned against pyrite or pyrrhotite, the conditions are more stringent; the ore fluid must have a very high Co/Ni ratio to balance out the Co enrichment in pyrite and pyrrhotite over chalcopyrite. It is likely that the magnitude of partitioning for the fluid versus mineral is larger for both Ni and Co than that of mineral A versus mineral B (see Eq. II) because the chemical potential difference between an aqueous complex and a solid phase is greater than between two solids. That is, the high Co/Ni ratio of minerals reflects the Co/Ni ratios of ore-bearing fluid in a qualitative way. Consequently, the changes of Co/Ni ratios likely reflect the changes in the fluid Co/Ni ratios. In this regard, changes in the physical nature (T,P) of ore fluid likely have a secondary effect on the mineral Co/Ni ratios, because both ratios $K_{Co}^{solid\text{-}fluid}/K_{Ni}^{solid\text{-}fluid}$ and $K_{Co}^{A\text{-}B}/K_{Ni}^{A\text{-}B}$ stay relatively constant with changing temperature due to the parallel changes of these partitioning coefficients. The constantly high Co/Ni ratios (> 1)

for the massive sulfides imply an open system for the process of mineralization, a more or less continuous supply of ore-depositing solution from the source.

It has been shown by Springer et al. (1964) that due to the lower solubility of Co in the aqueous sulfide solution than that of Ni and the fact that $K_{Co}^{py\text{-}fluid}$ is bigger than $K_{Ni}^{py\text{-}fluid}$, in a closed system where Rayleigh fractionation operates, early pyrites must be enriched in Co relative to Ni, while in late pyrites the reverse must be true. In our case the open system with a continuous supply of ore solution gives a higher rate of supply of Co to counterbalance the preferential removal of Co by the precipitating pyrites.

During the deposition of pyrite, iron is present in saturation amounts in the ore-depositing fluid. If Co and Ni were also present in saturation amounts, the Fe/Co and Fe/Ni and Co/Ni ratios in the fluid would be determined only by the relative solubilities. If a continuous supply of these elements is operative (i.e. we do not have a closed system), removal by the solid phase and partitioning do not effectively change the elemental ratios in the fluid.

Comparing the solubilities of Fe, Co and Ni mono- and disulfides in a_{H_2S} = 1 mole/litre solution at 300°C and pH = 1 (data from Springer et al., 1964), the solubility ratios for Co, Fe, Ni disulfides give Fe/Ni ≈ 10, Fe/Co ≈ 13, Co/Ni ≈ 0.8, so that Ni and Co were not present in saturation amounts. Solubility ratios for monosulfides also give the same result, although their order of magnitude ($Fe/Co \approx 10^3$) is bigger. This way it is highly probable

that if the metals were present in the solution as some kind of sulfide complexes, the solution was not saturated with Co and Ni.

Zoning in Pyrites

Chemical zoning in pyrites was not detectable by optical methods. Zoning was not apparent in many cases, even when coarse euhedral pyrites were analyzed with the electron microprobe. Some of the highest Co pyrites were selected and scanning X-ray pictures were made. The intensity of X-rays generated depends upon the concentrations of the element under examination. The relative brightness of different parts of the X-ray picture gives an indication of the relative concentration of the element. A definite zoning in the cobalt content of pyrite could be detected only in one case (the highest Co containing sample: 15P, disseminated pyrite from andesite).

Photograph 19 exhibits higher cobalt content at the centre of the 15P pyrite grain without a definite zonal arrangement. Photographs 20 and 21 show another pyrite grain from the same sample depicting the distribution of Co and Ni respectively. In this case cobalt shows a definite zonal arrangement; again the highest Co area is at the centre of the grain.

Photograph 21 exhibits a fairly even distribution of Ni in the same grain and zoning in the cobalt content was not followed by zoning in the nickel content. Pyrites from the massive sulfides do not have detectable zoning. Sample 1P, which is one of the highest

Co-containing pyrites from massive sulfide (1700 ppm Co), exhibits an even distribution of cobalt content on the X-ray photograph (Photograph 22). Brown and Bartholomew (1972) reported similar zoning in pyrite from a Zambian Cu-Co deposit, but opposite to this case, they found pyrites in which Ni presents a distribution paralleling that of Co. Springer et al. (1964) found that in synthetic $(Fe,Co)S_2$ crystallized from an acidic sulfide solution, the Co and Fe rich parts appear abruptly beside each other, while in $(Fe,Ni)S_2$ the zones are much less pronounced. In both the natural and synthetic assemblages the zoning was not uniform, some crystals show Co-rich internal zones with idiomorphic outlines, while others exhibit an irregular distribution of Co in the centre of the crystals.

Possible causes of zoning:

1. Changing value of the $K_{Co}^{py\text{-}fluid}$ partitioning coefficient with changing temperature.
2. Precipitation in a closed system with the progressive depletion of the chemical element less soluble in the ore fluid.
3. The ore depositing fluid changed its chemical composition due to changes in the source; i.e., we have an open system.

Springer found in his experiments that precipitation of pyrite in a closed system generates zoned crystals with Co-rich inner part. The rate of change of concentration depends on the amount precipitated and the magnitude of the $K_{Co}^{py\text{-}fluid}$ partitioning coefficient.

Due to the repeated appearance of Co-rich zones, even our disseminated pyrites from the andesitic host rock cannot be treated

as precipitates of a perfectly closed system, but in a shorter time interval (introduction of a new flood of the ore solution) the precipitation of pyrite can approximate a closed system type of crystallization. The X-ray picture (Photograph 20) of the zoned pyrite shows that after the precipitation of the central zone richest in Co, all the later Co-rich zones have a lower Co content compared to that of the core and are characterized by a smaller concentration gradient going from a Co-rich core towards a Co-poor rim. This implies that the removal of Co was dominant over the Co supply as the crystallization proceeded, so that it approaches closed system precipitation. We also have to mention another possible evidence of closed system precipitation in the case of disseminated pyrites. Only one pyrite grain was found to have a Co/Ni ratio lower than one. This pyrite comes from the same sample (15P) of disseminated pyrite as the zoned high Co pyrites. This low Co/Ni ratio can be expected on a theoretical ground (solubility and K values) in a closed system for late pyrites precipitating as the last, residual fraction. Now if we have a closed system and we consider that the zoning in Co content was not accompanied by a zoning in the Ni content, we can deduce the relative magnitude of $K_{Co}^{py\text{-}fluid}$ and $K_{Ni}^{py\text{-}fluid}$.

The high concentration gradient for Co and the very small gradient if any for Ni (see X-ray Photographs 20 and 21) implies a much bigger $K_{Co}^{py\text{-}fluid}$ than $K_{Ni}^{py\text{-}fluid}$ partitioning coefficient in agreement with the experimental results of Springer et al. (1964).

The absence of evident zoning in pyrites and of massive sulfides

can be either explained by open system precipitation with more perfect attainment of equilibrium at least on a hand specimen scale or by recrystallization and homogenization under metamorphic conditions (Bartholomew, 1972). Since overall evidence of recrystallization of the sulfides is absent, diffusion of Co following the deposition of ore is another feasible explanation.

Summary of the Genesis, Paragenesis, Equilibrium and Partitioning based on the Interpretation of the Co, Ni Analytical Data

1. Abundances of Co and Ni as well as the Co/Ni ratios of the sulfide minerals conform to the type of deposit and its geological environment and support a volcanogenic exhalative origin.
2. Based on the abundance of Co and from the Co/Ni ratios, three pyrite generations can be distinguished. The paragenetical position of pyrite and chalcopyrite cannot be clarified on the basis of Co, Ni data alone.
3. The near linear distribution of Ni between pyrite and chalcopyrite and that of Co between pyrite and pyrrhotite with K_{Co} and K_{Ni} values close to unity can either indicate tendency to equilibrium partitioning at very high and relatively constant temperature without a drastic change in the trace element composition of the ore fluid, or postdepositional homogenization (diffusion) of sulfide minerals.

It is not likely that chalcopyrite is saturated with Co above the 450 ppm level, particularly since the temperature of deposition

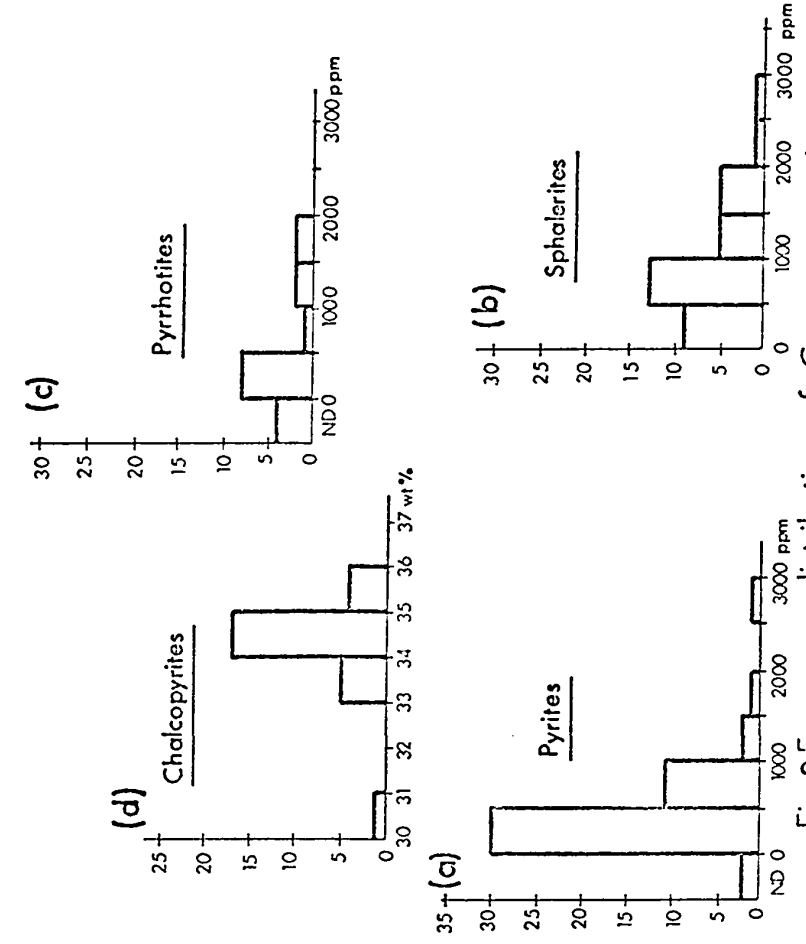

Fig.8.Frequency distribution of Cu concentrations

is high. Thus, the nature of the Co, Ni distribution is better explained by postdepositional effects. In this regard the degree of homogeneity of Co and Ni concentrations in the sulfide minerals would incidate that pyrites are affected the least and chalcopyrites the most in these postdepositional diffusion processes.

4. The zoned pyrites exhibiting original, depositional distribution of Co and Ni indicate, by and large, a closed system precipitation for the disseminated pyrites and a higher $K_{Co}^{py\text{-}fluid}$ than $K_{Ni}^{py\text{-}fluid}$ partitioning coefficient in agreement with experimental data on synthetic sulfides. From these experimental data and data on the Co/Ni ratios of pyrites, it follows that there was likely a somewhat higher concentration of Co than Ni in the ore-depositing fluid.

Results and Interpretation of the Cu-Zn Analysis

47 analyses of pyrite, 17 pyrrhotite, 27 chalcopyrite and 34 sphalerite were made for both Cu and Zn (see Appendix A 5-7).

The concentration of Cu in the pyrites ranges from the limit of sensitivity (some 50 ppm) to 2500 ppm (Fig. 8a). The frequency distribution has a pronounced peak between 0 and 500 ppm and it is asymmetric towards high Cu concentrations. Comparing our analytical data with literature data, these pyrites are characterized by a very low copper content. In his comprehensive review Fleischer (1955) reported that 10% of the total Cu analyses on pyrites had Cu concentrations of more than one weight percent. Frenzel and

Ottemann (1967) analyzed zoned pyrites by electron microprobe from Nukundamu, Fiji, which had up to 10 weight percent Cu, apparently in solid solution. This means that pyrite can take up almost as much Cu as Co in solid solution. The difference of an order of magnitude between the maximum Cu and maximum Co contents of the Kidd Creek pyrites also implies low level of Cu, perhaps prohibitive for an equilibrium coprecipitation between pyrite and chalcopyrite (i.e. for saturation of pyrite in regard to Cu). On the other hand, it was found that the ore type (mineralogical composition) establishes the Cu content of pyrites. Massive pyritic and sphaleritic ores with only traces of chalcopyrite have pyrites of the lowest Cu content (about 100 ppm). Disseminated pyrites from both the hanging wall and footwall are also characterized by very low Cu content. In this case again, chalcopyrite is absent or present only in form of microscopically small inclusions. Pyrites of highest Cu content (1000 ppm or more) are from chalcopyrite ores. The contradiction that although pyrite is not saturated with Cu (no equilibrium coprecipitation for pyrite and chalcopyrite) while pyrites coexisting with chalcopyrite have higher Cu content than those coexisting with other sulfide minerals can be resolved by assuming:

1. Coprecipitation of pyrite and chalcopyrite with only partial attainment of equilibrium.

2. Pyrites coexisting with chalcopyrite paragenetically preceded or followed chalcopyrite deposition at times when the ore depositing fluid was high in Cu content.

Arguing against the first alternative, even in the case of partial attainment of equilibrium, we should have much higher Cu content, close to that permitted by the FeS_2-$CuFeS_2$ binary at the temperature of deposition. In this regard there should be no difference where chalcopyrite is present only in trace amount, or when it makes up the bulk of the sulfides. On the contrary, high Cu pyrites usually are associated with massive chalcopyrite ore. These considerations suggest that diffusion of Cu in the solid state might have been operative. Within the temperature range of ore deposition the rate of diffusion of metal ions through sulfides is appreciable (Gill, 1960). Naturally this does not exclude the possibility that high Cu pyrites were partitioning against an ore fluid of higher Cu content and/or of lower temperature.

It is of interest to compare the minimum concentrations of Cu with that of Co and Ni. Despite the fact that Co and Ni were only trace constituents in the ore fluid during almost all of its history, every analysis of pyrite detected some hundred ppm of Co or Ni while in some pyrite the Cu content was below the analytical sensitivity. If the difference in partitioning conditions was inoperative, at certain stages of the ore fluid the abundances of trace metal constituents in the fluid was higher than that of Cu, which is a major element of the deposit.

The concentration of Cu in sphalerites exhibits exactly the same range as in the pyrites. The frequency distribution (Fig. 8b) has a peak between 500 and 1000 ppm, with the most abundant Cu

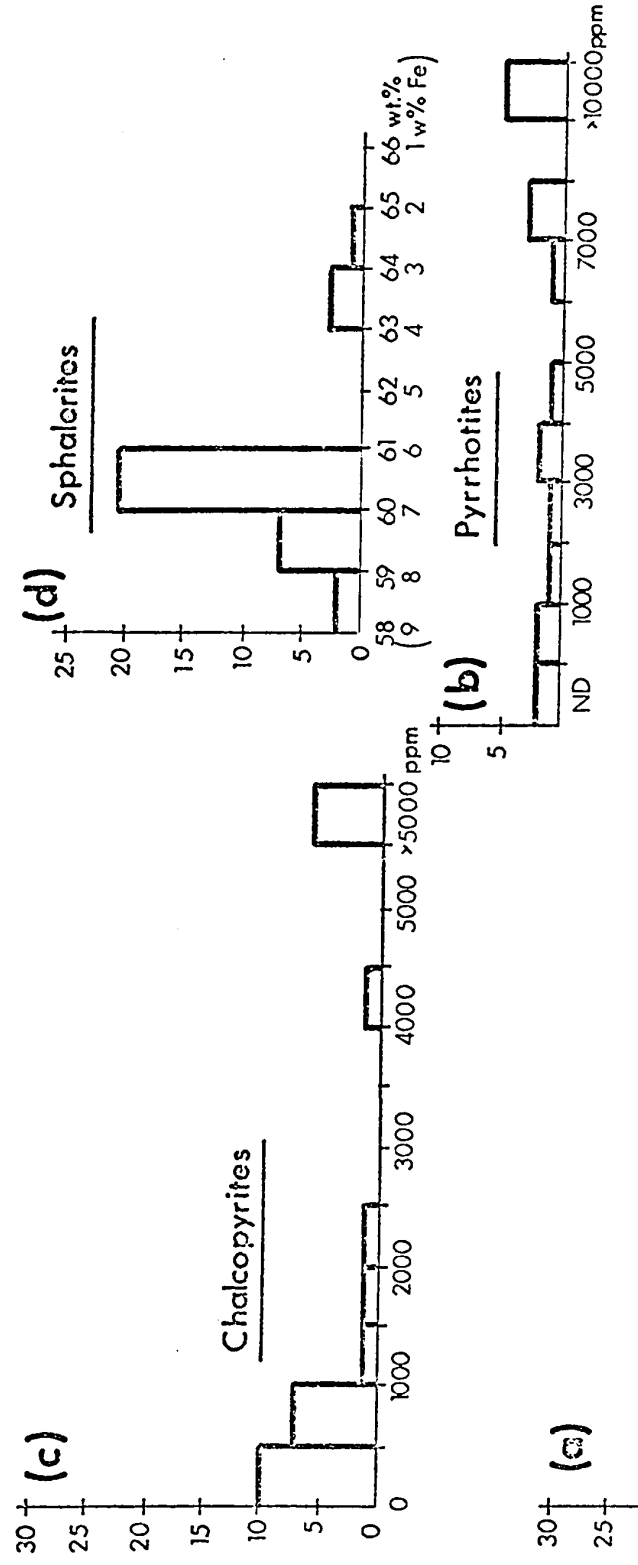

Fig. 9. Frequency distribution of Zn concentrations

concentrations shifted towards a higher concentration range compared with pyrites. Lack of analysis of Cu from sphalerites of volcanogenic sulfides hinders the comparison. Data on sphalerites of other deposit types suggests that the Kidd Creek sphalerites are low in copper. As in the case of pyrite, no relationship was found between the nature of host rock and abundance of Cu. On the other hand, it was found that mineralogical composition determines the Cu content of sphalerites. In general the presence of abundant chalcopyrite coincides with high Cu content in the sphalerites.

The concentration of Cu in pyrrhotites ranges from the limit of analytical sensitivity to 2000 ppm. The frequency distribution of Cu concentrations of pyrrhotites (Fig. 8c) is very similar to that of the pyrite and sphalerite copper frequency distribution.

No correlation was found between the nature of host rock and Cu content of pyrrhotites. Pyrrhotites from massive sphalerite or pyrite usually have low Cu content, those from massive chalcopyrite may have either high or low Cu content. In this case the relationship between mineralogical composition and Cu content of pyrrhotite is not pronounced.

The concentration of Zn in the pyrites ranges from the limit of the analytical sensitivity to 17720 ppm. The frequency distribution of Zn concentrations in pyrites (Fig. 9a) is U-shaped with two definite peaks at 0-500 ppm and above 5000 ppm. The minimum frequency range of Zn concentrations is not continuous but the discontinuity is small enough to be attributed to the insufficient

number of analyses rather than other factors such as paragenesis and partitioning.

It has been found again that mineralogical composition determines the chemical composition of pyrite, while there is no relationship with the nature of host rock. Disseminated pyrites from the hanging wall, footwall, and from the graphitic schist, together with pyrites from massive chalcopyrite, are the lowest in Zn.

All these samples had only traces of sphalerite, or none at all. Pyrites from massive sphalerite had the highest Zn content. Compared with literature data, these pyrites have a relatively high Zn content. Fleischer (1955) stated that out of all the Zn analyses of pyrite reported in the literature, only about 10% showed higher Zn concentrations than one weight percentage. Unfortunately there is no data on massive sulfides for comparison.

In examining pyrites associated with sphalerites, a very clear relationship was established between the textural and chemical properties, which further clarified some aspects of the mineral paragenesis. It has been shown by many investigators that precipitated sulfides can be redissolved by the ore depositing solutions, if the solutions become undersaturated with respect to the mineral leached. There are textural features of the Kidd Creek pyrites suggesting that this process was operative during the deposition. Texturally two different types of pyrites are present in the massive sphaleritic ores: coarse euhedral or subhedral pyrite and fine-anhedral pyrite. The coarse subhedral pyrites included

in sphalerite exhibit small rounded indentations or large embayments up to the extent of the lack of any idiomorphism. Pyrites with these scalloped outlines can be taken either as having a relict texture resulting from the redissolution of earlier pyrites by the later, sphalerite depositing solutions, or they can be interpreted as the products of simultaneous, equilibrium coprecipitation with sphalerite. In the latter case precipitation or dissolution of pyrite was the operative depending on the physical, chemical nature (T, P, fS_2, a_{FeS}) of the sphalerite depositing solution. In terms of paragenesis it means that these pyrites either crystallized before or during the sphalerite deposition and consequently they must differ in their Zn content if a certain degree of chemical equilibrium was attained during the deposition.

It has been found, analyzing these pyrites by the microprobe, that except in one case out of 12, subhedral pyrites with scalloped outline are characterized by a very high Zn content (above 5000 ppm) thus providing clear evidence of equilibrium coprecipitation between these pyrites and sphalerites.

Quantitatively these subhedral, scalloped pyrites are minor compared to the coarse euhedral pyrites, and even a smaller fraction of all the pyrites coexisting with sphalerite. Because relict pyrite textures are extremely rare, there was no appreciable leaching of pyrite by the sphalerite depositing solution, so that these solutions were also in equilibrium with the former generation of pyrite. More precisely, the solution at that particular temperature, pressure and fugacity of sulfur was saturated with FeS. Considering

the level of Zn (500-2000 ppm) found in coarse cubic pyrites included in sphalerite, these pyrites can either be formed before or after sphalerite when the ore solution was still high in Zn, but their idiomorphism definitely favours a pre-sphalerite age of crystallization.

As we mentioned before, Stanton (1960, 1964) concluded that sulfide minerals of stratiform volcanic ores are not deposited in a paragenetic (time) sequence, but rather the textures represent low temperature segregation during crystallization of an amorphous or cryptocrystalline sulfide mixture. On the basis of Co content alone, pyrites of the Texas Gulf deposit exhibit two distinct generations: an early and a late one. The late, low Co pyrites can be subdivided into two generations from their Zn content, and their paragenetical position compared to sphalerite can be determined. The chemical and textural evidence strongly favours the existence of a sequence of ore deposition at Kidd Creek.

The concentration of Zn in the pyrrhotites ranges from a few tens of ppm to 12870 ppm. The frequency distribution of Zn concentrations in pyrrhotites (Fig. 9b) has no pronounced peak, although it has some resemblance to the pyrite curve (Fig. 9a). Zn content of pyrrhotites depends on the mineralogical composition of the ore, and has no connection with the nature of the host rock. Pyrrhotites from massive sphalerites have the highest Zn content, while pyrrhotites from disseminated pyrite and from massive chalcopyrite are the lowest in Zn. Compared with other massive

sulfides, these pyrrhotites have high Zn content. Auger (1942) reported a relatively constant level of Zn (about 1000 ppm) from the Noranda pyrrhotites. A relationship between texture and chemical composition (as in the case of pyrites) was sought for pyrrhotites.

The rounded or shapeless blebs of pyrrhotite included in sphalerite are commonly believed to be a product of exsolution. These pyrrhotite blebs usually, but not invariably, exhibited a high content of Zn. A statistical study with high number of measurements would be necessary to prove or disprove the correlation between texture and chemical composition of pyrrhotites. In an ideal exsolution texture the exsolved phase is arranged along certain crystallographic directions of the host mineral. This cannot be recognized in this case, but it can happen that pyrrhotite inclusions of other origin (simple coprecipitation with sphalerite) and similar shape located at the sphalerite grain boundaries can mask any possible exsolution texture. The problem of exsolution will be discussed in more detail in relation to chalcopyrites. It is obvious from the chemical analysis that pyrrhotite coexisting with sphalerite represents a more or less equilibrium mineral pair.

The concentration of Zn in chalcopyrites ranges from the limit of analytical sensitivity (few tens of ppm) to 17150 ppm. The frequency distribution of Zn concentrations in chalcopyrites (Fig. 9c) is U-shaped with two peaks at 0-500 ppm and above 5000 ppm. There is a strong similarity between the frequency distribution of Zn in pyrite and in chalcopyrite. By and large the mineralogical composition

of the ore exhibits connection with the Zn content of chalcopyrites. Chalcopyrites from massive sphalerite are high in Zn, but some of the massive chalcopyrites still containing substantial amounts of sphalerite are low Zn chalcopyrites. Compared with literature data some of these chalcopyrites have very high Zn content. Fleischer cited analytical data from the literature on the Zn content of chalcopyrite with a maximum of one weight percent. Although the number of analyses does not allow us to make a generalization and the Zn analysis did not give an unequivocal answer, it seems that chalcopyrite blebs included in sphalerite with textures perhaps indicative of exsolution, usually have a very high Zn content.

Difficulties arose again in defining exactly which texture is indicative of exsolution and which one resulted from equilibrium coprecipitation with sphalerite. The first point which had to be clarified was whether or not this high Zn content in pyrrhotite and chalcopyrite is present in solid solution and whether or not these "exsolution blebs" have any compositional changes with respect to Zn. With the help of X-ray photographs it has been proved that Zn is present in solid solution in these pyrrhotites and chalcopyrites containing very high zinc values. The X-ray photographs did not detect any compositional changes within the "exsolution blebs" of pyrrhotite and chalcopyrite resulting from exsolution lamellae formed at different temperatures, so the existence of exsolution cannot be proved, but on the other hand, lack of exsolution lamellae is not an exclusive evidence against exsolution because these lamellae may

or may not be present in an exsolution product, depending mainly on the cooling history and surface tension of the exsolved phases.

X-ray photographs 23 and 24 are of a pyrrhotite bleb in sphalerite and depict the distribution of Zn and Fe within and around the pyrrhotite. If the exsolved phase (pyrrhotite) was only in surface equilibrium with the solvent phase (sphalerite) a halo with decreased content of the element (iron) extracted by the exsolved phase could be detected around the exsolved phase. On the other hand, both Fe and Zn in both the surrounding sphalerite and in the pyrrhotite inclusion exhibit a fairly even distribution. X-ray photograph 25 is a magnified image of the upper left part of the same pyrrhotite inclusion depicting the iron distribution at the sphalerite-pyrrhotite boundary. The diffuse distribution of iron at the sphalerite-pyrrhotite boundary can be interpreted as an equilibrium case for the two minerals, with a larger domain than that of a surface equilibrium. But again we do not have exclusive evidence against exsolution; it may well be the case that diffusion of iron and zinc in the solid phases homogenizes both the "solute" and "solvent", and gives rise to diffuse phase boundaries.

X-ray photographs 26 and 27 represent the Cu and Zn distribution within the chalcopyrite inclusion and in the surrounding sphalerite. The only definite conclusion is that the Zn is present in solid solution in the chalcopyrite.

In summary, it can be stated that both Cu and Zn content of sulfide minerals more or less showed relationship with the bulk mineralogical composition of ore suggesting that the diffusion of Cu

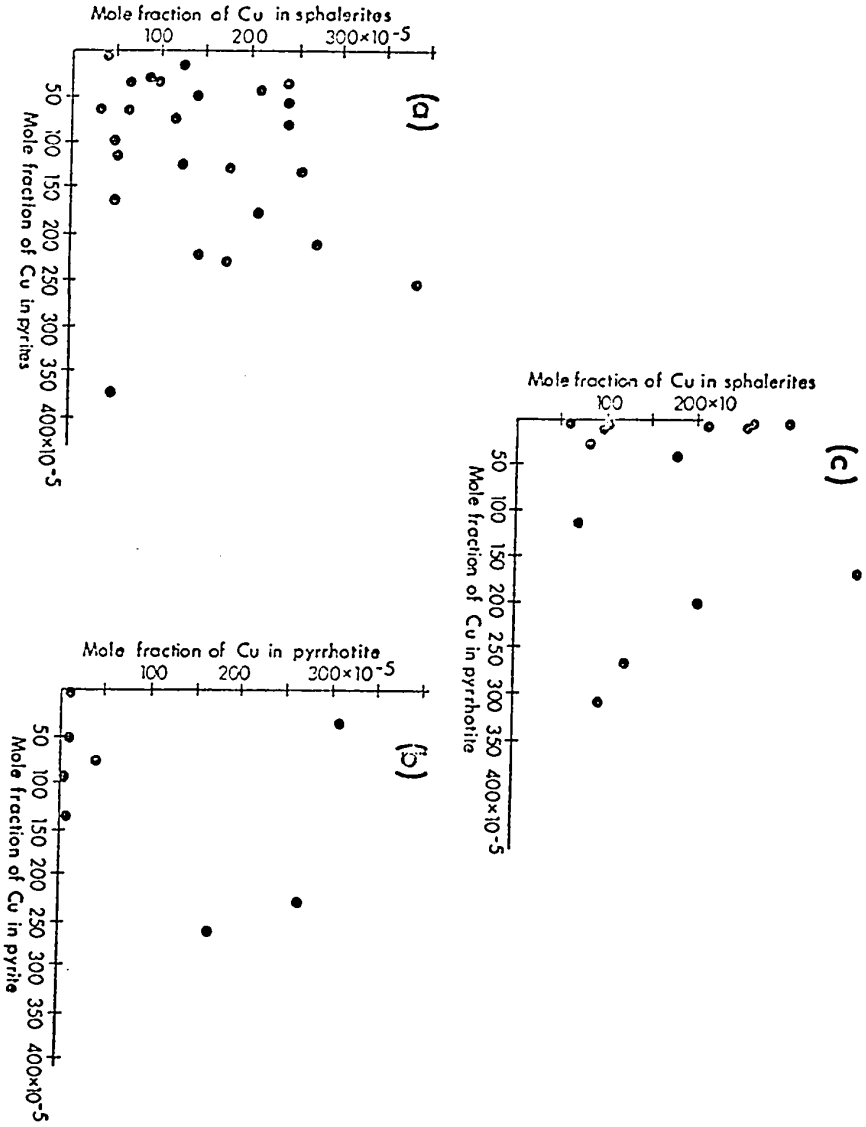

Fig.10. Partitioning of Cu.

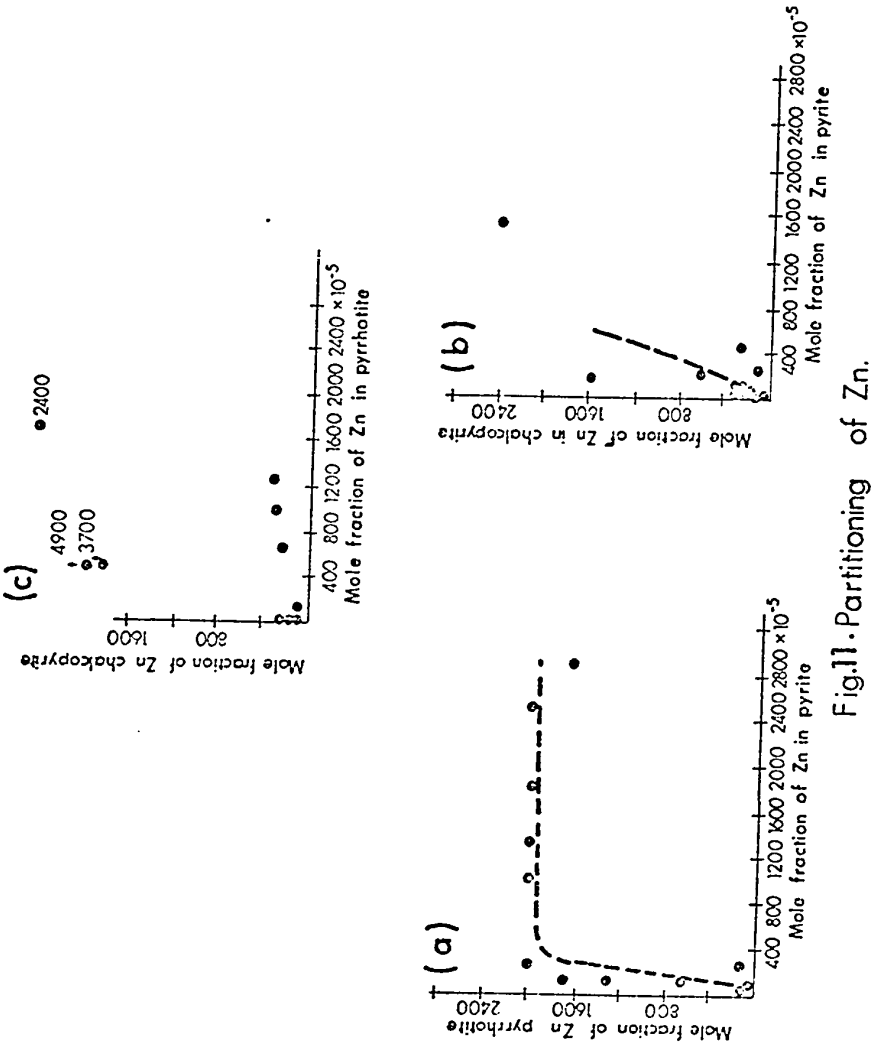

Fig.11. Partitioning of Zn.

and Zn through solid phase affected the original chemical composition. It has to be emphasized that solid state diffusion has only affected but did not erase the original chemical composition of minerals (e.g. pyrites are not homogenized, scalloped pyrites have distinctly high Zn content).

As secondary information, due to the simultaneous measurements of Cu and Zn, we also obtained data on the Cu content of chalcopyrites. They usually have stoichiometric amounts of Cu (Fig. 8d). Low Cu content is followed by high Zn content in almost every case.

Partitioning of Cu and Zn between the sulfide minerals

On Fig. 10a, b, c are plotted the mole fraction of Cu in pyrite-sphalerite, pyrite-pyrrhotite and pyrrhotite-sphalerite, respectively. In all three cases we have a scattered type of partitioning pattern.

Figures 11a, b and c represent the partitioning of Zn between pyrrhotite-pyrite, chalcopyrite-pyrite and chalcopyrite-pyrrhotite. The partitioning is of the discontinuous type for the pyrrhotite-pyrite mineral pair and scattered for the chalcopyrite-pyrite and chalcopyrite--pyrrhotite mineral pairs. (In the latter case there may be a curvilinear distribution of Zn, but there is not enough data to draw a definite conclusion).

The scattered type partitioning patterns for Cu and Zn can be explained by either coprecipitation of sulfides without attainment of equilibrium or by postdepositional changes affecting the

distribution of Cu and Zn. Since both elements show a relationship with the bulk mineralogical composition (amount of chalcopyrite or sphalerite) postdepositional diffusion of Cu and Zn is the more feasible explanation.

On Fig. 12a depicting the distribution of Zn between pyrite and pyrrhotite, pyrrhotites from massive sphaleritic ore plot along the horizontal part of the curve. The high and reasonably constant Zn content of these pyrrhotites can best be explained by postdepositional diffusion of Zn from sphalerite to pyrrhotite. Saturation of pyrrhotite with Zn at this (2000 ppm) concentration level is not likely since several analyses indicated more than 1 weight % Zn in pyrrhotite. The Zn distribution between pyrrhotite and pyrite in the low Zn concentration range is not scattered and shows a definite enrichment ($K_{Zn}^{po-py} \simeq 6$) of Zn in pyrrhotite (no homogenization of the two minerals). Therefore, an original, depositional distribution of Zn with tendency to equilibrium rather than a later, diffusional distribution is the better interpretation.

Summary of the Paragenesis, Equilibrium and Partitioning based on the Interpretation of the Cu-Zn Analytical Data

1. Based on the abundance of Zn it is possible to discriminate between two pyrite generations which do not coincide with the high and low Co pyrite generations. There is a pronounced relationship between textural features of pyrite simultaneously deposited with sphalerite and its Zn content.

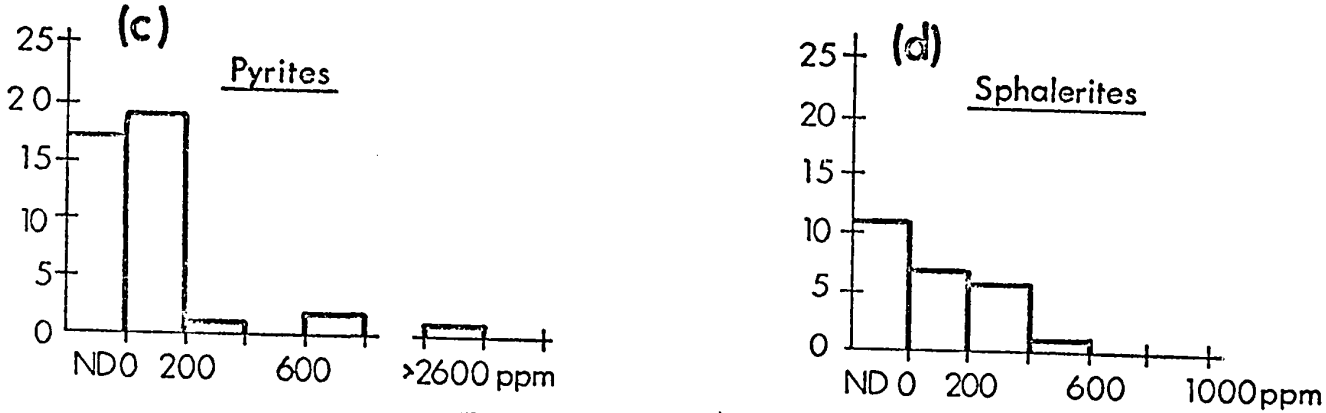

Frequency distribution of Ag.

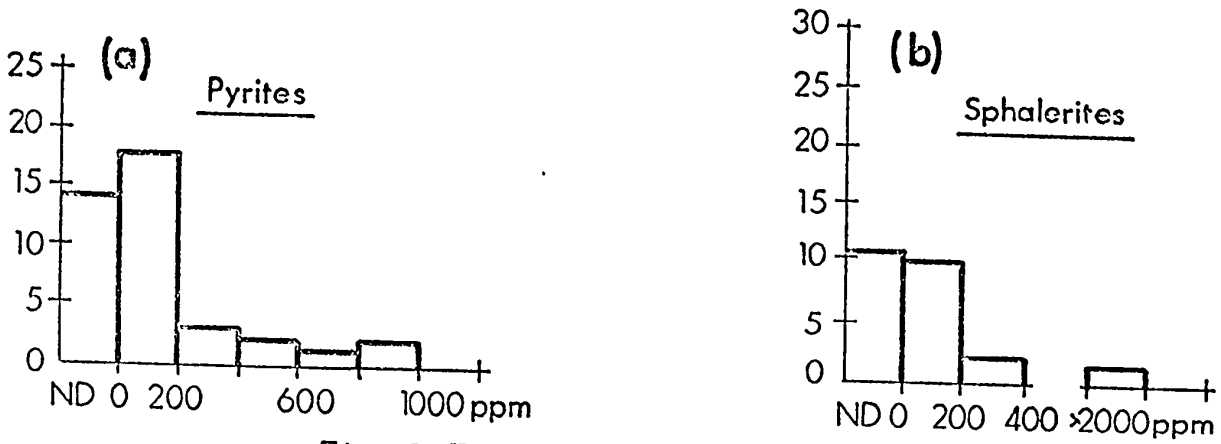

Fig.12. Frequency distribution of Sn.

2. The postdepositional nature of the Cu and Zn distribution between the sulfide minerals is very likely. Since both elements show relationship with the bulk mineralogical composition (amount of chalcopyrite or sphalerite) postdepositional diffusion of Cu and Zn is a feasible explanation. The effect of solid state diffusion is different for different elements and minerals. The distribution of Zn between pyrrhotite and pyrite is likely the least effected.
3. Compared with Co and Ni, which exhibited a narrow range of concentrations in these sulfides, Cu and Zn concentration of sulfides which carry these elements as trace constituents show two or three orders of magnitude variation. This is likely a result of the large concentration gradients for Cu and Zn facilitating their diffusion and possible coprecipitation with chalcopyrite and sphalerite.

Results and Interpretation of the Sn-Ag Analysis

40 analyses of Sn and Ag were performed on pyrites and 25 on sphalerites. In addition some galena was analyzed in order to have more information about the mode of occurrence and distribution of silver.

Tin content of pyrites varies from the limit of analytical sensitivity to 1000 ppm with the most frequent concentrations encountered between 0-200 ppm (Fig. 12a). The Sn concentration is highly variable, some samples exhibit the total range of values (Sample 18P).

The Kidd Creek deposit, like other Canadian massive sulfides of Archean age has a high tin content (Roscoe, 1965). The average Sn content of the deposit is 0.14% (Mulligan, 1972).
As was mentioned in connection with the mineralogy of the ore, trace amounts of cassiterite are present in the deposit. Idiomorphic to subidiomorphic cassiterite grains with grain size of 10-100 micron size are present in pyrite, sphalerite, galena and also in the gangue minerals. One microprobe analysis of cassiterite gave 82.5 weight % Sn which is slightly more than that of the stoichiometrical cassiterite (79.1 weight %) suggesting the lack of substitution of Sn by Fe or other elements. This latter feature may be characteristic of cassiterites of massive sulfide deposits since they formed at lower temperature compared to cassiterites of vein or disseminated type tin deposits. In high temperature pneumatolitic cassiterites up to 1/6 of the Sn can be substituted for by Fe. The prismatic habit of Kidd Creek cassiterites also suggest a lower, hydrothermal temperature for their formation. These considerations and the observed, frequent occurrence of cassiterite inclusions in sulfides, can suggest that the sulfides and cassiterite are paragenetically closely related, or even that late cassiterite was coprecipitated with sulfides. Unfortunately on the ground of Sn content of sulfides we could not decide whether or not cassiterite was coprecipitated with the enclosing sulfides. Compared with Co or Ni the average Sn content of pyrites is low, about an order of magnitude lower than that of Co. Different partition conditions are not

likely to be responsible for this difference, but the substantially lower solubility of Sn in pyrite is the reason. An indefinite host rock - tin content of pyrite relationship exists; pyrites from rhyolitic host rock seem to have higher Sn contents, but low tin pyrites were also encountered in the acidic volcanics (Sample 14P) which do not exhibit hydrothermal alteration. Sphalerites have a similar but slightly lower Sn content than pyrites (Fig. 12b). Only one analysis shows a higher Sn content than that of pyrite (Sample 3P with 2260 ppm Sn) but this can perhaps be attributed to the presence of submicroscopic cassiterite inclusions. The tin content of sphalerites is very variable without a consistently higher value of tin in the vicinity of acidic host rocks. Because of the highly variable Sn concentrations from grain to grain and values near to the analytical sensitivity with a consequently high analytical error, a regular partitioning of Sn between pyrite and sphalerite cannot be obtained. The other reason for the undecipherable, scattered partitioning pattern may be simply the lack of equilibrium.

A general conclusion with some further implications can be made on the genesis of ore in connection with Sn. The granitoid rocks - tin association has been known for a long time. Because Sn is probably derived and deposited from the same fluid as the sulfides themselves, the source rock of the ore depositing fluid must be sialic. It is thought that cassiterite forms by the hydrolysis reaction of tin halides (and by reaction of tin halides with SiO_2). All these reactions increase the pH of the depositing solution.

Because SnO_2 is stable in neutral or alkaline oxidizing media, the rising ore solutions must have been neutralized by reaction with the wall rocks in order to precipitate the cassiterite; i.e. the development of ore solution was from acidic to neutral. Stability conditions of carbonates which were coprecipitated with sulfides also exclude an acidic ore solution during sulfide deposition. To check this assumption a detailed study on the distribution of Sn and cassiterite would be necessary, relating Sn content to the amount and nature of the gangue minerals (carbonates, chert, chlorite).

Silver content of pyrite varies from the limit of analytical sensitivity to 800 ppm, with the most frequent concentration range between 0 and 200 ppm (Fig. 12c) (a pyrite grain with 2670 ppm Ag is suspected to have minute native silver inclusions). The silver content is highly variable even in a single polished section. On the average the Kidd Creek deposit is extremely rich in silver, but Ag is not particularly concentrated in the pyrites. The average Ag content of pyrites is about 50-60 ppm (this value rather should be taken as an estimate because Ag concentrations were often near to or below the level of analytical sensitivity). Silver content of pyrites does not show a relationship with the nature of host rock or mineralogical composition. Pyrite samples in contact with rhyolites or andesites and samples with or without silver minerals have no consistently different silver content. Ag content of sphalerites shows a similar range to that of pyrites, but on the

average sphalerite has about twice as much silver content (around 100 ppm or about 3 oz/ton). For comparison, the average Ag content of the deposit is 4.85 oz/ton. If we also consider that sphalerite contains minute inclusions of Ag-minerals it is obvious that most of the silver is associated with sphaleritic ores. All the analyzed galenas are low in Ag (below the limit of detectability of 50 ppm) so that they do not contribute much to the average Ag content of ore. Ag content of sphalerites also has no connection with the nature of host rock or mineralogical composition.

Regular partitioning of Ag between pyrite and sphalerite could not be tested due to the high analytical error in the determination of Ag. Naturally a disequelibrium situation is also possible, particularly if we consider that there are at least three different phases carrying Ag as a major element, and all these may have formed at a different time (paragenetic restriction on partitioning) in a different physical-chemical environment (widely varying partitioning conditions).

Ag Minerals

The presence of native silver in pyrite was proved by electron microprobe analysis. The size of native silver inclusions is generally around ten microns. The shape of Ag grains, as depicted by an X-ray photograph, is irregular with a slight diffuse boundary (Photograph 28), almost certainly due to the finite size of the volume excited by the electron beam.

Sphalerites contain two (?) different silver minerals: antimonial silver and allargentum. They appear as 10 micron-sized rounded or drop-shaped inclusions. Sometimes these inclusions are arranged along a straight line suggesting localization along the crystallographic directions of the sphalerite host. Microprobe analysis was made on two grains. One seems to be antimonial silver with a composition Ag = 94.1 Sb = 4.5%. A small amount of As, and perhaps Bi and S may be present, making up the sum of the analysis to 100%.

The other grain showed a very definite zoning with regard to its Sb content. Because of the small grain size Sb and S were measured simultaneously in order to avoid obtaining erratic data which can result from the partial excitation of surrounding sphalerite. Sb content at the centre of grain was 13.6%, at the outermost part, 6.7% Sb was present. Sulfur was constant at 0.2%. Ag content was measured only at the centre (85.7%) but it can be assumed that a decrease in Sb content was followed by an increase in Ag.

An X-ray photograph (Photograph 29) was made to depict the distribution of Ag. It shows a diffuse boundary against sphalerite suggesting equilibrium between antimonial silver and sphalerite. The brighter spot at the lower left corner of the picture is an antimonial silver grain.

Early studies (Schwartz, 1928; Broderick and Ehret, 1931) on the Ag-Sb system concluded that the solubility of Sb in silver (excluding the dycrasite field) is about 10 weight % at low temperature, and about 13 weight % at 450°C. More recent investigations

(Barstad, 1959) conducted at 400°C indicate that up to 6.9% Sb a cubic phase exists, from 10.3 to 16.3% Sb there is a hexagonal phase and finally from 23.3 to 28.7% Sb an orthorhombic phase is stable. There is no stable phase between 6.9 and 10.3% Sb content. Mineralogical findings do not support the lack of solid solution between 6.9 and 10.3% Sb. The range of composition for relevant Ag-Sb minerals are (Ramdohr and Strunz, 1967).

Animikite (antimonial silver) up to 11% Sb	(cubic)
Allargentum: from 10 to 15% Sb	(hexagonal)
Dyscrasite: about 21% Sb	(orthorhombic)

It is suspected that Ag-rich dyscrasites are actually intergrowths of two phases: dyscrasite and allargentum or antimonial silver (Schwartz, 1928). Because allargentum and antimonial silver also occur as intergrowths, it may well be that many analyses were made on a mixture of the two phases, and there is really a solubility gap between 6.9 and 10.3% Sb content as indicated by the phase studies. Because of the small size of the grain on which our analysis was made, we could not test whether the Sb content decreases gradually or changes abruptly; i.e. whether or not there are two phases present with a distinct solubility gap with regard to their Sb content. We do not know about other microprobe analyses made on these minerals, so we are unable to make further comparison.

Both allargentum and antimonial silver can be formed by exsolution. Studies of Ag ore deposits reveal that dyscrasite forms

exsolution intergrowth with allargentum often with segregation of antimonial silver (Markham and Lawrence, 1962).

Our evidence supporting exsolution is:

1. Drop-shaped grains
2. Localization of these grains along crystallographic directions of the sphalerite host.
3. Changing composition with Sb-rich central part, as it can be expected for the early exsolved material.

A detailed examination of these phases would be necessary involving heating experiments with the determination of homogenization temperature.

There is another Ag-containing mineral which occurs in galena: grain size varies from 10 to about 100 microns, optical properties are close to freibergite or polybasite (Photographs 17 and 30).

Microprobe analysis indicated: Ag = 25.8%
Sb = 21.5%
S = 15.2%

Apart from these elements a spectral scan detected the presence of abundant Cu. The chemical composition suggests freibergite $(Cu,Ag)_3SbS_{3-4}$ rather than polybasite.

CHAPTER IV: GEOBAROMETRY AND GEOTHERMOMETRY

Iron Content of Sphalerite and its use in Geobarometry

Zn, Cu and in some cases Mn and Cd content of sphalerites were measured. Cu and Cd are present usually around the 100 ppm level and the Mn content is even much lower. Knowing the concentrations of Zn, Cu and Cd we can calculate the amount of iron present in the sphalerite with a fair accuracy. The frequency distribution of Zn and that of the calculated Fe content of sphalerites is represented on Figure 9d.

The physical-chemical variables defining the iron content of sphalerite in the Zn-Fe-S system are temperature, fugacity of sulfur and total pressure. Since in divariant assemblages (pyrite + sphalerite or pyrrhotite + sphalerite) the equilibrium f_{S_2} is not buffered, the iron content of sphalerite can vary to a greater extent than in the three phase assemblages (pyrite + pyrrhotite + sphalerite). In the three phase assemblages the equilibrium fugacity of sulfur is fixed by the pyrite - pyrrhotite buffer system, therefore the iron content of sphalerite is more restricted, it is only the function of the total pressure at a given temperature.

In accordance with these general physical-chemical considerations in the Zn-Fe-S system, we found that sphalerites coexisting only with pyrite have an iron content varying from 5 to 10 mole %. Sphalerites coexisting with pyrite + pyrrhotite have a narrow range of iron content varying from 8 to 10 mole %. Sphalerites coexisting only with pyrrhotite have a less variable iron content than those coexisting only with pyrite. In fact they show a very similar iron content to

those sphalerites which coexist with both pyrite and pyrrhotite. Consequently, during the deposition of pyrrhotite + sphalerite the partial pressure of sulfur was near to that defined by the pyrite - pyrrhotite solvus. These findings prove the existence of chemical equilibrium between sphalerite and the iron sulfides. All these sphalerites are low in iron which is a general characteristic of sphalerites from massive sulfides of volcanogenic exhalative origin (Hutchinson, 1965).

Scott and Barnes (1971) re-examined and clarified the properties of the controversial Zn-Fe-S system and the question of sphalerite geothermometry. They have found that in the three phase assemblage pyrite + pyrrhotite + sphalerite the sphalerite composition is constant with 20.7 $\pm$ 0.6 mole % FeS below 550°C, therefore the iron content of sphalerite cannot be used as a geothermometer. On the other hand, the pressure effect on the FeS content of sphalerite is large enough to use sphalerite as a geobarometer.

In estimating the pressure of ore deposition we considered only the iron content of sphalerites (average 10 mole %) coexisting with both pyrite and pyrrhotite and used the graphical representation of Scott's and Barnes' data on the composition of sphalerite as a function of temperature and total pressure.

Our sphalerites indicate a pressure range between 5.3 and 6.3 kilobars in the temperature interval 350-450°. Similarly high pressures (5.5 $\pm$ 0.5 kb) of ore deposition were calculated for Quemont Mine, Noranda, Quebec (Scott and Barnes, 1971). Since the isobars of Scott and Barnes are extrapolated ones at pressures higher than one kilobar

these pressure values describing the ore deposition are only tentative. It also has to be mentioned that in all these experiments Scott and Barnes equilibrated the high temperature hexagonal pyrrhotite with pyrite + sphalerite. Below 308°C the conversion from hexagonal to low temperature monoclinic pyrrhotite adds a new phase to the system whose composition is critical in terms of chemical equilibrium in the Fe-Zn-S system. If this conversion takes place after the deposition, it probably does not affect the iron content of sphalerite because "the iron content of sphalerite is unusually resistant to postmineral changes" (Barnes, 1967).

Certainly the pressure of deposition as deduced from the sphalerite geobarometer is too high to be geologically reasonable if the ore is volcanogenic.

Partitioning of Mn and Cd between Galena and Sphalerite, and its use in Geothermometry

The distribution coefficients for Mn and Cd between coexisting galena and sphalerite were determined experimentally over the temperature range 600-800°C and their value was extrapolated to lower temperatures (Bethke and Barton, 1971). They pointed out that the distribution of Mn and Cd obeyed Henry's Law throughout the concentration ranges encountered in natural sphalerites and galenas. The effect of pressure on the partitioning was calculated from molar volume data and appeared to be insignificant, making the partitioning applicable in estimating the temperature of formation of sphalerite and galena. The distribution of Mn and Cd between coexisting sphalerite and galena is described by the following equations:

$$\log K_{Cd}^{sph\text{-}gn} = \frac{2080 + 0.0264P}{T_K^\circ} - 1.08$$

$$\log K_{Mn}^{sph\text{-}gn} = \frac{1410 + 0.0261P}{T_K^\circ} - 0.01$$

We analyzed five samples of galena and sphalerite making repeated measurements on different areas of the same sample. All the analyses were obtained by line counts, thus the domain of equilibrium studied is rather on hand specimen scale than grain to grain scale. In order to reduce the analytical error, peak readings were increased from the usual 5 to 15 for each Mn and Cd analysis pair. Both the Mn and Cd

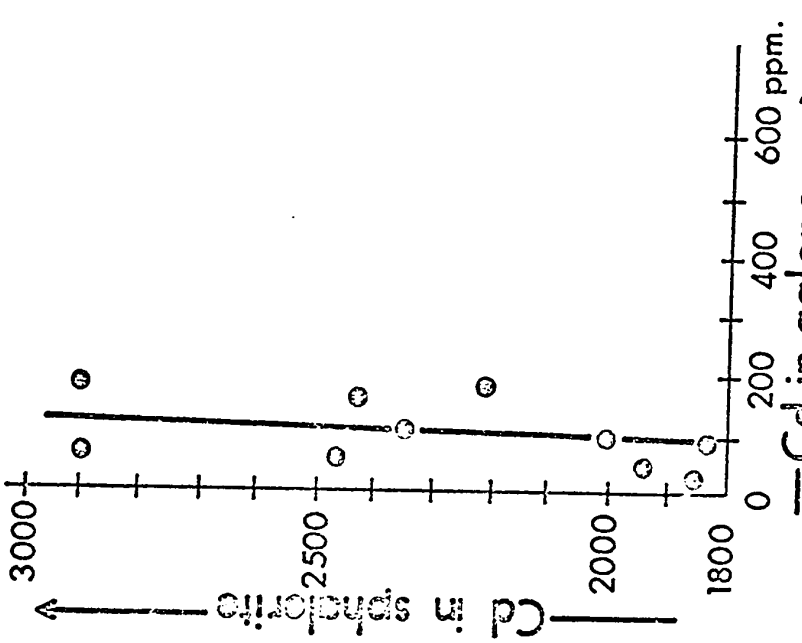

Fig.13. Partitioning Plots for Cd.

content of sphalerites (particularly Mn) are low, while galena has about an average Mn and Cd content compared with galena and sphalerite of hydrothermal ore deposits (Fleischer, 1955). Mn in sphalerite ranges from 40 to 230 ppm and Cd from 1830 to 2890 ppm. Mn in galena varies from 20 to 120 ppm and Cd from 20 to 180 ppm.

Mn does not show any definite partitioning between coexisting sphalerite and galena, galena has a very similar Mn content to that of sphalerite. The near unity partitioning coefficient K_{Mn}^{sph-gn} implies lack of equilibrium distribution for Mn. At 400°C Mn is more than one hundred times enriched in sphalerite over galena if equilibrium is attained. On the other hand, Cd shows a definite partitioning with enrichment in sphalerite over galena.

Utilizing Barton and Bethke's equation describing the distribution of Cd between coexisting sphalerite and galena, the following temperatures of crystallization have been calculated:

Sample Number	K_{Cd}^{sph-gn}	Temperature (°C)
2P	39	505
2P	22	585
2P	13	675
5P	41	499
18P	20	600
18P	> 50	475
62C	16	637
62C	40	502
66C	15	649

Figure 13 is a plot of the partitioning of Cd between sphalerite and galena. The visually estimated best fit line of the partitioning diagram gives a K_{Cd}^{sph-gn} value of about 30.

As can be seen from the data above, the partitioning coefficients are not very consistent. Temperatures of deposition indicated by individual K_{Cd}^{sph-gn} values are too high to be geologically feasible, despite the fact that they were calculated without pressure correction. If a pressure of deposition of 5.5 kb was of the right order of magnitude, and was utilized for pressure correction on the partitioning, all the temperature data reported above should be increased by about 50°C. On the other hand, if we consider the magnitude of analytical errors in determining 50-70 ppm of Cd, some of the temperatures may be lower or higher by 40-50°C.

Instead of giving a detailed discussion of other reasons for too high a temperature of deposition obtained from partitioning, we list only the important ones and refer back to the detailed discussion of the problem of partitioning we made in connection with Co and Ni.

1. Long extrapolation of the experimental data of Bethke and Barton.
2. Different and more complex partitioning conditions in natural environments (chemical composition of sphalerite and galena). Alternating sphalerite and galena bands indicate changing physical chemical conditions during deposition.
3. Postdepositional changes.

In relation to the last point, we observe that although there are textural features suggesting partial recrystallization of fine-grained pyrite and sphalerite, this is not obvious from the partitioning data. We did not measure higher partitioning coefficients

for samples having relict colloform textures (Sample 62C), which would indicate lower temperature postdepositional reequilibration (metamorphism).

The question still to be answered remains: why does the Mn not show any partitioning between coexisting sphalerite and galena? It is not unusual that one element shows a definite partitioning between two phases while another element does not. Hall et al.(1971) measured equilibrium or near equilibrium partitioning for Mn and Cd between coexisting sphalerite and galena, but not for Se.

CONCLUSIONS

1. Abundances of Co and Ni in the sulfide minerals of the Kidd Creek deposit conform to the type of deposit and its geological environment, supporting the volcanogenic origin. Co and Ni content of pyrites and their Co/Ni ratios indicate three different generations of this mineral.

2. The near linear distribution of Ni between pyrite and chalcopyrite and that of Co between pyrite and pyrrhotite with K_{Co} and K_{Ni} values close to unity can either indicate tendency to equilibrium partitioning at very high and relatively constant temperature without drastic change in the trace element composition of the ore fluid or postdepositional homogenization of sulfide minerals by diffusion processes. Because the former explanation requires very stringent physical-chemical conditions for the deposition of the sulfide minerals, the nature of the Co, Ni distribution is better explained by postdepositional effects. In this regard the degree of homogeneity of Co and Ni concentrations in the sulfide minerals would indicate that pyrites are affected the least and chalcopyrites the most in these postdepositional diffusion processes.

3. The zoned pyrites exhibiting original, depositional distribution of Co and Ni indicate, by and large, a closed system precipitation

for the disseminated pyrites and a higher $K_{Co}^{py\text{-}fluid}$ than $K_{Ni}^{py\text{-}fluid}$ partitioning coefficient in agreement with experimental data on synthetic sulfides. From these experimental data and data on the Co/Ni ratios of pyrites, it follows that there was likely a somewhat higher concentration of Co than Ni in the ore-depositing fluid.

4. The postdepositional nature of the trace element distribution is even more likely in the case of Cu and Zn. In this case the distribution of Zn between pyrrhotite and pyrite is the least affected by diffusion. Based on the abundance of Zn it is possible to discriminate between two pyrite generations which do not coincide with the high and low Co pyrite generations. Cu content of pyrite does not favour equilibrium coprecipitation for the pyrite-chalcopyrite mineral pair.

5. The paragenetic sequence of mineralization is very difficult to establish from the partitioning data. The superimposed postdepositional changes in the chemical composition of sulfides and reequilibrated mineral textures both probably result from the slow cooling history of the deposit, but the effect is not complete, original textures and chemical compositions are preserved. The generally accepted view stating the lack of paragenetic sequence in massive sulfide mineralization cannot be substantiated in relation to the Texas Gulf deposit because: (a) the partitioning data does not support diagenetic or metamorphic recrystallization of the sulfides; (b) the

difference in chemical composition of pyrites indicates different generations of this mineral.

6. Iron content of sphalerite which is resistant to postmineral changes indicates equilibrium deposition for pyrite, pyrrhotite and sphalerite as well as equilibrium fugacity of sulfur. Pressure of deposition calculated from the iron content of sphalerite is about 5.5 kilobars. Temperature of deposition obtained from the partitioning of Cd between sphalerite and galena is about 550°C. The mineralogical composition of ore (presence of Co, Sn, Ag minerals, lack of Fe oxide minerals) and perhaps the high temperature and pressure of deposition reflect the significant differences in geological-chemical environment of ore formation between Archean massive sulfides and massive sulfides of younger geological age.

REFERENCES

ARTHUR, R. and KINKEL, J.R., 1966. Massive pyritic deposits related to volcanism and possible methods of emplacement. Econ. Geol., vol. 61, pp. 673-694.

AUGER, P.E., 1942. Zoning and district variations of the minor elements in pyrite of Canadian gold deposits. Econ. Geol., vol. 36, pp. 401-423.

BARNES, H.L., 1967. Geochemistry of hydrothermal ore deposits. Holt, Rinehart and Winston.

BARSTAD, J., 1959. Phase relations in the system Ag-Sb-S at 400°C. Acta Chem. Scand., vol. 13, p. 1703.

BETHKE, P.M. and BARTON, P.B., 1971. Distribution of some minor elements between coexisting sulfide minerals. Econ. Geol., vol. 66, pp. 140-163.

BRODERICK, J. and EHRET, W., 1931. An X-ray study of the alloys of silver with bismuth, antimony and arsenic. J. Phys. Chem., vol. 35, p. 2631.

BROWN, A.C. and BARTHOLOMEW, P., 1972. Inhomogeneities in cobaltiferous pyrite from the Chihuluma Cu-Co deposit, Zambia. Mineral. Deposita (Berl.)., vol. 7, pp. 100-105.

BURNS, R.G., 1970. Mineralogical applications of crystal field theory. Cambridge University Press.

DOUGLAS, R.J.W., 1970. Geology and Economic minerals of Canada. Department of Energy, Mines and Resources, p. 191.

DUNCUMB, P. and REED, S.J.B., 1968. The calculation of stopping power and backscatter effects in electron probe microanalysis. Nat. Bur. Standards, Sp. Publ. 298, pp. 133-151.

FIGGIS, B.N., 1966. Introduction to ligand fields. Interscience, New York.

FLEISCHER, M., 1955. Minor elements in some sulfide minerals. Econ. Geol. 50th Anniv. Vol., pp. 970-1024.

FRENZEL, G. und OTTEMANN, J., 1967. Eine sulfidparagenese mit kupferhaltigem zonapyrit von Nukundamu, Fiji. Mineral. Deposita, vol. 1, pp. 307-316.

GHOSH-DASTIDAR, P., PAJARI, G.E. and TREMBATH, L.T., 1970. Factors affecting the trace element partition coefficients between coexisting sulfides. Econ. Geol., vol. 65, pp. 815-837.

GILL, J.E., 1960. Solid diffusion of sulphides and ore formation. 21st Internat. Geol. Gong., pt. 16, pp. 209-217.

HALL, W.E., ROSE, H.J. and SIMON, J., 1971. Fractionation of minor elements between galena and sphalerite, Darwin lead-silver--zinc Mine, Inyo County, California and its significance in geothermometry. Econ. Geol., vol. 66, pp. 602-606.

HAWLEY, J.E. and NICHOL., I., 1961. Trace elements in pyrite, pyrrhotite. Econ. Geol., vol. 56, pp. 467-487.

HEINRICH, K.F.J., 1967. The absorption correction model for microprobe analysis. Trans. 2nd Nat. Conf. Electron Microprobe Analysis, Boston, Paper 7, 2 p.

HOLLEBONE, B.R., 1971. Pseudo-halide complexes of transition metals, Part II. Jour. Chem. Soc., pp. 481-486.

HUTCHINSON, R.W., 1965. Genesis of Canadian massive sulphides reconsidered by comparison to Cyprus deposits. C.I.M. Trans., vol. LXVIII, pp. 286-300.

KALLIOKOSKI, J., 1965. Metamorphic features in North American massive sulfide deposits. Econ. Geol., vol. 60, pp. 485-505.

LOFTUS-HILLS, G. and SOLOMON, M., 1967. Cobalt, nickel, and selenium in sulphides as indicators of ore genesis. Mineral. Deposita, vol. 2, pp. 228-242.

McINTIRE, W.L., 1963. Trace element partition coefficients - a review of theory and applications to geology. Geochim. Cosmochim. Acta, vol. 27, pp. 1209-1264.

MARKHAM, N.L. and LAWRENCE, L.J., 1962. Primary ore minerals of the Consols Lode, Broken Hill, N.S. Wales. Proc. Austral. Inst. Min. Metall., No. 201, p. 43.

MULLIGAN, R., 1972. Canada's lithophile minerals: tin in short supply. Northern Miner, vol. 58, no. 37, p. 96.

PHILIBERT, J., 1963. A method for calculating the absorption correction in electron probe microanalysis, in X-ray optics and X-ray microanalysis. Academic Press, New York, pp. 379-392.

PYKE, D.R. and MIDDLETON, R.S., 1971. Distribution and characteristics of the sulphide ores of the Timmins Area. C.I.M. Trans., vol. LXXIV, pp. 157-168.

RAMDOHR, P. and STRUNZ, H., 1967. Lehrbuch der Mineralogie. Verlag, Stuttgart.

REED, S.J.B., 1965. Characteristic fluorescence corrections in electron probe microanalysis. Brit. Jour. Appl. Phys., vol. 16, pp. 913-926.

ROSCOE, S.M., 1965. Geochemical and isotopic studies, Noranda and Matagami Areas. C.I.M. Trans., vol. LXVIII, ppl 279-285.

ROSE, A.W., 1967. Trace elements in sulfide minerals from the Central District, New Mexico and the Bingham District, Utah. Geochim. Cosmochim. Acta, vol. 31, pp. 547-585.

SCHWARTZ, G.M., 1928. Dyscrasite and the silver-antimony constitution diagram. Amer. Mineral., vol. 13, pp. 495.

SCOTT, S.D. and BARNES, H.L., 1971. Sphalerite geothermometry and geobarometry. Econ. Geol., vol. 66, pp. 653-669.

SINCLAIR, W.D., 1971. A volcanic origin for the No. 5 zone of the Horne Mine, Noranda, Quebec. Econ. Geol., vol. 66, pp. 1225-1231.

SMITH, D.G.W., and TOMLINSON, M.C., 1970. An APL language computer program for use in electron microprobe analysis. Computer Contribution 45, State Geol. Survey, University of Kansas, Lawrence.

SPRINGER, G., SCHACKNER-KORN, D. and LONG, J.P.V., 1964. Metastable solid solution relations in the system FeS_2-CoS_2--NiS_2. Econ. Geol., vol. 59.

STANTON, R.L., 1960. General features of the conformable "pyritic orebodies". C.I.M.M. Trans., vol. LXIII, pp. 22-36.

STANTON, R.L., 1964. Abundances of copper, zinc and lead in some sulfide deposits. Jour. Geol., vol. 66, pp. 484-502.

STANTON, R.L., 1964. Mineral interfacies in stratigorm ores. Inst. Min. Metall. Trans., vol. 74, pp. 45-79.

STANTON, R.L., 1964. Textures of stratiform ores. Nature, vol. 202, pp. 173-174.

VERHOOGEN, J., 1962. Oxidation of iron-titanium oxides in igneous rocks. Jour. Geol., vol. 70, pp. 168-181.

APPENDIX I

PRECISION OF THE MICROPROBE ANALYSIS FOR DIFFERENT ELEMENTS AT DIFFERENT CONCENTRATIONS

Concentration of Element	$I_p - I_b - 2.6\left(\frac{I_p}{t_p} + \frac{I_b}{t}\right)^{\frac{1}{2}}$	Standard deviation	Confidence level (%)
Cobalt (ppm)			
200	+ 0.7275	9.54	100
300	+ 1.1234	13.17	100
Nickel (ppm)			
70	- 0.0239	2.34	98
80	- 0.0183	2.41	98.4
90	+ 0.035	2.97	99.7
100	+ 0.041	3.01	99.74
120	+ 0.1345	4.02	100
Copper (ppm)			
50	- 0.1369	1.10	72
80	- 0.0577	1.97	95
120	+ 0.0202	2.82	99.5
140	+ 0.0610	3.26	98.8
180	+ 0.1587	4.31	100
Zinc (ppm)			
80	- 0.1176	1.413	84
90	- 0.1028	1.58	88
150	+ 0.0356	2.98	99.7
170	+ 0.1000	3.78	99.98

Concentration of Element	$I_p - I_b - 2.6(\frac{I_p}{t_p} + \frac{I_b}{t_b})^{\frac{1}{2}}$	Standard deviation	Confidence level (%)
Tin (ppm)			
10	- 0.102	0.42	33
20	- 0.053	1.12	74
30	- 0.0279	1.77	92
40	- 0.0081	2.36	98
50	+ 0.0116	2.94	99.7
60	+ 0.0259	3.32	99.9
80	+ 0.0741	4.42	100
120	+ 0.1699	7.50	
Silver (ppm)			
40	- 0.05734	1.07	71
60	- 0.03297	1.68	90
80	- 0.01776	2.13	96
100	+ 0.0020	2.65	99.2
120	+ 0.0264	3.33	99.92
180	+ 0.0812	4.73	100
Cadmium (ppm)			
50	- 0.04273	1.26	79
60	- 0.03277	1.57	88
70	- 0.0228	1.88	94
90	- 0.00287	2.50	98.7
160	+ 0.0569	4.94	100
180	+ 0.0768	5.76	

Results of the Microprobe Analysis

Sample No	Mineral	Concentrations in ppm Co	Ni
1P	py	1910	190
		1820	50
	cp	570	170
		410	120
1P'	py	1510	100
	cp	320	220
		440	200
1P"	py	590	180
		17840	1870
		16130	1720
	cp	390	250
		370	140
	po	1210	470
		1210	470
2P	cp	380	200
		280	140
	po	1140	200
2P'	py	990	240
		800	260
		600	260
2P"	py	810	460
		750	430
	cp	360	230
3P	po	630	60
		670	130
	cp	200	ND
		290	ND
3P'	cp	400	230

Sample No.	Mineral	Concentrations in ppm Co	Ni
4P	py	1730	180
		1320	130
		1030	120
	cp	430	120
	po	1050	430
		1110	540
5P	py	740	ND
		600	ND
		500	ND
	po	1060	ND
6P	py	960	80
		860	60
	cp	460	160
		280	110
6P'	py	1170	120
	cp	450	110
7P	py	1010	270
		800	60
7P'	cp	310	20
	po	1310	530
		1230	560
8P	py	710	170
	cp	400	120
	po	860	250

Concentrations in ppm

Sample No.	Mineral	Co	Ni
10P	py	640	50
		610	40
	cp	430	ND
14P	py	680	300
		580	280
		670	260
	cp	380	ND
14P'	py	730	310
15P	py	800	3830
		1940	310
		27670	240
	cp	230	300
16P	py	710	70
		690	ND
	cp	490	30
17P	py	1450	110
		1040	90
	cp	430	ND
		460	ND
17P'	py	16200	1710
		15120	1690
18P	py	620	120
		660	ND
18P'	py	600	160
		690	270
19P	py	620	630
19P'	py	580	400
		770	330
	cp	310	310
		430	230

Concentrations in ppm

Sample No.	Mineral	Co	Ni
II	py	510	ND
		390	ND
	cp	220	ND
		380	110
IV	py	1260	ND
		550	ND
	cp	490	ND
	po	1360	180
		1330	160
VIII	cp	480	180
	po	1330	400
IX	cp	590	240
	po	870	250
		1380	450
XV	py	680	190
57.c	py	1440	20
	cp	460	90
	po	1220	490

Sample No.	Mineral	Concentrations in ppm or weight percentage Cu	Zn
1P'	cp	35.11%	1260
		34.69%	440
	po	190	ND
	sph	550	60.212%
1P	py	140	5950
		50	170
		140	13650
	sph	260	60.227%
		570	60.603%
2P	cp	34.96%	940
	po	720	6200
	sph	490	60.89%
		480	60.81%
2P'	py	160	10260
		530	690
		ND	17720
	sph	370	60.158%
2P"	py	180	2690
		690	1880
	cp	35.02%	830
3P	cp	34.80%	430
		34.97%	440
3P'	py	490	150
	cp	35.93%	430

Sample No.	Mineral	Concentrations in ppm or weight percentage Cu	Zn
4P	py	620	2520
		1040	700
	sph	850	60.157%
		680	60.507%
5P	py	1190	400
	cp	34.88%	480
	po	1070	370
	sph	2610	60.331%
5P'	py	470	80
		1740	8480
		380	6140
	po	ND	12870
		ND	12460
	sph	340	59.852%
6P	cp	33.97%	11240
	po	1250	3500
	sph	1370	60.466%
		970	60.284%
6P'	py	380	490
		340	13500
	cp	34.53%	4380
		34.48%	10070
	sph	1600	59.983%
		790	60.175%
	po	260	10610

Sample No.	Mineral	Cu	Zn
7P	py	80	180
	cp	34.11%	17150
7P'	cp	33.65%	15030
	po	ND	3660
		20	2500
	sph	660	58.672%
		740	58.561%
8P	py	ND	490
	cp	34.99%	970
	po	50	7970
10P	py	130	ND
		400	ND
14P	py	200	170
		120	250
	cp	41.19%	790
14P'	py	170	ND
	po	1960	110
	cp	34.39%	750
	sph	650	60.179%
15P	py	180	90
		210	180
16P	py	190	4810
		230	1100
		850	11610
	po	50	12350
	sph	1400	60.179%
17P	py	590	120
		2500	150
	cp	34.75%	420
		34.65%	290

Sample No.	Mineral	Cu	Zn
18P	py	160	510
		170	16240
		320	11690
		280	130
	sph	420	60.787%
		440	60.426%
18P	py	30	1140
		770	6780
	sph	340	60.606%
		220	59.394%
19P	py	180	250
		260	280
	cp	33.90	610
	sph	1560	63.246%
		1630	63.439%
57.c	py	1070	1190
	cp	35.07%	280
	po	1690	950
	sph	850	60.021%
I	py	990	1410
		640	590
	cp	34.76	1870
	sph	1860	60.003%
I'	py	600	740
	cp	33.65%	7480
		34.92%	2170
	sph	1230	59.5%
		1180	60.257%
II	py	80	690
		230	270
	cp	31.04%	220
	sph	850	64.566%
		950	63.041%

Sample No.	Mineral	Cu	Zn
IV	py	640	590
	cp	34.77%	740
	po	ND	4180
	sph	1710	59.845%
VIII	po	50	7970
		80	7590
	sph	650	59.699%
IX	cp	34.79%	390
	po	40	ND
	sph	2020	60.107%
		1460	59.874%
XV	py	120	310

Concentrations in ppm

Sample No.	Mineral	Sn	Ag
1P	py	190	200
		200	40
		300	630
	sph	90	450
		140	80
2P	py	80	ND
	sph	ND	ND
		10	ND
3P'	sph	2260	ND
		ND	ND
4P	py	530	790
		ND	ND
	sph	ND	190
		ND	270
5P	py	60	120
		40	120
		530	180
		30	ND
	sph	120	ND
	gn	750	ND
		90	ND
7P	py	30	ND
7P'	py	60	ND
		110	ND
	sph	ND	ND
10P	py	20	ND
		800	30
		ND	90
	gn	ND	ND
14P	py	ND	ND
		ND	100
16P	py	120	ND
	sph	120	ND

Concentrations in ppm

Sample No.	Mineral	Sn	Ag
18P	py	950	2670
		260	200
		170	360
		60	60
		ND	40
	sph	180	170
		280	40
	gn	160	ND
19P	py	130	100
		110	ND
	sph	200	140
57.c	py	ND	ND
		ND	80
		ND	60
	sph	ND	230
I'	sph	ND	ND
		ND	ND
II	py	ND	ND
		ND	110
	sph	80	230
		40	140
IV	py	80	ND
		ND	ND
	sph	ND	80
		ND	ND
VIII	py	ND	ND
		ND	ND
		ND	40
	sph	160	0
	gn	ND	
IX	py	530	180
		20	ND
		60	100
		1040	180
	sph	ND	230

Concentrations in ppm

Sample No.	Mineral	Mn	Cd
2P	sph	220	1940
		210	2000
		230	2230
	gn	20	50
		80	90
		30	180
5P	sph	60	2460
	gn	120	60
18P	sph	90	1830
		60	1860
	gn	70	90
		50	ND
62.c	sph	40	2890
		40	2890
	gn	70	180
		100	70
66.c	sph	40	2430
	gn	40	160

ND = the element was not detected

Samples assigned with prime differ only in gross sulfide mineral composition

Location and Description of Samples

Samples from the open pit:

1P South orebody; quartz and sphalerite with traces of pyrite, chalcopyrite and pyrrhotite.

2P Bench 9 - Middle of the South orebody; quartz, massive sphalerite with some pyrite and chalcopyrite.

3P Bench 9 - Middle Zone of the South orebody, contact with the hanging wall. Massive chalcopyrite with minor sphalerite and pyrrhotite.

4P Bench 9 - South end of South orebody; massive sphalerite with pyrite, massive chalcopyrite.

5P North part of South orebody, contact with the hanging wall; massive sphalerite with galena, massive chalcopyrite.

6P North part of the South orebody, 30 feet from the contact with the hanging wall; massive sphalerite with pyrite and chalcopyrite.

7P North part of the South orebody, contact with the footwall; massive sphalerite with traces of pyrite and pyrrhotite.

8P Shear zone between the two orebodies; quartz and chalcopyrite, traces of pyrite.

9P Shear zone between the two orebodies; sericite schist with chalcopyrite and pyrrhotite.

10P 10th Bench - North orebody, contact with the footwall; graphitic schist with disseminated pyrite.

11P Main rampa, NE wall; altered massive rhyolite.

12P 7th Bench - NE rampa; massive black rhyolite.

13P 10th Bench - North orebody footwall; carbonaceous andesite.

14P 10th Bench - North orebody; massive black rhyolite with traces of pyrite.

15P 10th Bench - North orebody; andesite with traces of pyrite.

16P 10th Bench - North orebody; massive sphalerite with pyrite.

17P 10th Bench - North orebody; massive chalcopyrite in cherty breccia.

18P 10th Bench - North orebody; massive pyrite with sphalerite and galena.

Samples from the No. 204 Drill Hole:

57.c from 2960 feet; massive sphalerite with pyrite and chalcopyrite.

62.c from 3025 feet; massive sphalerite with pyrite.

66.c from 3050 feet; massive pyrite with sphalerite.

Underground samples from the 800 feet level:

I	Contact with footwall; sericitic schist, massive chalcopyrite and sphalerite.
II	Tuff agglomerate with elongated sphalerite lenses and cataclastic pyrite.
III	Rhyolite tuff without sulfides.
IV	Calcite from joint in altered rhyolite. Some pyrite and chalcopyrite.
V	Massive andesite or diorite with quartz-carbonate vein.
VI	35 crosscut; massive sphalerite with pyrite.
VII	35 crosscut; massive sphalerite, traces of pyrite.
VIII	35 crosscut; massive sphalerite, traces of chalcopyrite and pyrite.
IX	35 crosscut; contact with rhyolite; massive chalcopyrite and sphalerite.
X	Sericite schist.
XI	39 crosscut; dacite with quartz eye phenocrysts.
XII	39 crosscut; massive chalcopyrite and sphalerite.
XIII	39 crosscut; rhyolite tuff agglomerate at hanging wall or ore.
XIV	from 802 DR; siliceous rhyolite tuff agglomerate.
XV	from 801-810 N DR; rhyolite tuff agglomerate.
XVI	Dacite agglomerate
XVII	Graphitic schist from contact.
XVIII	End of crosscut; massive pyrite with sphalerite.

APPENDIX II

Results of the Sulfur Isotope Analysis

Sample Number	Description	δS^{34} (‰)
2P	Massive sphalerite	-1.16
	Galena from massive sphalerite	-2.03
5P	Massive sphalerite	+0.72
	Massive chalcopyrite	-1.34
6P	Massive sphalerite	-1.26
7P	Massive sphalerite	-0.95
	Disseminated pyrite from host rock	+2.02
10P	Disseminated pyrite from graphitic schist	+1.46
14P	Disseminated pyrite from rhyolite	+4.22
15P	Disseminated pyrite from andesite	+0.18
18P	Galena from sphalerite	-1.56
	Massive sphalerite	-0.77
	Pyrite	+0.68
19P	Disseminated pyrite from graphitic schist	+1.55
	Pb concentrate	-1.0711
	Zn concentrate	-2.072
	Cu concentrate	-0.55

Sample Number	Description	δS^{34} (‰)
II	Massive pyrite	0.00
	Disseminated pyrite	+1.10
VIII	Massive sphalerite	-0.53
IX	Massive sphalerite	-0.56
	Massive chalcopyrite	-0.81
XII	Massive chalcopyrite	-1.266
	Massive sphalerite	-1.35
XVIII	Chalcopyrite from quartz vein	-1.07
19C	Disseminated pyrite from 1595 feet No. 204 drill hole	+4.67
26C	Pyrite mineralization from rhyolite breccia from 2114 feet No. 204 drill hole	+0.10
29C	Pyrite mineralization from 2199 feet No. 204 drill hole	-0.11
32C	Pyrite mineralization from 2295 feet No. 204 drill hole	+0.87
38C	Disseminated and massive chalcopyrite mineralization from 2548 feet No. 204 drill hole	-1.44
39C	Disseminated and massive chalcopyrite mineralization from 2570 feet No. 204 drill hole	-1.77
45C	Massive chalcopyrite from 2760 feet No. 204 drill hole	-0.74
49C	Disseminated sphalerite from 2850 feet. No. 204 drill hole	-0.65

Sample Number	Description	δS^{34}(‰)
62C	Massive sphalerite from 3030 feet No. 204 drill hole	-0.17
	Pyrite from massive sphalerite	-0.49
63C	Galena from quartz vein from 2037 feet. No. 204 drill hole	-2.30
74C	Pyrite mineralization from 3125 feet No. 204 drill hole	-0.52
76C	Massive sphalerite from 3140 feet No. 204 drill hole	-1.03
	Pyrite from massive sphalerite	-1.65
78C	Galena mineralization from 3178 feet No. 204 drill hole	-1.41

Discussion of the Sulfur Isotope Data

Sulfur isotope ratios were measured on 40 sulfide samples from the open pit, from the No. 204 drill hole and from the 800' level. Pyrite, chalcopyrite, sphalerite and some galena samples were analyzed.

A binocular microscope was used for hand separation of pure sulfide minerals. Samples were burned at 1100°C directly to SO_2, using Cu_2O as the oxidizing agent. A twelve-inch 90°-magnetic-analyzer gas source mass spectrometer (equipped for simultaneous collection of mass 64 and mass 66) was used. Samples were compared with a reservoir standard having δS^{34} = +1.75‰ (vs. troilite from Maverthorpe meteorite).

From the measured mass 66/64 ratios, the S^{32}/S^{34} ratios were calculated using the following expression:

$$\delta S^{34}\ (‰) = \frac{F \times R_x - R_{std}}{R_{std}} \times 1000$$

where: R = mass 66/mass 64 for standard (std) and for unknown (x).

F is a correction factor for mass 66 to correct for contribution to mass 66 from $S^{32}O^{16}O^{18}$.

δS^{34} values of sulfide minerals range from +4.67 to -2.3‰ giving a total spread close to 7‰ (see Appendix A-13). The

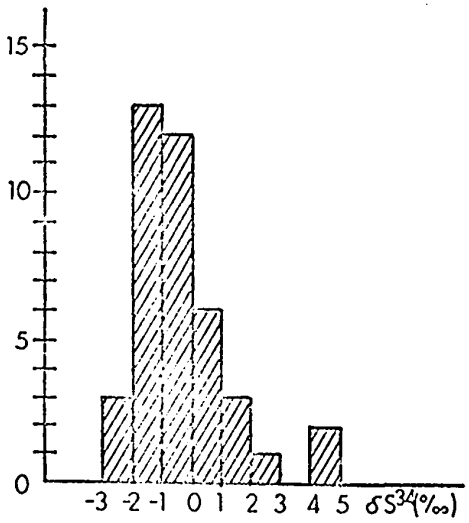

Frequency distribution of δS^{34} values

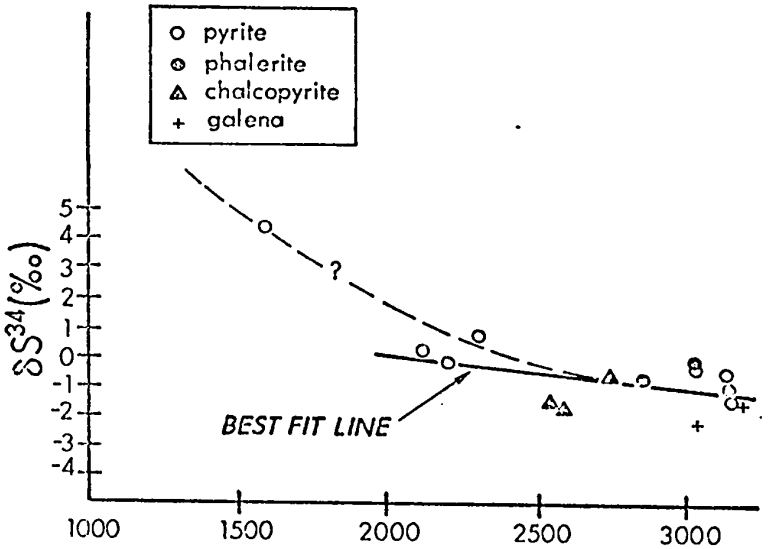

Depth in feet (Drill hole No.204)

Sulfur isotope distribution with depth

FIGURE 14.

frequency distribution of δS^{34} values of all the sulfide minerals are plotted in Fig. 14. The mean δS^{34} is close to zero (-0.32‰) essentially the same as for meteoritic sulfur. The standard deviation for the 40 δS^{34} values is ±1.51‰, and indicates the narrow range of sulfur isotopic composition. The mean sulfur isotopic composition of the Kidd Creek sulfides is not significantly different from that of the meteoritic sulfur; samples with near zero δS^{34} values have 82% confidence level.

The average isotopic composition of magmatic sulfur is slightly positive (Jensen, 1967), but the range of values also includes a few with permil values lighter than meteoritic sulfur.

S^{34}/S^{32} ratios in sulfide minerals are determined by the following factors:

1. Sulfur isotopic composition of source which depends on:
    a) Ratio of magmatic to sedimentary sulfur. Possible sedimentary sources can be seawater sulfate, sulfide minerals and other compounds of sulfur.
    b) Ratio of exhalative loss of volatile sulfur compounds (and their average isotopic composition) to the total sulfur content of the ore-depositing fluid.
    c) Isotopic fractionation processes accompanying the incorporation or loss of sulfur (e.g. fractionation against seawater sulfate.

2. Eh, pH and temperature of the ore solution. Sakai (1968) and Ohmoto (1972) have shown that pH, Eh and T° influence the relative concentrations and isotopic composition of aqueous sulfur species. Fractionation between H_2S and the other aqueous sulfur species increases with increasing alkalinity and decreasing temperature.

3. Isotopic fractionation between the ore-depositing solution and sulfide minerals and between the sulfide minerals. Lengthy paragenesis (reservoir effects), hypogene zoning (different thermal conditions), a change in physical-chemical conditions of ore-deposition (Eh, pH) can induce substantial isotopic variation.

4. Postdepositional changes.

The narrow range of sulfur isotopic composition of the Kidd Creek sulfides (with a near magmatic mean value) indicate a homogeneous source of sulfur with little or no assimilation of sedimentary sulfur, in agreement with the overall geological picture in which rocks of sedimentary origin are subordinate. δS^{34} values of pyrites from the graphitic schist are not different from those of pyrites associated with the massive orebody. The isotopic data (in accordance with the trace element data) suggest that these pyrites are not biogenic in nature and are derived by the same volcanogenic processes as the ore body itself.

Since changing physical-chemical conditions, particularly

partial pressure of oxygen and pH, can induce isotopic variation in the aqueous sulfur species despite a homogeneous source of sulfur in the ore solution, it is possible to have a very wide range of isotopic composition in the sulfide minerals; particularly if the deposition occurs in oxidizing alkaline environment (Ohmoto, 1972). Mineral stability relationships applied to the Kidd Creek deposit, presence of cassiterite, lack of magnetite, coexistence of pyrite and pyrrhotite indicate an ore depositional environment with low f_{O_2}, f_{S_2}, low or neutral pH, and consequently H_2S as the predominant sulfur species in the ore-depositing solution.

In the low f_{O_2} and low to neutral pH range, δS^{34} of aqueous H_2S and that of the precipitating minerals is little affected by changes in f_{O_2} or pH (Ohmoto, 1972). Sulfide minerals precipitating from such a solution exhibit homogeneous δS^{34} values similar to the mean sulfur isotopic composition of the ore-depositing solution.

These considerations suggest that the sulfur isotopic composition of the solution depositing the Kidd Creek sulfides was magmatic (crustal average) with δS^{34} near to zero. Mixing of the ore-forming solution with seawater sulfate and fractionation against seawater sulfate are ruled out.

Isotopic fractionation between the sulfide minerals of the Kidd Creek deposit is usually small. Pyrite is generally, but not invariably, heavier than other sulfide minerals. Disseminated

pyrites from the andesite or rhyolite host rock seem to be slightly heavier than pyrite associated with the massive sulfides due to either slightly different physical-chemical conditions of deposition or different paragenetic position from that of the massive pyrites. The δS^{34} separation between pyrite and sphalerite varies from 1.45‰ (Sample 18P) to 2.97‰ (Sample 7P), but in the later case pyrite is from the andesite host rock while sphalerite is from the massive ore contacting the andesite. For other samples (62C and 76C) the Δpyrite-sphalerite value is near zero or even negative, indicating either lack of equilibrium coprecipitation or lack of any coprecipitation for the mineral pair. The permil separation between sphalerite and galena shows a fair consistency between two analyses (Sample 2P and 18P) with values 0.79 and 0.87‰ possibly indicative of high temperature (above 400°C) deposition.

Isotopic composition of 15 sulfide samples from the No. 204 drill hole give measurements over a cross-section of the orebody from rhyolite through the hypogene mineral zones of pyrite--chalcopyrite-sphalerite and galena. These samples were measured in order to examine the possible sulfur isotope variation with depth. Data plotted on Fig.14 indicates a progressively lighter sulfur in going from the base of the mineralization (pyrite zone in the rhyolite) towards the top.

The equation of the regression line is:

$\delta S^{34}‰ = -0.05 - 0.000975x$ where x is distance in feet

A pyrite sample located at 1595 feet was not considered in the linear regression, being too far from the other samples. Over a distance of 1200 feet there is 1.2‰ decrease in the δS^{34} values of sulfides. The standard deviation of the values is 0.8‰. The ratio between the total permil change along the regression line to the standard deviation is 1.5‰.

The somewhat large standard deviation and the scatter of points along the regression line can be explained by the fact that we plotted δS^{34} values of four different mineral species.

Sphalerite samples from the open pit (5P, 6P, 7P) also have heavier sulfur at the contact with the rhyolite (+0.72‰) than at the top of the orebody (-0.95‰). A similar trend can be observed on sphalerites from the 800 feet level (Samples VII, IX, XII). There can be two possible explanations for the changing isotopic composition with depth:

1. Reservoir effect. First precipitates, particularly pyrite, are enriched in S^{34}, giving rise to progressively lighter sulfur in the ore fluid and sulfides.

If we consider that the magnitude of the total sulfur content of the orebody (30-40 million tons of sulfur), even a lower crust source for sulfur probably cannot act as an unlimited reservoir during the sulfide deposition process, particularly because the deposition must have occurred in a short time interval.

2. Thermal effect. A temperature gradient in the orebody, operative during or after the deposition of the ore, can give rise to diffusion of the sulfur isotopes with a higher rate for the lighter isotope and consequently more negative δS^{34} values away from the heat of source. A thermal gradient can perhaps exist during the deposition of ore with a higher temperature near to the source of the mineralizing solutions (rhyolite).

The presence of a basic intrusive located about 1000 feet away from the orebody can much better account for a high thermal gradient and isotopic diffusion. In drill hole No. 204, the contact of rhyolite and basic intrusive is at 950 feet, so that increasing distance on Fig.14 means increasing distance from the heat of source.

The small isotopic fractionation between different sulfide minerals and the homogeneous isotopic composition of samples of a given mineral species spatially close to each other, also support postdepositional remobilization of sulfur in a diffusion process and enforces the similar explanation for the trace element distribution.

In summary it can be stated that:

1. The narrow range of sulfur isotopic composition of Kidd Creek sulfides (with a near magmatic mean value) indicate a homogeneous source of sulfur with no assimilation of sedimentary sulfur.
2. The isotopic composition of the depositing solution was magmatic (crustal average with δS^{34} near to zero).

3. Postdepositional remobilization of sulfur in a diffusion process induced by a basic intrusive located only 1000 to 1500 feet away from the orebody, or later granitic intrusions of the area, is the most likely explanation for the observed trend in sulfur isotopic composition.

References Cited:

Jensen, M.L., 1967. Sulfur isotopes and mineral genesis, In Barnes, H.L., ed., Geochemistry of Hydrothermal Ore Deposits. New York, Holt, Rinehart and Winston, Inc., pp. 143-165.

Sakai, H., 1968. Isotopic properties of sulfur compounds in hydrothermal processes. Geochem. Jour. 2, pp. 29-49.

Ohmoto, H., 1972. Systematics of sulfur and carbon isotopes in hydrothermal ore deposits. Econ. Geol. 67, pp. 551-579.

PLATE I Microphotographs

1. Colloform sphalerite and chalcopyrite included in pyrite (x65).

2. Partially recrystallized colloform texture. At the centre of the photograph pyrite still has radial appearance (x65).

3. Banded ore. Pyrite band in massive sphalerite (x23).

4. Rhombohedral calcite included in chalcopyrite. No sign of replacement (x65).

5. Subhedral calcite in a fine-grained pyritic band included in massive sphalerite (x65).

6. Pyrite in contact with carbonate. Pyrite is a late interstitial filling, its outline follows the rhombohedral crystal faces of carbonate. No sign of replacement (x65).

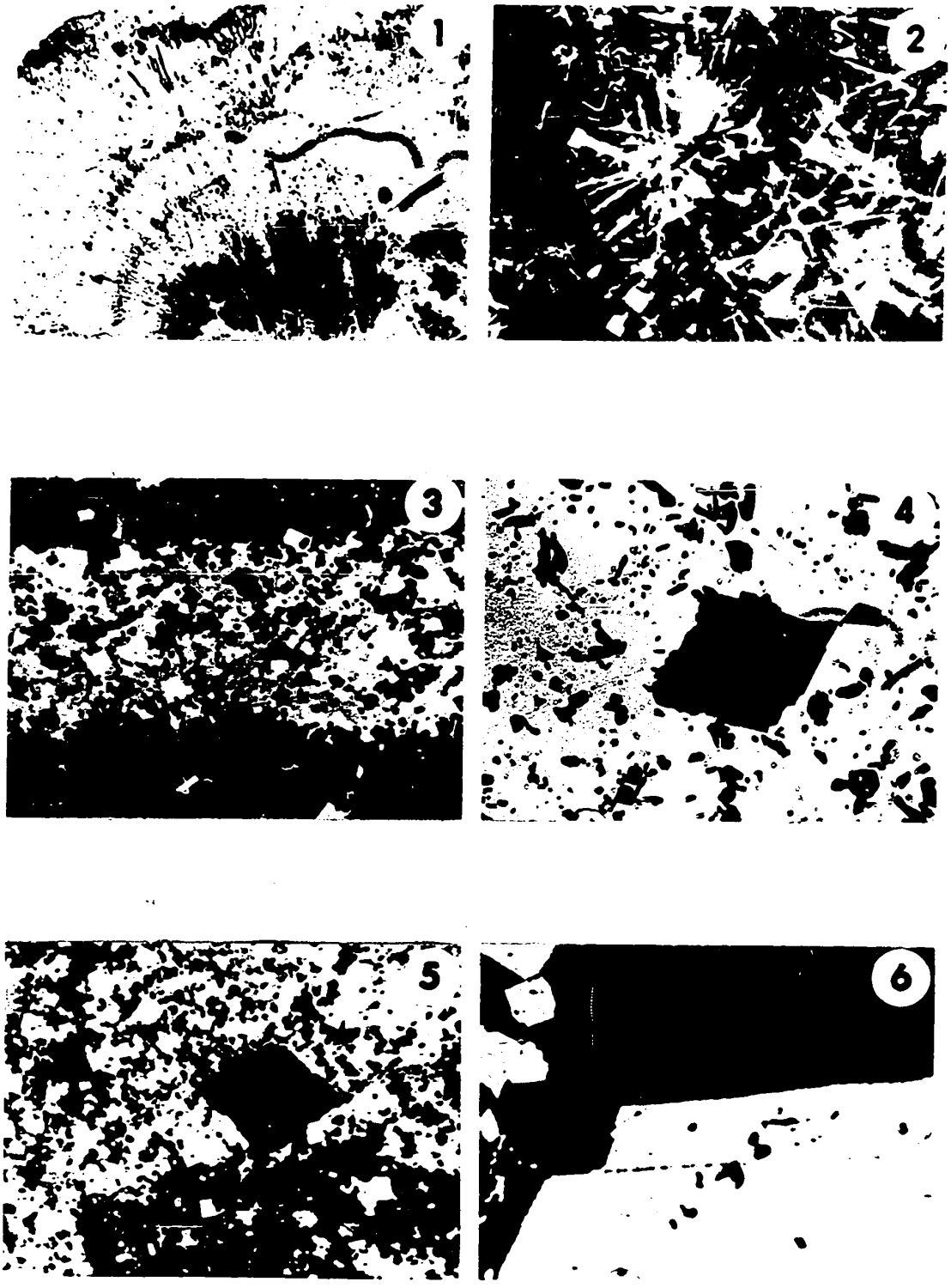

PLATE I.

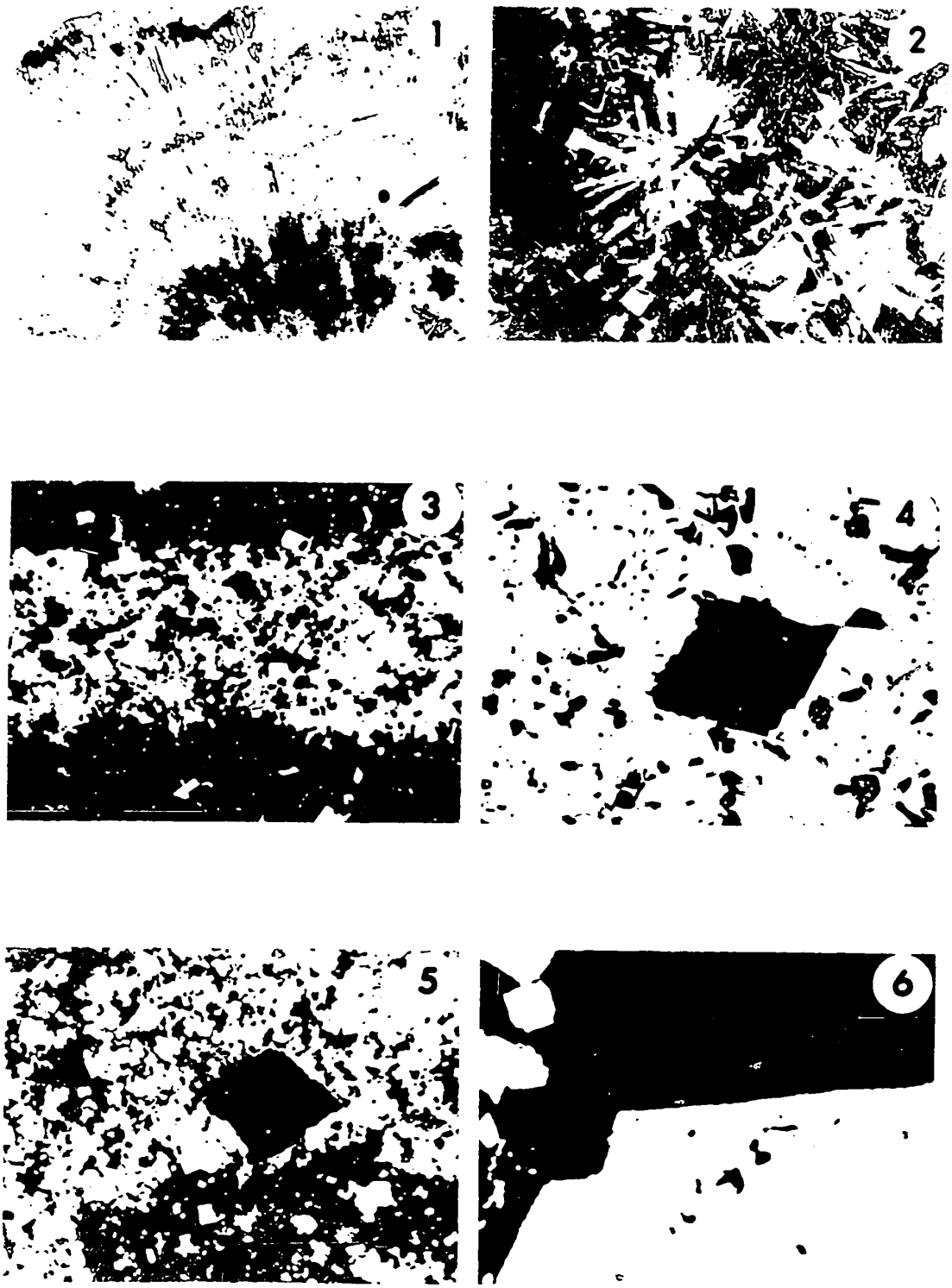

PLATE I.

PLATE II Microphotographs

7. Sphalerite embayment in pyrite. Pyrite is euhedral to subhedral (x65).

8. Sphalerite embayment in pyrite. Some anhedral pyrite grains (x65).

9. Sheared cataclastic pyrite, the openings are filled up by sphalerite and some chalcopyrite (x65).

10. Tension fractures in slightly oriented quartz-carbonate gangue, filled up by chalcopyrite (x23).

11. Sheared cataclastic pyrite, groundmass is cherty silica. Note pitted surface, the strained material is hard to polish (x65).

12. Pyrite included in the chalcopyrite band is subhedral and unfractured (lower right corner of photograph). Pyrite included in the silicate band is strongly fractured (upper part of the photograph) (x23).

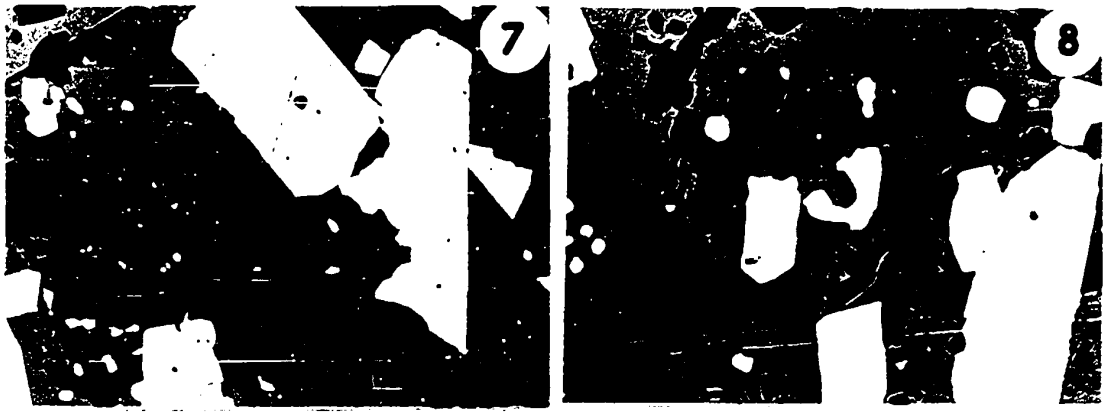

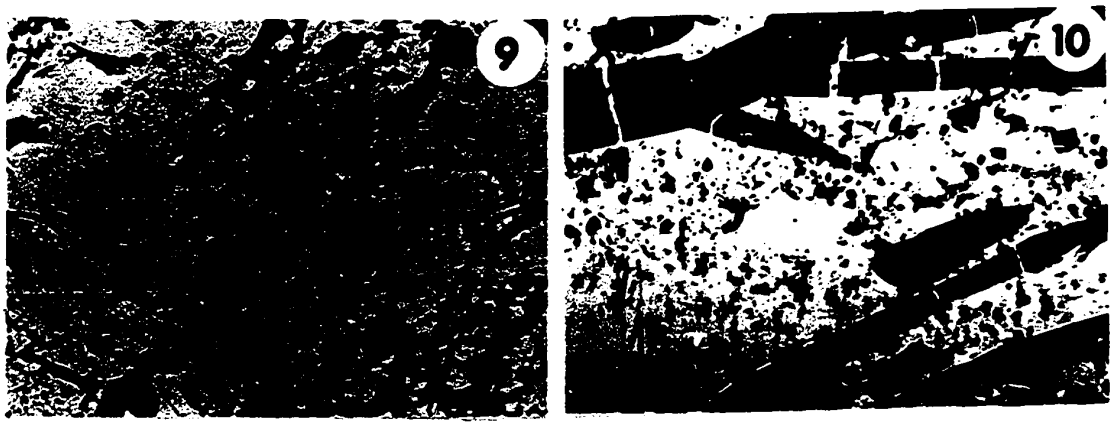

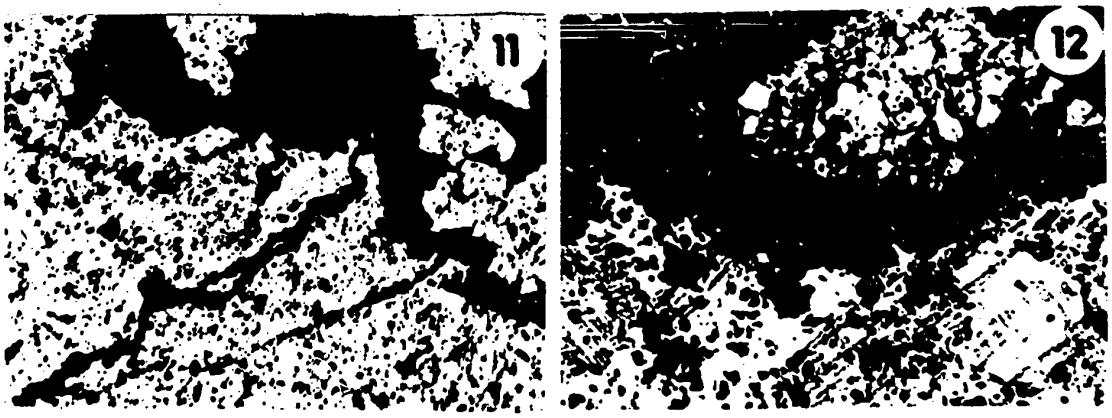

PLATE II.

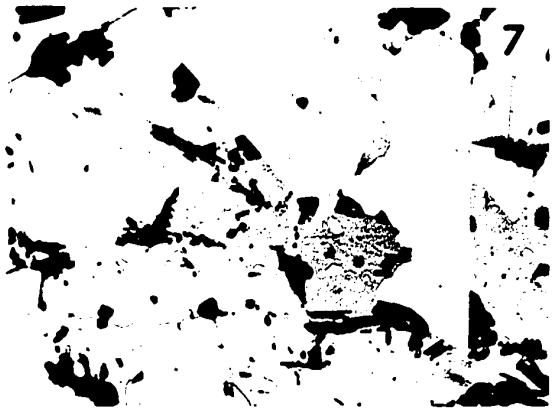

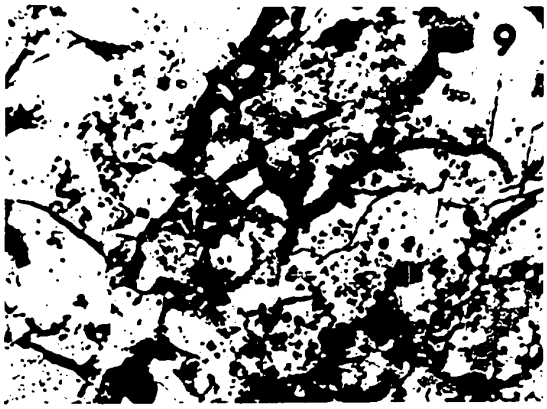

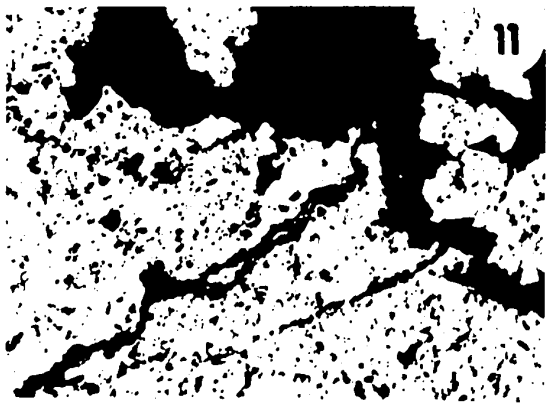

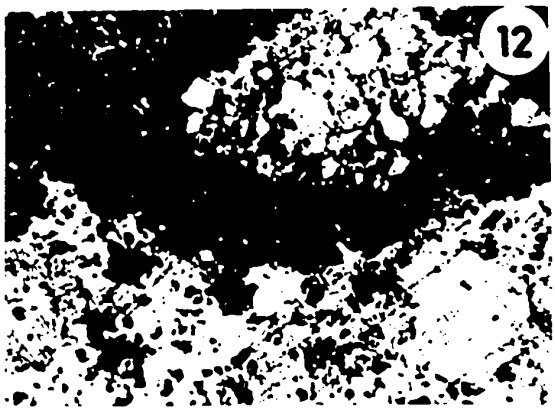

PLATE II.

PLATE III Microphotographs

13. Plastic deformation of sphalerite. Sphalerite grains are elongated parallel to the stresses (x65).

14. Plastic deformation of galena. The cleavage planes are slightly bent (x65).

15. Orientation of gangue minerals in sphalerite due to late metamorphic deformation of the ore (x65).

16. Aggregates of fine-grained pyrite with tendency to recrystallization to cubes (x65).

17. Silver-bearing tetrahedrite (freibergite) in galena (x175).

18. Titaniferous magnetite and illmenite lamellae (exsolution or oxidation or both) from andesite (x65).

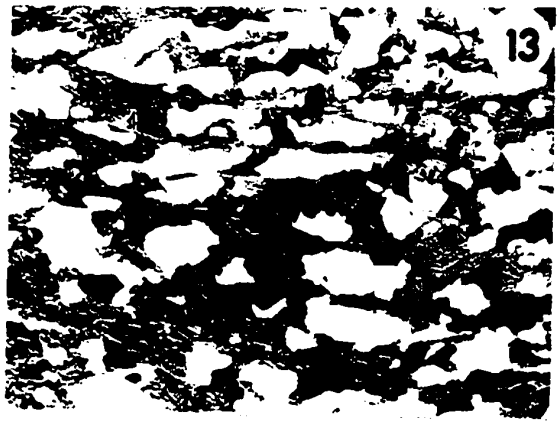

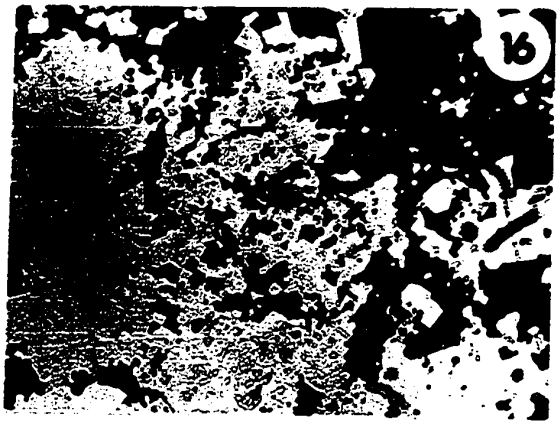

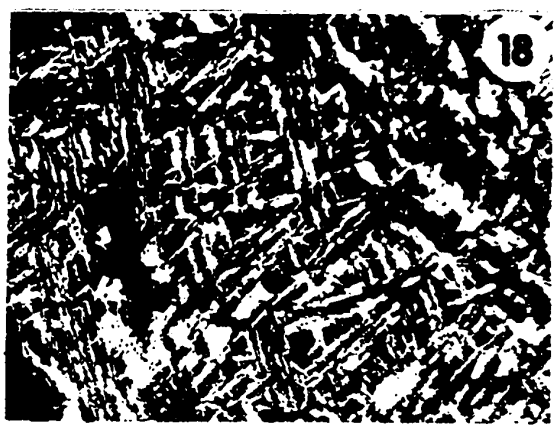

PLATE III.

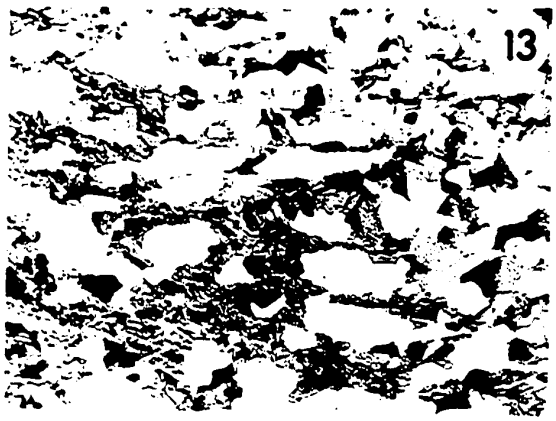

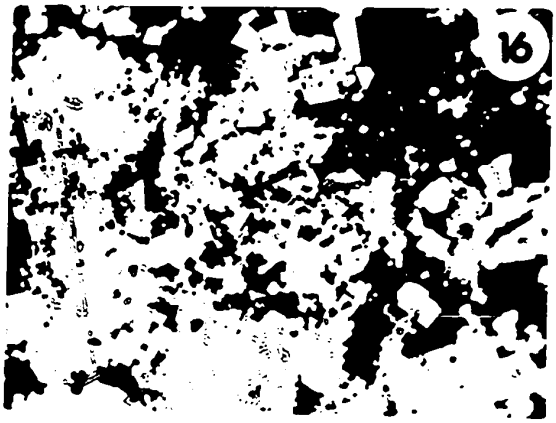

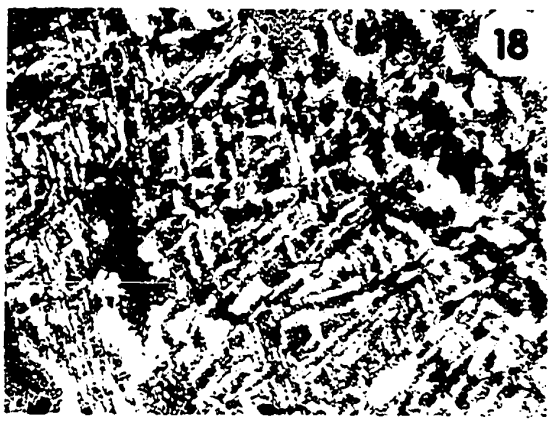

PLATE III.

PLATE IV X-ray Photographs

19. Distribution of Co in a pyrite crystal. High Co (light) areas at the centre (x122).

20. Zoning of Co content in pyrite; a definite zonal arrangement of high Co areas as contrasted to Photograph 19 (x122).

21. A fairly even distribution of Ni in the same pyrite grain above on Photograph 20 (x122).

22. Cobalt distribution in pyrite from massive sulfide. Homogenous distribution of Co (x244).

23. Distribution of Zn in a pyrrhotite inclusion occurring in sphalerite. Sphalerite: white area; pyrrhotite: dark grey (x488). Zn is present in solid solution. No exsolution lamellae or solid inclusions.

24. Same pyrrhotite grain as above showing the distribution of Fe in and around the pyrrhotite inclusion. Sphalerite: dark grey area; pyrrhotite: white (x244).

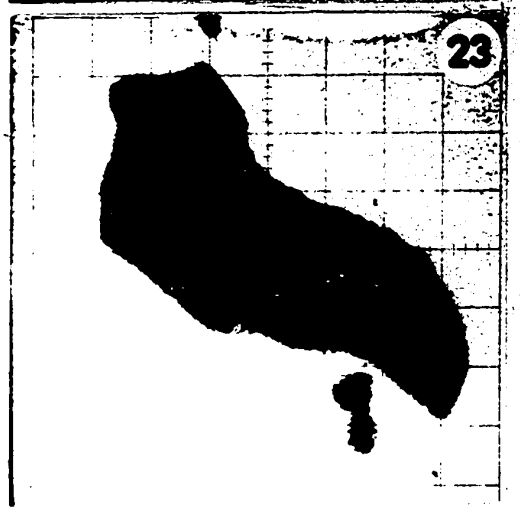

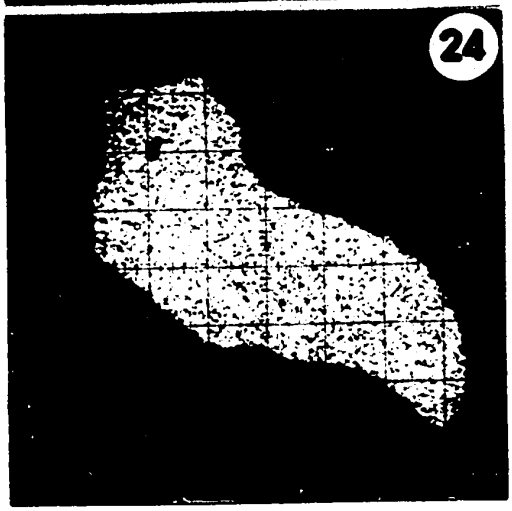

PLATE IV.

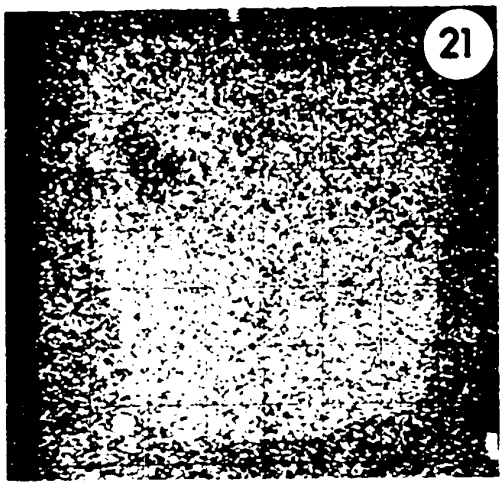

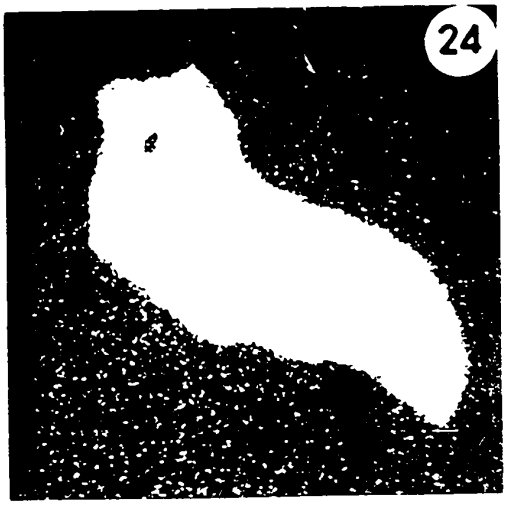

PLATE IV.

PLATE V X-ray Photographs

25. Magnified image of the upper left part of th- same pyrrhotite inclusion represented on Fig. 24, depicting the distribution of Fe at the sphalerite-pyrrhotite boundary (x3900). There is no evidence that pyrrhotite is an exsolution product.

26. Distribution of Cu in a chalcopyrite inclusion and in the surrounding sphalerite. Dark area: sphalerite; light: chalcopyrite (x976). Cu is present in solid solution in the sphalerite inclusion. No evidence of exsolution.

27. Distribution of Zn in the same chalcopyrite inclusion. Dark area: chalcopyrite; white: shalerite (x976). Zn is present in solid solution. No evidence of exsolution.

28. Native silver inclusion in pyrite (Ag is photographed) (x488).

29. Antimonial silver (smaller inclusion at the lower left corner of photograph) and allargentum in sphalerite (Ag is photographed) (x976).

30. Silver-bearing tetrahedrite inclusion in galena (Ag is photographed) (x244).

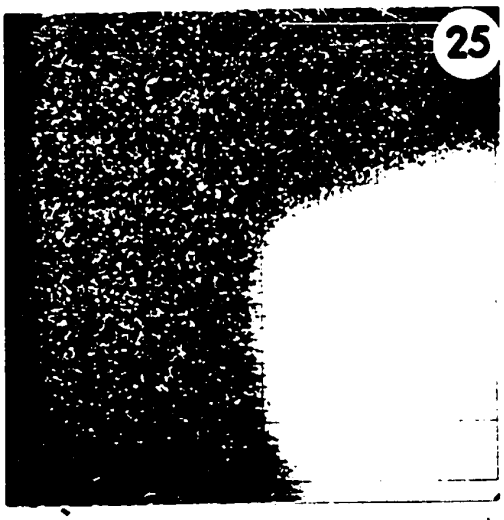

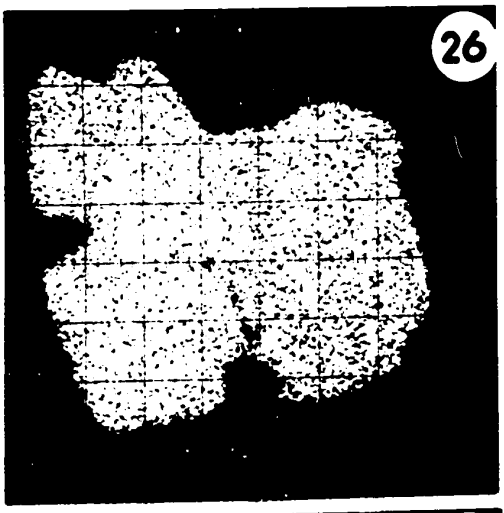

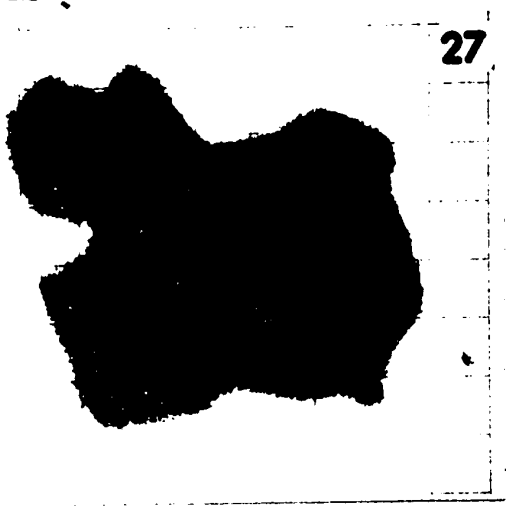

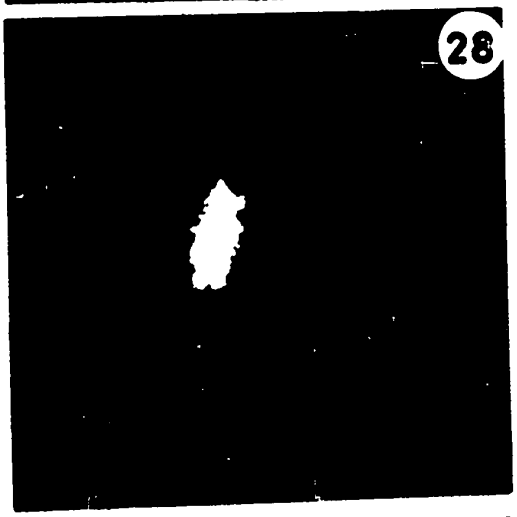

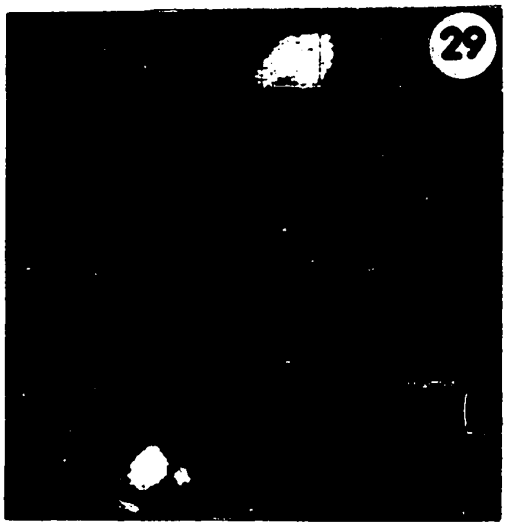

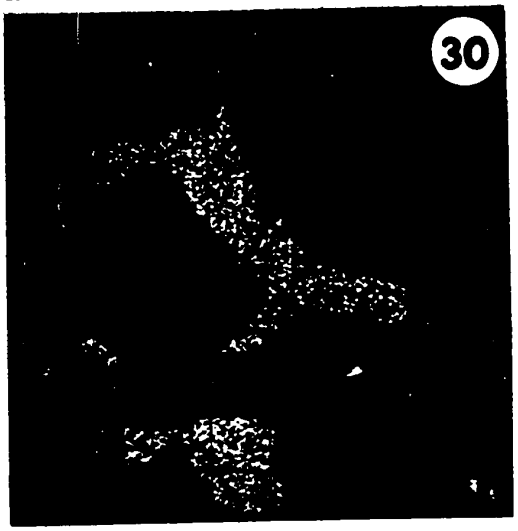

PLATE V.

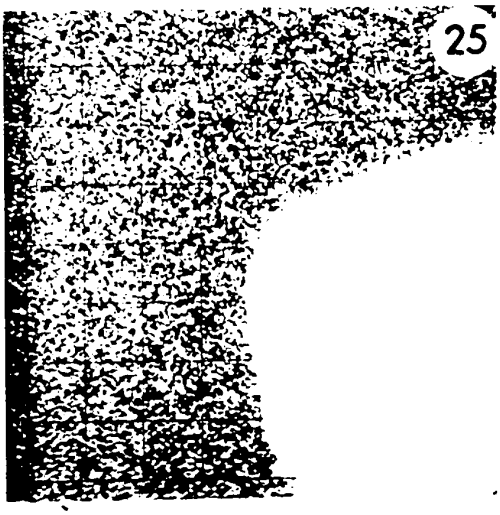

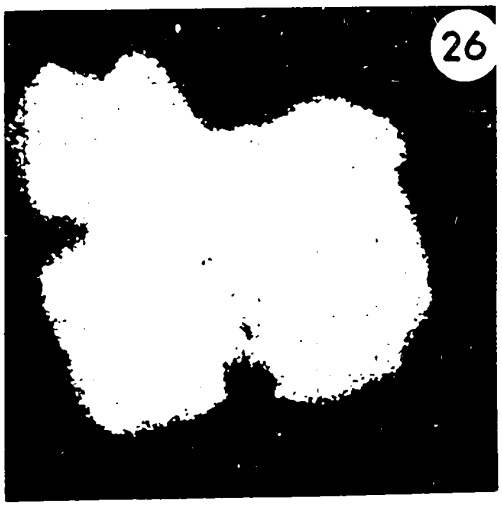

27

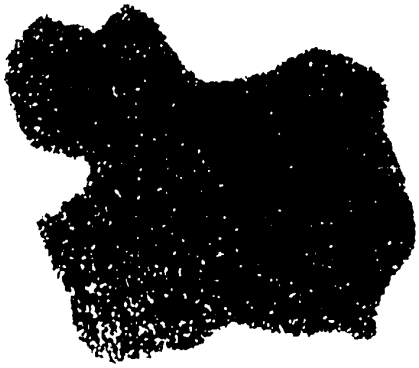

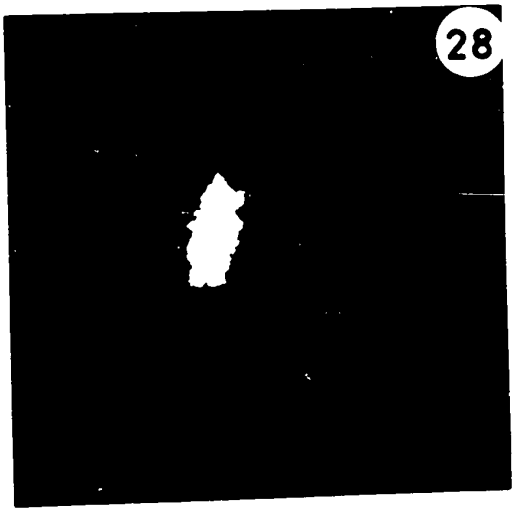

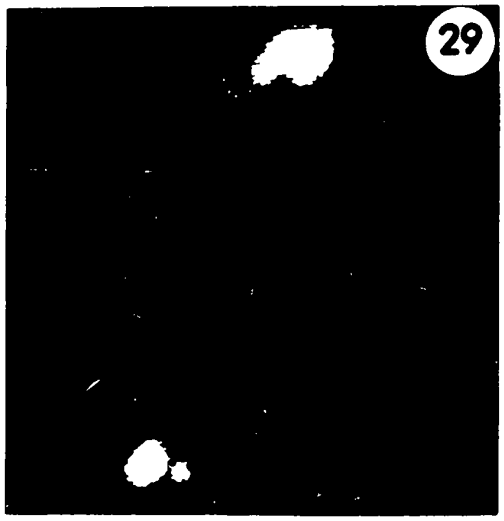

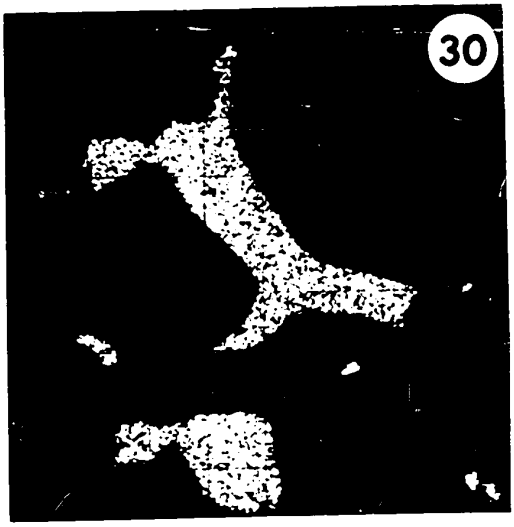

PLATE V.

END OF REEL

ARC-30